

# **Resonating-Valence-Bond Approaches to High-Temperature Superconductivity**

Samuel BIERI

Ecole Polytechnique Fédérale de Lausanne

A dissertation submitted to the Swiss Federal Institute of Technology in Lausanne for the  
degree of Doctor ès Sciences

Lausanne EPFL  
2008



## Version abrégée

Cette thèse est consacrée à l'étude théorique de la supraconductivité à haute température critique, décrite comme un isolant de Mott dopé. Dans cette optique, le modèle  $t$ - $J$  sur réseau carré est analysé par les approches variationnelles et champ moyen. La thèse est focalisée sur la construction des excitations et sur les propriétés spectrales dans le cadre du concept (dû à Anderson) de fonctions d'onde dite "resonating-valence-bond" (RVB). Le modèle quantique de dimères comme modèle pour la phase RVB des isolants de Mott est aussi exploré.

Dans la première partie de la thèse, on analyse les fonctions de Green dans la phase supraconductrice à l'aide des fonctions d'onde variationnelles pour le modèle  $t$ - $J$ . Il est démontré que le poids spectral totale est diminué par une renormalisation dépendante de l'impulsion, et que la projection de Gutzwiller produit une asymétrie particule-trou dans la renormalisation des poids spectraux.

La deuxième partie est consacrée à l'analyse des fonctions de Green dans la phase pseudogap des cuprates à l'aide d'une approche  $SU(2)$  de champ moyen où le paramètre d'ordre fluctue entre le supraconducteur  $d$ -wave et l'état staggered-flux non-supraconducteur. Ce modèle prédit un spectre de photoémission avec un gap asymétrique qui interpole entre le gap supraconducteur centré sur l'énergie de Fermi et le gap asymétrique de l'état staggered-flux. Cette asymétrie du gap change de signe aux points où la surface de Fermi croise la diagonale  $(0, \pi)$ - $(\pi, 0)$ .

Dans la dernière partie de la thèse, on considère les excitations de trous et de vortex dans la phase liquide du modèle quantique de dimères Rokhsar-Kivelson sur réseau triangulaire. On montre que le mouvement d'un trou lié à une excitation topologique est fortement contraint du fait des effets d'interférence.

**Mots clefs:** supraconductivité à haute température critique, resonating valence bond, pseudogap, modèles sur réseau, électrons fortement corrélés, modèle  $t$ - $J$ , Monte Carlo variationnel, fonction d'onde de Gutzwiller, isolant de Mott dopé, modèle de dimères quantique



# Abstract

This thesis is devoted to a theoretical study of high-temperature superconductivity from the viewpoint of a doped Mott insulator. To this end, the square-lattice  $t$ - $J$  model is analyzed by variational and mean-field approaches. The thesis focuses on the construction of excitations and on spectral properties in the framework of Anderson's concept of resonating-valence-bond wavefunctions. The quantum dimer model as a toy model for the resonating-valence-bond phase of Mott insulators is also explored.

In the first part of the thesis, the single-particle Green's functions in the superconducting phase are analyzed using Gutzwiller-projected variational wavefunctions for the  $t$ - $J$  model. It is found that the overall spectral weight is reduced by a momentum-dependent renormalization, and that the projection produces a particle-hole asymmetry in the renormalization of the spectral weights.

The second part analyzes the Green's functions in the pseudogap phase of the cuprates within an  $SU(2)$  mean-field approach where the order parameter fluctuates between the  $d$ -wave superconductor and the non-superconducting staggered-flux state. The model predicts a photoemission spectrum with an asymmetric gap structure interpolating between the superconducting gap centered at the Fermi energy and the asymmetric staggered-flux gap. This gap asymmetry changes sign at the "hot-spots" where the Fermi surface crosses the diagonal  $(0, \pi)$ - $(\pi, 0)$ .

In the last part of the thesis, single hole and vortex excitations in the liquid phase of the triangular-lattice Rokhsar-Kivelson quantum dimer model are considered. It is found that the motion of a hole bound to a topological excitation is strongly constrained due to interference effects.

**Keywords:** high-temperature superconductivity, resonating valence bond, pseudogap, lattice models, strongly correlated electrons,  $t$ - $J$  model, variational Monte Carlo, Gutzwiller-projected wavefunction, doped Mott insulator, quantum dimer model



# Contents

<b>1. Introduction</b>	<b>1</b>
1.1. A brief history of superconductivity . . . . .	1
1.2. Phenomenology of high-temperature superconductors . . . . .	4
1.3. Doping a Mott insulator: physics of strongly interacting electrons . . . . .	6
1.3.1. Mott transition . . . . .	6
1.3.2. From Hubbard to the $t$ - $J$ model . . . . .	7
1.3.3. Zhang-Rice singlets . . . . .	9
1.4. Outline of this thesis . . . . .	11
1.5. Notational conventions and abbreviations . . . . .	12
<b>2. Resonating-valence-bonds: a variational view on high-temperature superconductivity</b>	<b>15</b>
2.1. Anderson's wavefunction . . . . .	16
2.1.1. (Re-)introduction of double occupancy . . . . .	19
2.1.2. Variational Monte Carlo method . . . . .	20
2.1.3. Gutzwiller approximation . . . . .	24
2.2. Quantum dimer models . . . . .	26
2.2.1. Introduction . . . . .	26
2.2.2. Topological degeneracy and topological order . . . . .	28
2.2.3. The square-lattice Rokhsar-Kivelson quantum dimer model . . . . .	29
2.2.4. Static and dynamical correlation functions at Rokhsar-Kivelson points . . . . .	31
2.2.5. The triangular-lattice Rokhsar-Kivelson quantum dimer model and topological sectors . . . . .	32
2.2.6. Topological excitations in the dimer liquid . . . . .	34
2.2.7. Doping quantum dimer models . . . . .	36
<b>3. Strongly correlated superconductors and their electronic properties</b>	<b>37</b>
3.1. Introduction . . . . .	37
3.1.1. Key experimental technique: angle-resolved photoemission spectroscopy . . . . .	37
3.2. Analysis of the spectra within the resonating-valence-bond picture and the $t$ - $J$ model . . . . .	40
3.2.1. Spectral sum rules in the $t$ - $J$ model . . . . .	40
3.2.2. The Gutzwiller-projected BCS state and its excitations . . . . .	42
3.2.3. Effective Fermi surface for the coherent quasiparticle . . . . .	47

3.3. Spectral weight of a Gutzwiller-projected $d$ -wave superconductor . . . . .	49
3.3.1. Introduction . . . . .	49
3.3.2. The model . . . . .	50
3.3.3. Quasiparticle spectral weights . . . . .	52
3.3.4. Superconducting order parameter . . . . .	56
3.3.5. Fermi surface . . . . .	58
3.4. An SU(2) approach to the pseudogap phase . . . . .	60
3.4.1. Introduction . . . . .	60
3.4.2. The model . . . . .	62
3.4.3. Pure states . . . . .	64
3.4.4. Averaged state . . . . .	69
3.4.5. Experimental implications . . . . .	73
<b>4. Single hole and vortex excitation in the doped Rokhsar-Kivelson quantum dimer model on the triangular lattice</b>	<b>75</b>
4.1. Non-vison excitation branch . . . . .	77
4.2. Vison excitation branch . . . . .	78
4.3. Summary . . . . .	81
<b>A. Nonperturbative proof of the 4-fold degeneracy of the vison branch</b>	<b>83</b>
<b>Bibliography</b>	<b>87</b>
<b>Acknowledgements</b>	<b>99</b>
<b>Curriculum Vitae</b>	<b>100</b>







# Chapter 1.

## Introduction

### 1.1. A brief history of superconductivity

Superconductivity was first observed by Kammerlingh Onnes in 1911. When he cooled mercury to the temperature of liquid helium at 4 Kelvin ( $-269\text{ }^{\circ}\text{C}$ ), its resistivity dropped to an unmeasurably small value. Subsequent experimental advances were able to produce even lower temperatures and it was found that most *metals* are in fact superconductors at very low temperature.

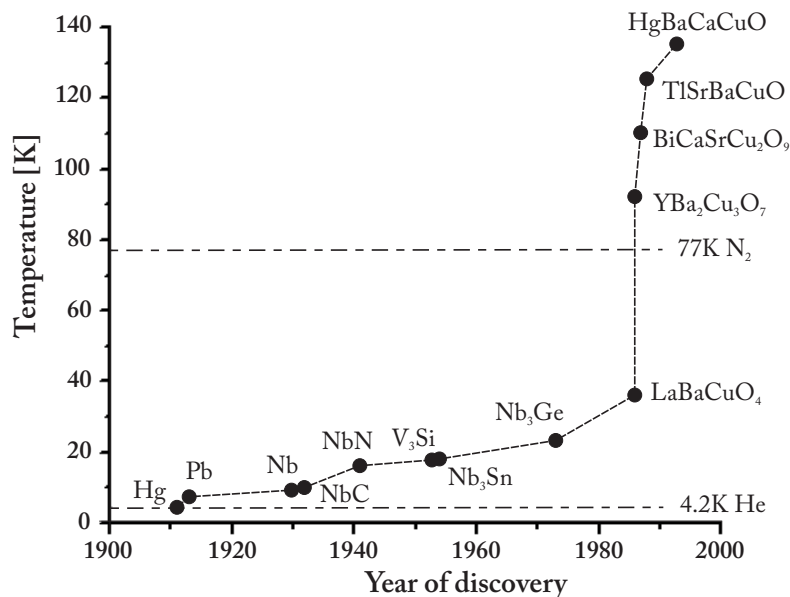


**Figure 1.1.:** Critical temperature of some superconductors as a function of their year of discovery [8].

In 1957, Bardeen, Cooper, and Schrieffer (BCS) [1] proposed a microscopic theory which described the superconducting state as a superfluid of paired electrons. In the BCS theory, these so-called *Cooper pairs* of electrons are in a bound state due to the exchange of lattice vibration modes called *phonons*. The phonons induce an effective attraction between electrons. Within BCS theory, all superconductors which were known at this time could be well understood.<sup>1</sup>

The superconductors known at that time had relatively low critical temperatures, above which they are well-conducting metals. It came therefore as a surprise to the physics community when in 1986, Bednorz and Müller [2] reported the discovery of a superconductor that broke this rule. They found that the  $\text{La}_{2-x}\text{Sr}_x\text{CuO}_4$  (LSCO) compound, a bad conductor at higher temperatures, starts to be superconducting already at 30 Kelvin. A few months later, this  $T_c$  could be improved to spectacular 90 Kelvin in the similar YBCO compound and exceeded for the first time the boiling point of nitrogen (77 Kelvin).<sup>2</sup> The superconductivity at relatively high temperature in metal-oxide compounds, which had previously been known as electric insulators, indicated that a new class of materials had been discovered. This initiated the field of research which is called high-temperature (or unconventional) superconductivity today.

In the 20 years following the discovery of the first high-temperature superconductor, several other compounds with even higher critical temperatures were synthesized. The highest critical temperature under ambient pressure reported so far is 139 K in a mercury-barium-thallium-copper-oxide compound. All these chemically very complicated compounds share similar structures. They are built from layers of copper-oxide (hence their name *cuprates*), separated by layers of rare-earth or alkaline-metal salts.

Despite intense effort during the last 30 years, no unifying theoretical description of high-temperature superconductivity has been found to date. A plethora of theoretical approaches and ideas were proposed, many were abandoned, others are competing or subject to controversy. Starting for example from the viewpoint of strong-correlation physics (which I will make more precise later), the high-temperature-superconductivity problem is very similar to quantum chromodynamics at finite fermion density [3]. Unfortunately, most if not all conventional tools of theoretical physics are not applicable to such systems.

In the meantime, empirical efforts have not been hindered by the lack of theoretical understanding. Enormous quantities of experimental data are available today. The quest for an understanding of these materials has been the driving force in pushing experimental techniques like photoemission spectroscopy or tunneling microscopy to an unprecedented accuracy and reliability.

The recent developments in the research on high-temperature superconductivity indicate that, apart from the high critical temperature  $T_c$ , the superconducting phase of the cuprates is

---

<sup>1</sup>The Nobel prize for the work of BCS was awarded in 1972.

<sup>2</sup>Bednorz and Müller received the Nobel prize for their discovery only one year later, in 1987.

rather conventional. The superconducting cuprates share many properties with conventional metallic superconductors. In contrast to this, the “*anomalous*” *normal state* above the critical temperature shows very unusual and surprising properties which indicate that a radically new state of matter may have been discovered.

Apart from the fundamental scientific interest in these materials, we should not forget that the research has been motivated over the decades by the enormous technological impact that superconductivity at room temperature would undoubtedly have on our society. Lossless transport of electric current is only one application, the possibility to create or measure magnetic fields another. However, as the history of fundamental research shows, the most important applications are rarely foreseen in advance.

## 1.2. Phenomenology of high-temperature superconductors

In order to get a picture of the high-temperature superconductors (HTSC), let me introduce the compound  $\text{La}_{2-x}\text{Sr}_x\text{CuO}_4$  (LSCO) as an example. The chemical structure of this compound is depicted in Fig. 1.2. All cuprates show a similar layered structure with a plane of copper atoms arranged on a rather perfect square lattice. The inplane oxygen atoms sit on the bonds of the square lattice between the copper atoms. The different cuprate materials are mainly distinguished by the insulating crystal between the copper-oxide layers. In the case of LSCO, the interlayer structure is built up of lanthanum.

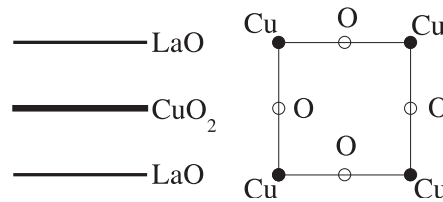


**Figure 1.2.:** Crystal structure of the  $\text{La}_2\text{CuO}_4$  compound. Left are copper-oxide and lanthanum layers in the  $c$ -direction, right is a single copper-oxide layer. The inplane distance between copper atoms is roughly  $a \simeq b \simeq 5\text{\AA}$  and the distance between copper-oxide layers is  $c \simeq 13\text{\AA}$  [9]. Upon doping, the lanthanum atoms are replaced by strontium or barium atoms. Picture taken from [7].

By doping the out-of-plane crystal structure, i.e. by replacing some of these atoms, the experimentalist can control the number of charge carriers in the  $\text{CuO}_2$  plane. In the case of LSCO, doping can be achieved by replacing lanthanum by strontium or barium atoms. Depending on the dopant atom, one may either *add* electrons to the copper-oxide plane (electron doping) or *remove* electrons from the copper-oxide plane (hole doping). Both electron and hole doping have similar effects on the cuprates. However, in this thesis, I am concentrating on the hole-doped cuprate superconductors.

A typical experimental phase diagram of a hole-doped cuprate superconductor as a function of temperature and doping is sketched in Fig. 1.3. At *half filling* (in absence of a dopant) and below the ordering temperature  $T_N \simeq 325\text{ K}$  [10], the material is antiferromagnetically ordered and insulating. As the hole-dopant concentration is increased, the system goes through the *pseudogap* phase and finally becomes superconducting. At small doping, the superconducting transition temperature starts to rise and reaches a maximum at *optimal doping*. Then, the superconductivity vanishes again at a higher doping. Inside this *superconducting dome*, the material has all the well-known characteristics of a superconductor: zero electrical resistivity, Meissner effect (expulsion of electromagnetic fields), etc. Cuprate superconductivity is of type II, i.e. a strong magnetic field produces vortices inside the superconductor and a sufficiently strong field can completely destroy the superconductivity. At higher doping (far in the *overdoped* region, above optimal doping) or at temperatures above the *pseudogap temperature*  $T^*$ , the material covers all aspects of a conventional metal with a gapless Fermi

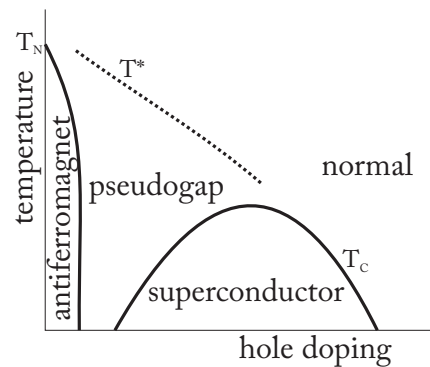


**Figure 1.3.:** A typical experimental phase diagram of the hole-doped cuprates. Close to half filling, an antiferromagnetic insulator is found with a Neel temperature  $T_N$  of several hundreds of Kelvin. As holes are doped into the copper plane, a superconducting phase appears between 5% and 25% doping, optimal doping is reached around 17% in LSCO.

surface and a finite resistivity. The nature of the pseudogap phase appearing at intermediate temperature (between  $T_c$  and  $T^*$ ) in the *underdoped* part of the phase diagram (below optimal doping) is still under debate. Ongoing experiments are trying to characterize this phase. It appears that the pseudogap phase is normal in the sense that it is not superconducting. However, angle-resolved photoemission experiments show a partially gapped Fermi surface or *Fermi arcs*. This property is highly unusual and not observed in normal metals. For this reason, the pseudogap phase was also called *strange metal* by Anderson [11]. In Section 3.4 of this thesis, I propose a theoretical model for this phase.

The electronic properties of the superconducting phase of HTSC is an important subject of this thesis. From the experimental point of view, it is now well established that the symmetry of the superconducting gap is not *s-wave*, as it is for most conventional superconductors. The superconducting order parameter has *d-wave* symmetry, i.e. the gap vanishes at a point in the Brillouin zone (at the *nodal point*) and the order parameter changes sign when the plane is rotated by 90 degrees.<sup>3</sup>

There are many more experimental aspects of high-temperature superconductivity. However, I do not want to go into greater detail at this point, but introduce further aspects in due course.

<sup>3</sup>The symmetry of the superconducting order parameter led to considerable controversy among experimentalists which was settled only a few years ago. The correct theoretical prediction, however, was given in the late 1980s (see Section 2.1).

### 1.3. Doping a Mott insulator: physics of strongly interacting electrons

The approaches and results of this thesis are rooted in the strong-coupling point of view. Based on this view, the striking phenomena in cuprate superconductors have their origin in the large Coulomb repulsion between the charge carriers. This repulsion energy between the charge carriers is much larger than their kinetic energy in the solid and this makes traditional tools of solid state theory, like band theory or perturbation in the interaction strength, of little use. In this section, I will introduce the strong-coupling approach to the problem of unconventional superconductivity.

Let me first remind the electronic configuration of the atoms in the  $\text{CuO}_2$  plane (Fig. 1.2). The copper ions on the square lattice have  $\text{Cu}^{2+}$  charge with a single electron missing in the  $3d$ -shell. The oxygen atoms on the bonds of the lattice carry a single negative charge.

It was proposed by P. W. Anderson [12] that the electrons in the partially filled  $d$ -shell of the copper atom are delocalized in a single band of the 2-dimensional solid. Due to the large on-site Coulomb integral  $U$  of the  $d_{x^2-y^2}$  orbitals, these itinerant electrons on the same site strongly interact and their quantum mechanics is well approximated by the single-band Hubbard model (1.1) [13]. The nearest-neighbor hopping integral  $t$  involves the intermediate oxygen atom and is therefore rather small,  $U \simeq 12t$ . Further-neighbor hoppings are even smaller due to the geometry of the  $d_{x^2-y^2}$ -orbitals. The dopant removes electrons from the copper site ( $\text{Cu}^{3+}$ -ions are formed) and holes are introduced into the Hubbard model.

$$H_U = - \sum_{i,j,\sigma} t_{ij} c_{i\sigma}^\dagger c_{j\sigma} + \frac{U}{2} \sum_{i,\sigma} c_{i\sigma}^\dagger c_{i\sigma} c_{i\bar{\sigma}}^\dagger c_{i\bar{\sigma}} \quad (1.1)$$

#### 1.3.1. Mott transition

In the limit  $U \rightarrow \infty$ , it is easy to see that the ground state(s) of the half-filled Hubbard model (1.1) is localized with exactly one electron per site,

$$|\text{MI}\rangle = \prod_i c_{i\sigma_i}^\dagger |0\rangle. \quad (1.2)$$

This limit is an example of a so-called *Mott insulator*, in contrast to the more conventional *band insulator*. In a band insulator, the conduction electrons occupy a completely filled band and the band gap prohibits conduction. In a Mott insulator on the other hand, the electrons need to overcome the (large) Mott gap  $U$  to create doubly occupied sites and to delocalize.

In the other limit,  $U \rightarrow 0$ , the electrons are completely delocalized. E.g. in the case of nearest-neighbor hopping, the electrons are in a band  $\varepsilon_{\mathbf{k}} = -2[\cos k_x + \cos k_y]$ . In this limit,



the exact ground state is also known. It is the completely filled Fermi sea,

$$|\text{Fs}\rangle = \prod_{\epsilon_{\mathbf{k}} < 0} c_{\mathbf{k}\uparrow}^\dagger c_{\mathbf{k}\downarrow}^\dagger |0\rangle. \quad (1.3)$$

For intermediate  $U$ , the ground state is much more complicated. It is believed that there is a critical  $U_c \simeq 4t$  where the *Mott transition* [14] from a conductor to a Mott insulator takes place.<sup>4</sup>

In the cuprates, the valence electrons occupy a half-filled band and they would be conducting if the Coulomb integral  $U$  was moderate. However, the on-site Coulomb repulsion in cuprates is so large that the undoped material is deep in the Mott-insulating phase ( $U \simeq 12t$ ).

### 1.3.2. From Hubbard to the $t$ - $J$ model

The Hubbard model in the limit  $U \gg t$  can be transformed to a low-energy effective model in the subspace with less than two electrons per site ( $n_i < 2$ ) [15]. Doubly occupied sites cost a large energy of order  $U$  and can be neglected at low temperature. One can find a unitary transformation  $S$  which block-diagonalizes the Hubbard model by eliminating matrix elements that mix singly occupied with doubly occupied states (this is the so-called *Schrieffer-Wolff transformation*),  $H^{eff} = e^{-iS} H_U e^{iS}$ . The unitary transformation  $S$  can be found to any order in  $t/U$ . In the following, I will restrict myself to a model with uniform nearest-neighbor hopping. Without going through the details, the result to second order in  $t/U$  is [5, 15]:

$$\begin{aligned} H^{eff}|_{n_i < 2} = & -t P_d \sum_{\langle i,j \rangle, \sigma} c_{i\sigma}^\dagger c_{j\sigma} P_d \\ & + \frac{t^2}{U} P_d \sum_{i, \tau_1, \tau_2, \sigma} [c_{i+\tau_1\sigma}^\dagger c_{i\sigma}^\dagger c_{i\sigma} c_{i+\tau_2\sigma} - c_{i+\tau_1\sigma}^\dagger n_{i\sigma} c_{i+\tau_2\sigma}] P_d + O\left(\frac{t^3}{U^2}\right). \end{aligned} \quad (1.4)$$

where  $H^{eff}|_{n_i < 2}$  is the matrix acting only on the low-energy space of vectors without doubly occupied sites.  $i + \tau$  denotes a site which is nearest neighbor to site  $i$ . The *Gutzwiller projector*  $P_d$  in (1.4) is needed to ensure that the hopping remains in this low-energy space. It is defined as

$$P_d = \prod_i [1 - n_{i\downarrow} n_{i\uparrow}]. \quad (1.5)$$

---

<sup>4</sup>This discovery is due to Sir Nevil Francis Mott, who won the Nobel price for his work on strongly correlated electrons in 1977, together with P. W. Anderson and J. van Fleck.

The terms in the sum with  $\tau_1 = \tau_2$  of the effective model (1.4) gives an antiferromagnetic interaction between the electron spins on nearest-neighbor sites:

$$H_J = \frac{t^2}{U} \sum_{i,\tau,\sigma} [c_{i+\tau,\sigma}^\dagger c_{i\bar{\sigma}}^\dagger c_{i\bar{\sigma}} c_{i+\tau,\sigma} - c_{i+\tau,\sigma}^\dagger n_{i\bar{\sigma}} c_{i+\tau,\sigma}] = J \sum_{\langle i,j \rangle} [\mathbf{S}_i \cdot \mathbf{S}_j - \frac{n_i n_j}{4}] \quad (1.6)$$

with  $J = \frac{4t^2}{U}$  and  $\mathbf{S} = \frac{1}{2} \sum_{\alpha,\beta} c_\alpha^\dagger \boldsymbol{\sigma}_{\alpha\beta} c_\alpha$ . The remaining term,

$$H_3 = \frac{J}{4} \sum_{i,\tau_1 \neq \tau_2, \sigma} [c_{i+\tau_1,\sigma}^\dagger c_{i\bar{\sigma}}^\dagger c_{i\bar{\sigma}} c_{i+\tau_2,\sigma} - c_{i+\tau_1,\sigma}^\dagger n_{i\bar{\sigma}} c_{i+\tau_2,\sigma}], \quad (1.7)$$

is the so-called *3-site-hopping term*.

The *t-J model*, in which I am mainly interested here, is this effective model without the 3-site-hopping term:

$$H_{t,J} = -t P_d \sum_{\langle i,j \rangle, \sigma} c_{i\sigma}^\dagger c_{j\sigma} P_d + J \sum_{\langle i,j \rangle} [\mathbf{S}_i \cdot \mathbf{S}_j - \frac{n_i n_j}{4}]. \quad (1.8)$$

In the limit of vanishing doping ( $x \rightarrow 0$ ), it is clear that the Gutzwiller-projected hopping term  $P_d c^\dagger c P_d$  is zero: every site is singly occupied and the hopping necessarily creates a doubly occupied site. In terms of the so-called Gutzwiller approximation (Section 2.1.3), the Gutzwiller-projected hopping matrix element is reduced by a factor of order  $x$ . In the same sense,  $H_3 \sim xt^2$ , and the 3-site-hopping term is negligible with respect to  $H_J \sim t^2$  at low doping. At half filling, the electrons are localized and the only remaining term is  $J \mathbf{S}_i \cdot \mathbf{S}_j$  with  $J > 0$ . This is the *antiferromagnetic Heisenberg model*. The antiferromagnetic interaction between the electron spins can be understood intuitively from the concept of virtual hopping: Even though the electrons are localized, opposite spins on nearest-neighbor sites are favored because they have in principle the possibility to hop. On the other hand, the same spin state on nearest-neighbor sites are forbidden to hop because of the fermionic statistics of the electrons (the Pauli principle).

Note that a perfect two-dimensional antiferromagnetic Heisenberg model orders only at zero temperature ( $T_N=0$ ). In cuprates, however, there is a weak interlayer coupling which explains the observed ordering at finite temperature in these materials.

The  $t$ - $J$  model can conveniently be written in terms of Gutzwiller-projected creation and annihilation operators,

$$\tilde{c}_\sigma = c_\sigma [1 - n_{\bar{\sigma}}]. \quad (1.9)$$

This replaces the Gutzwiller projector in the Hamiltonian (1.8) and the hopping term of the model is simply

$$\sum_{\langle i,j \rangle, \sigma} \tilde{c}_{i\sigma}^\dagger \tilde{c}_{j\sigma}. \quad (1.10)$$

### 1.3.3. Zhang-Rice singlets

There is an alternative way to directly construct an effective  $t$ - $J$  model for the  $\text{CuO}_2$  layers which was proposed by Zhang and Rice [16]. The undoped material is clearly an antiferromagnet for the  $d$ -holes on the  $\text{Cu}^{2+}$ -ions. This motivated Zhang-Rice to start from the Heisenberg model. In the Zhang-Rice scenario, doping does not remove a further  $d$ -electron to create a  $\text{Cu}^{3+}$ -ion, but instead it removes a  $p$ -electron from the oxygen atom in the plane. Hybridization favors a singlet superposition of a  $p$ -hole delocalized on the four oxygen atoms surrounding a  $\text{Cu}^{2+}$ -ion and the  $d$ -hole of the central copper atom. Zhang-Rice constructed Wannier states for such a singlet. A  $p$ -hole in this state can tunnel to a nearest-neighbor site and form another singlet, but only if no singlet is already occupying the site. This results in the constrained hopping of holes in the antiferromagnetic background, precisely described by the  $t$ - $J$  model.



## 1.4. Outline of this thesis

The remaining part of this thesis is organized in the following way. In Chapter 2, I introduce the theoretical tools which I use to study high-temperature superconductivity and doped Mott insulators. I give an introduction to Anderson's variational resonating-valence-bond construction and to the theoretical developments that emerged from Anderson's proposal. In the case of the variational Monte Carlo method, some technical details developed by myself are also given.

In Chapter 3, I analyze the electronic properties of doped Mott insulators and I discuss their experimental implications. In the first part, the general properties of spectra within a Gutzwiller-projected Hilbert space are studied. In the second part, I analyze the spectral properties of Gutzwiller-projected variational wavefunctions in the superconducting phase of cuprates. In the last part of that chapter, I study the spectral properties in the disordered phase of the pseudogap region at the mean-field level.

Chapter 4 is devoted to a toy model for the resonating-valence-bond liquid phase: the quantum dimer model on the triangular lattice. This model provides an example of a topological phase and is therefore interesting on general grounds. There are proposals and indications that the cuprate superconductors close to half filling may be in such a topological phase. In this last chapter, I analyze dynamical properties of a single hole in such a phase in the presence and absence of a topological excitation.

## 1.5. Notational conventions and abbreviations

In this thesis I use the following notations and conventions.

- (i)  $c_{i\sigma}$  is the annihilation operator for an electron with spin  $\sigma$  in the Wannier state localized at the lattice site  $\mathbf{r}_i$ .  $c_{i\sigma}^\dagger$  is the corresponding creation operator. These operators follow the usual anti-commutation relations  $\{c_{i\sigma}, c_{j\sigma'}\} = 0$  and  $\{c_{i\sigma}, c_{j\sigma'}^\dagger\} = \delta_{ij}\delta_{\sigma\sigma'}$ . The spin index  $\sigma$  takes values  $\uparrow$  and  $\downarrow$  and the opposite spin to  $\sigma$  is written as  $\bar{\sigma}$ .
- (ii)  $c_{\mathbf{k}\sigma}$  is the Fourier transform,  $c_{\mathbf{k}\sigma} = \frac{1}{\sqrt{L}} \sum_j e^{-i\mathbf{k}\cdot\mathbf{r}_j} c_{j\sigma}$  and  $L$  is the total number of lattice sites.
- (iii) The electron-number operator is denoted by  $n_{i\sigma} = c_{i\sigma}^\dagger c_{i\sigma}$  and  $n_i = \sum_\sigma n_{i\sigma}$ .
- (iv) The vacuum state for electrons is denoted by  $|0\rangle$ , i.e.  $c_{i\sigma}|0\rangle = 0$ .
- (v) The hole-doping level (concentration of holes with respect to half filling when there is exactly one electron per site) of the cuprate layer is denoted by  $x = \frac{L-N}{L}$ . It takes values  $x \in [0, 1]$ . To avoid confusion, I use  $\hat{N} = \sum_i n_i$  to denote the total number operator and  $N$  for the total number of electrons.
- (vi)  $\langle i, j \rangle$  denotes pairs of indices on nearest-neighbor sites and  $\langle\langle i, j \rangle\rangle$  denotes pairs of indices on next-nearest neighbor sites of a lattice.
- (vii)  $\{\sigma_i, i = 1, 2, 3\}$  are the Pauli matrices:  

$$\sigma_1 = \begin{pmatrix} 0 & 1 \\ 1 & 0 \end{pmatrix}, \sigma_2 = \begin{pmatrix} 0 & -i \\ i & 0 \end{pmatrix}, \sigma_3 = \begin{pmatrix} 1 & 0 \\ 0 & -1 \end{pmatrix}.$$
- (viii) “column-vectors” ( $N \times 1$ -matrices) are written in bold font. A superscript T denotes matrix transposition:  $\mathbf{v}^T = (v_1, v_2, \dots)$ . The cartesian product may be written with a dot:  $\mathbf{u} \cdot \mathbf{v} = \sum_i u_i v_i$ .
- (ix) The spin operator for electrons is defined as  $\mathbf{S} = \frac{1}{2} \sum_{\alpha, \beta} c_\alpha^\dagger \boldsymbol{\sigma}_{\alpha\beta} c_\beta$ . The raising operator is  $S^+ = S^{-\dagger} = c_\uparrow^\dagger c_\downarrow$ .
- (x) The symbol # is sometimes used as abbreviation for “number of”.
- (xi) the curly brackets stand for the anti-commutation,  $\{A, B\} = AB + BA$ . The square brackets stand for the commutation,  $[A, B] = AB - BA$ .
- (xii) I use the physicist’s jargon for the word “finite”. A number is finite if it is real and not zero.
- (xiii) The Gutzwiller-projection operator is denoted by  $P_d = \prod_i [1 - n_{i\uparrow} n_{i\downarrow}]$ .
- (xiv) The projection operator to a given number of particles  $N$  is denoted by  $P_N = \int_0^1 d\alpha e^{2\pi i(\hat{N}-N)\alpha}$ .

---

The following abbreviations are used in this thesis.

---

AF	antiferromagnet(-ic)
ARPES	angle-resolved photoemission spectroscopy
BCS	Bardeen-Cooper-Schrieffer
FS	Fermi surface
GA	Gutzwiller approximation
HTSC	high-temperature superconductivity
MC	Monte Carlo
QDM	quantum dimer model
QP	quasiparticle
RK	Rokhsar-Kivelson
RVB	resonating-valence-bond
SC	superconductor / superconductivity
SF	staggered-flux
VB	valence bond
VBS	valence-bond-solid
VMC	variational Monte Carlo

---





## Chapter 2.

# Resonating-valence-bonds: a variational view on high-temperature superconductivity

In the introductory Chapter 1, I have argued that there are good reasons to believe that many phenomena of cuprate superconductors can be understood within repulsive, large- $U$  fermionic Hubbard or  $t$ - $J$  models (for  $U \simeq 12t$  or  $t \simeq 3J$ ). However, these strong-coupling models are difficult to explore theoretically, because there is no small parameter which would allow to expand around a known limit. For example, doping as small parameter is not suitable: Even a single mobile hole in the antiferromagnetic background introduces a new degree of freedom (the charge) and may affect the system in a nonperturbative way. Unbiased numerical approaches like *exact diagonalization* or *quantum Monte Carlo methods* are either bound to very small clusters (even on modern computers) or suffer from fermionic sign problems [17]. In this thesis, I adopt a different approach, a *variational* one. Although this approach is biased (by hopefully correct physical insight), it has the advantage of being nonperturbative and can be applied to large systems.

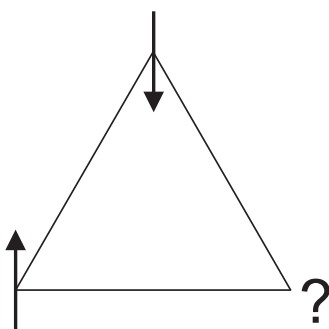


**Figure 2.1.:** An artist's view of geometric frustration: three classical spins with antiferromagnetic interaction on a triangle. Two of the spins minimize their energy by pointing up and down, respectively. The third spin is frustrated because it cannot minimize the interaction energy on the two bonds simultaneously.

## 2.1. Anderson's wavefunction

In the undoped case, the square-lattice Heisenberg model is known to have a ground state with antiferromagnetic long-range order. However, this conclusion is not very robust. For example, the Mermin-Wagner-Hohenberg theorem [18, 19, 20] implies immediate destruction of long-range order at finite temperature. Other effects like geometric frustration (e.g. on the triangular lattice or by further-neighbor interactions on the square lattices; see Fig. 2.1) or a mobile hole may destroy the antiferromagnetic ground state. In the year 1972, even before the discovery of HTSC, Anderson considered alternative ground-state wavefunctions on the square lattice which can compete with the Neel antiferromagnet [21]. Anderson was inspired by L. Pauling's work, who had successfully described the chemical structure of benzene molecules as quantum-mechanical superpositions of different valence-bond configurations [hence the name *resonating-valence-bond* (RVB); see Fig. 2.2]. Pauling had also applied these ideas to valence electrons in solids [22]. After the discovery of HTSC, Anderson developed the RVB idea further and adapted it to the case of the cuprates [12].

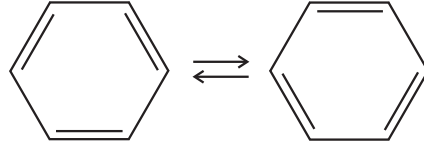


**Figure 2.2.:** The double-bonds in benzene are not localized and may be pictured as a quantum-mechanical superposition of two classical states. Such states were named *resonating-valence-bonds* (RVB) by L. Pauling.

Anderson was motivated by the fact that for an antiferromagnetic Heisenberg model on an unfrustrated lattice with coordination number  $z$ , the Neel state has a variational energy of  $-\frac{Jz}{4}$  per site. On the other hand, if we imagine a product state with pairs of (AF-coupled) spins in a singlet state, then a variational energy of  $-\frac{3J}{8}$  per spin is obtained. For a chain ( $z = 1$ ), the singlet state is a better variational state than the Neel state.<sup>1</sup> As we go to higher coordination numbers, the Neel state becomes a better variational state. Anderson proposed that such a product state of spin singlets could be stabilized even in two dimensions by letting the singlet bonds resonate between different sites.

More formally, we define

$$b_{ij}^\dagger = \frac{1}{\sqrt{2}}[c_{i\uparrow}^\dagger c_{j\downarrow}^\dagger - c_{i\downarrow}^\dagger c_{j\uparrow}^\dagger] \quad (2.1)$$

<sup>1</sup>Indeed, it is known from Bethe's solution that the antiferromagnetic spin chain has a singlet ground state [23, 24].

the creation operator for a singlet on bond  $(i, j)$ . A state in a “valence-bond” configuration may be constructed by

$$|\text{VB}\rangle = \prod_{(i,j)} b_{ij}^\dagger |0\rangle \quad (2.2)$$

where  $(i, j)$  are pairs of sites which *cover the entire lattice* and *no site is repeated in the product*. The last point is important, because if sites were repeated in the product, this would create doubly occupied sites in terms of  $c$ -electrons,  $c_{i\uparrow}^\dagger c_{i\downarrow}^\dagger$ . Such states are not in the Hilbert space of the Heisenberg Hamiltonian or, in terms of electronic models, they cost a large energy of order  $U$ . There are many VB states possible on a given lattice and the counting of them may be formulated in terms of close packing of *hardcore dimers* on the lattice.<sup>2</sup> Chapter 4 will be devoted to the quantum dynamics of such dimer coverings. Note that the singlet-product states corresponding to different close-packed dimer coverings are not orthogonal in general. Note also that the state  $|\text{VB}\rangle$  is a spin singlet, i.e.  $\mathbf{S}_{tot}^2 |\text{VB}\rangle = 0$ .

A wavefunction with resonating singlets and no translational symmetry breaking (termed *spin liquid* by Anderson) may be constructed in the following way:

$$|\text{RVB}\rangle = P_d \left[ \sum_{i,j} \tilde{a}(\mathbf{r}_i - \mathbf{r}_j) b_{ij}^\dagger \right]^{N/2} |0\rangle = P_d \left[ \sum_{i,j} a(\mathbf{r}_i - \mathbf{r}_j) c_{i\uparrow}^\dagger c_{j\downarrow}^\dagger \right]^{N/2} |0\rangle \quad (2.3)$$

where  $a(\mathbf{r}) = \tilde{a}(\mathbf{r}) + \tilde{a}(-\mathbf{r})$  and  $N$  is the (even) number of electrons on the lattice.  $N = L$  is chosen for a spin wavefunction (half filling) and  $N < L$  for an electronic (doped) wavefunction. The sum in (2.3) creates spin singlets between the sites  $\mathbf{r}_i$  and  $\mathbf{r}_i + \mathbf{r}$  with probability  $a(\mathbf{r})$  for all  $i$ . The product produces states containing  $\frac{N}{2}$  singlets. Those states which contain doubly occupied sites are then removed by the Gutzwiller projector,  $P_d = \prod_i [1 - n_{i\uparrow} n_{i\downarrow}]$ .  $|\text{RVB}\rangle$  is a superposition of all singlet-product states with bond occupation probability  $a(\mathbf{r})$ . I do not want to go into the details of the classification or phenomenology of quantum spin liquid states, but instead refer to the literature [59, 60]. Let me just note that such spin states (at half filling) are not characterized by a broken symmetry and conventional order parameter (like e.g. the Neel state is). Spin liquid states are instead characterized by *topological order*. I will illustrate this concept in the case of the quantum dimer model.

Written in Fourier space, the RVB state (2.3) turns out to be a Gutzwiller-projected BCS-wavefunction at fixed particle number, as it can be easily seen from the following calculation,

$$\begin{aligned} |\text{RVB}\rangle &= P_d \left[ \sum_{\mathbf{k}} a_{\mathbf{k}} c_{\mathbf{k}\uparrow}^\dagger c_{-\mathbf{k}\downarrow}^\dagger \right]^{N/2} |0\rangle \propto P_d P_{\frac{N}{2}} e^{\sum_{\mathbf{k}} a_{\mathbf{k}} c_{\mathbf{k}\uparrow}^\dagger c_{-\mathbf{k}\downarrow}^\dagger} |0\rangle \\ &= P_d P_{\frac{N}{2}} \prod_{\mathbf{k}} [1 + a_{\mathbf{k}} c_{\mathbf{k}\uparrow}^\dagger c_{-\mathbf{k}\downarrow}^\dagger] |0\rangle \propto P_d P_{\frac{N}{2}} |\text{BCS}\rangle. \end{aligned} \quad (2.4)$$

<sup>2</sup>Also known in mathematics as the *perfect matching of a graph*.

I have used the projection to a given number of electrons,  $P_N = \int_0^1 d\alpha e^{2\pi i(\hat{N}-N)\alpha}$ , and  $a_{\mathbf{k}} = \sum_i a(\mathbf{r}_i) e^{-i\mathbf{r}_i \cdot \mathbf{k}}$ , the Fourier transform of the singlet distribution function. In BCS terminology [25],  $u_{\mathbf{k}} = \frac{1}{\sqrt{1+a_{\mathbf{k}}^2}}$ ,  $v_{\mathbf{k}} = \frac{a_{\mathbf{k}}}{\sqrt{1+a_{\mathbf{k}}^2}}$ , and  $|\text{BCS}\rangle = \Pi_{\mathbf{k}}[u_{\mathbf{k}} + v_{\mathbf{k}} c_{\mathbf{k}\uparrow}^\dagger c_{-\mathbf{k}\downarrow}^\dagger] |0\rangle$ .

Anderson's proposal to understand high-temperature superconductors as a doped spin liquid is very elegant and appealing. If the Gutzwiller-projected BCS wavefunction has particle-hole mixing (i.e.  $0 < u_{\mathbf{k}}^2 < 1$ ), then superconductivity will naturally emerge from the same wavefunction, as holes are added. To understand this, consider the off-diagonal long-range order parameter that characterizes a superconducting state [6, 26],

$$\Phi_{ij}^{SC} = \lim_{r \rightarrow \infty} \langle c_{i\sigma} c_{j\bar{\sigma}} c_{i+r\sigma}^\dagger c_{j+r\bar{\sigma}}^\dagger \rangle. \quad (2.5)$$

From combinatorial arguments, known as Gutzwiller approximation (see Section 2.1.3), one can understand that this quantity vanishes like  $\Phi_{ij}^{SC} \propto x^2 \Phi_{ij}^0$  as doping  $x$  goes to zero.  $\Phi_{ij}^0$  is the off-diagonal long-range order of the unprojected wavefunction. The vanishing is due to the Gutzwiller projector and is not a property of the wavefunction before projection. On the other hand, magnetic correlations of the form

$$\langle S_i^z S_j^z \rangle \quad (2.6)$$

are only weakly affected by the Gutzwiller projector near half filling.

Indeed, it was found by Gros [27] and Yokoyama *et al.* [28] in 1988 that a BCS wavefunction with a  $d$ -wave gap symmetry,

$$u_{\mathbf{k}}^2 = \frac{1}{2} \left[ 1 + \frac{\Delta(\cos k_x - \cos k_y)}{\sqrt{(\cos k_x + \cos k_y - \mu)^2 + \Delta^2(\cos k_x - \cos k_y)^2}} \right], \quad (2.7)$$

is a favored variational state of the  $t$ - $J$  model for a large range of doping. The energy gain of this state is mainly due to the spin-exchange term as we expect from Anderson's arguments. It took many years until the experimental technique of angle-resolved photoemission spectroscopy (ARPES) [29, 30] was accurate enough to confirm the  $d$ -wave gap symmetry in the superconducting phase of the cuprates. In fact, the first unambiguous experimental confirmation came from phase sensitive measurements with Josephson junctions [31, 32]. Since these early studies, the variational approach to the  $t$ - $J$  model has been refined and extended by many research groups [33, 34, 35, 36] and today we enjoy a quite complete variational picture of the  $t$ - $J$  model and the cuprate superconductors within this framework. The main results were summarized in recent review articles [3, 4, 5, 6]. In the following chapters, I will remind some of these results where necessary.

### 2.1.1. (Re-)introduction of double occupancy

The RVB wavefunction (2.4) is a variational state for the  $t$ - $J$  model. However, one may also want to use this type of wavefunction to study the Hubbard model. There are two approaches in the literature which allow to introduce doubly occupied sites and to extend this variational approach to the Hubbard model.

In the first approach, one rotates the wavefunction back to the Hubbard model using the inverse Schrieffer-Wolff transformation introduced in Section 1.3.2:

$$|\text{RVB}, U\rangle = e^{-iS}|\text{RVB}\rangle = |\text{RVB}\rangle + \frac{t}{U}S_1|\text{RVB}\rangle + \dots \quad (2.8)$$

Doubly occupied sites can be reintroduced to any desired order in  $t/U$  and small quantitative changes of some matrix elements were reported for the cuprates [27, 33]. However, no qualitatively different conclusions are expected if we are deep in the Mott-insulating phase  $t \ll U$ .

An alternative approach is the so-called *partial-projection operator*  $P_g$  instead of the Gutzwiller projector [36].  $P_g$  has an additional variational parameter  $g$  and the states with doubly occupied sites are not completely suppressed but only reduced by a factor  $1 - g$ :

$$P_g = g^{\sum_i n_{i\uparrow} n_{i\downarrow}} = \prod_i [1 - (1 - g)n_{i\uparrow} n_{i\downarrow}]. \quad (2.9)$$

Such wavefunctions are particularly useful in the case of intermediate  $U$ , when the system is in the vicinity of a Mott transition. The disadvantage when studying superconductivity in a doped Mott insulator is that partially projected wavefunctions generally (super-)conduct in the half-filled limit,  $x \rightarrow 0$ . The possibility that such states are realized in the cuprates was proposed by R. Laughlin who called them *gossamer superconductors* [37, 38]. Note, however, that due to the invertibility of  $P_g$ , it is easy to write down a Hamiltonian for which the  $P_g$ -“projected” mean-field state is an exact eigenstate.<sup>3</sup> This is not possible for the Gutzwiller projector  $P_d = P_{g=0}$  and the limit  $g \rightarrow 0$  is clearly not analytic.

In this thesis, I choose to work with the pure  $t$ - $J$  model without perturbative or explicit inclusion of doubly occupied sites.

---

<sup>3</sup>Note that the terminology “partial projection” is unfortunate, since  $P_g$  is not a true projection operator (i.e.  $P_g^2 \neq P_g$ ).

### 2.1.2. Variational Monte Carlo method

The shift of problem from solving the full Hubbard Hamiltonian (1.1) to working with variational wavefunctions of the  $t$ - $J$  model has simplified our task. However, it is still formidable to make quantitative predictions. The local constraint implemented by the Gutzwiller projector  $P_d$  is difficult to handle both analytically and numerically. This is expected, since  $P_d$  incorporates the strong interaction between the electrons in the copper-oxide layer which makes this problem so distinct from traditional mean-field theories or other weak-coupling expansions of many-body physics. In this thesis, I mainly rely on the approaches described in this and the following sections.

The variational Monte Carlo method (VMC) [27, 28] is a numerical tool that allows to compute the expectation value of an operator in a given many-body wavefunction within small error bars. Here, I apply it to electronic wavefunctions on finite lattices, where it is highly efficient: It allows to handle wavefunctions on large clusters up to 500 sites within a reasonable time frame of the order of days on modern computer processors. A particular advantage of VMC is that it allows to implement the Gutzwiller constraint  $n_i < 2$  exactly.

A Markov-chain random walk is performed in the  $S_z$ -basis for a given wavefunction. This allows to write the matrix element of an operator as an average taken over the random walk,

$$\frac{\langle \psi | O | \psi \rangle}{\langle \psi | \psi \rangle} = \sum_{\alpha} \frac{\langle \psi | \alpha \rangle \langle \alpha | O | \psi \rangle}{\langle \psi | \psi \rangle} = \sum_{\alpha} \frac{|\langle \psi | \alpha \rangle|^2}{\langle \psi | \psi \rangle} \frac{\langle \alpha | O | \psi \rangle}{\langle \alpha | \psi \rangle} \quad (2.10)$$

The states  $|\alpha\rangle$  and  $|\beta\rangle$  are real-space spin states ( $S_z$  eigenstates). The form (2.10) suggests a discrete probability distribution on the states  $|\alpha\rangle$ ,

$$p(\alpha) = \frac{|\langle \psi | \alpha \rangle|^2}{\langle \psi | \psi \rangle}; \quad p(\alpha) > 0; \quad \sum_{\alpha} p(\alpha) = 1 \quad (2.11)$$

Such a probability distribution can be generated by a random walk with transition probability

$$P(\alpha \rightarrow \alpha') = \min\left[1, \frac{p(\alpha')}{p(\alpha)}\right] = \min\left[1, \left|\frac{\langle \alpha' | \psi \rangle}{\langle \alpha | \psi \rangle}\right|^2\right]. \quad (2.12)$$

This transition probability satisfies the detailed balance condition and is known to generate the equilibrium distribution  $p(\alpha)$  [17, 39]. The task is now to efficiently generate a new spin configuration from a given one. I do this by picking a random site and exchange the spin or hole on this site with one on a random neighboring site of the square lattice. The projection of a fermionic wavefunction to a given electron configuration (non-magnetic, with  $N_{\uparrow} = N_{\downarrow}$ ) is a  $N_{\uparrow} \times N_{\uparrow}$  Slater determinant

$$\langle \alpha | \psi \rangle \propto \det a_{ij}. \quad (2.13)$$

In the case of a mean-field wavefunction  $|\psi\rangle = |\text{RVB}\rangle$ , the matrix  $a_{ij}$  is precisely the singlet-bond distribution function  $a(\mathbf{r})$  which appeared in the definition of the RVB wavefunction (2.3):

$$a_{ij} = a(\mathbf{r}_{i\uparrow} - \mathbf{r}_{j\downarrow}), \quad (2.14)$$

where  $\mathbf{r}_{i\uparrow}$  and  $\mathbf{r}_{j\downarrow}$  are the positions of the up and down spins, respectively, in the state  $|\alpha\rangle$ . Note that I need to choose a particular ordering of the sites  $i = 1 \dots L$ , in order to uniquely define the sign of  $\langle\alpha|\psi\rangle$ . The advantage of exchanging particles to generate a random walk becomes now apparent: The new position of an up spin amounts to replacing a row, a new position for a down spin amounts to replacing a column in the matrix  $a_{ij}$ . Using well-known formulas from linear algebra, one can efficiently calculate the new determinant in terms of the inverse matrix. By storing and updating both the matrix  $a_{ij}$  and its inverse, one can greatly improve the speed of the Monte Carlo (MC) algorithm, an idea due to Ceperley and Chester [40].

In the following, I will give an example where a MC step proposes to exchange an up spin on site  $\mathbf{r}_{i_1}$  with a hole on site  $\mathbf{r}_{i_2}$ . The sites are ordered ( $i = 1 \dots L$ ) and we need to keep track of the sign change for the determinant due to the fermionic commutation. Let  $b_n = a(\mathbf{r}_{i_2} - \mathbf{r}_n)$  where  $\mathbf{r}_n$  are the positions of the down spins. The new matrix  $\tilde{a}_{ij}$  and its determinant after the MC step are given by

$$\tilde{a}_{ij} = \begin{cases} b_j & \text{for } i = i_2, \\ a_{ij} & \text{otherwise.} \end{cases} \quad (2.15)$$

$$\frac{\det \tilde{a}_{ij}}{\det a_{ij}} = (-)^{\#(i_1, i_2)} \sum_n b_n [a^{-1}]_{ni_2}.$$

where  $\#(i_1, i_2)$  is the number of particles between sites  $i_1$  and  $i_2$ . The acceptance probability of this step is then given by (2.12), simply using the ratio of the determinants squared,  $(\det \tilde{a}_{ij} / \det a_{ij})^2$ . As already mentioned, it is therefore efficient to store and update  $a_{ij}$  as well as its inverse matrix  $[a^{-1}]_{ij}$  after every accepted MC step. The acceptance probabilities for exchanging two spins is computed analogously.

The random walk explained in the last paragraph provides a sample of states  $|\alpha\rangle$  with probability distribution  $p(\alpha)$ . The expectation value of an operator can now be computed approximately,

$$\frac{\langle\psi|O|\psi\rangle}{\langle\psi|\psi\rangle} = \sum_{\alpha} p(\alpha) \frac{\langle\alpha|O|\psi\rangle}{\langle\alpha|\psi\rangle} \simeq \sum_{\{\tilde{\alpha}\}} \frac{\langle\tilde{\alpha}|O|\psi\rangle}{\langle\tilde{\alpha}|\psi\rangle} \quad (2.16)$$

where  $\{\tilde{\alpha}\}$  denotes the generated MC sample. I estimate the error of the expectation value by its variance over different MC runs.

The generation of an MC sample for a given wavefunction is identical for all operator expectation values. The average over the MC sample (2.16), however, needs to be implemented

for each operator  $O$  that we are interested in. This is easiest for operators which are diagonal in spin space, like  $O = n_i n_j$  or  $O = S_i^z S_j^z$  etc. For example,  $n_i n_j$

$$\frac{\langle \alpha | n_i n_j | \psi \rangle}{\langle \alpha | \psi \rangle} = \begin{cases} 1 & \text{if } \mathbf{r}_i \text{ and } \mathbf{r}_j \text{ are occupied in } |\alpha\rangle, \\ 0 & \text{otherwise.} \end{cases} \quad (2.17)$$

Hopping operators of the form  $O = c_{i\sigma}^\dagger c_{j\sigma}$  are also straightforward to compute since this is very similar to the MC steps explained in (2.15):

$$\frac{\langle \alpha | c_{i\uparrow}^\dagger c_{j\uparrow} | \psi \rangle}{\langle \alpha | \psi \rangle} = \begin{cases} (-)^{\#(i,j)} \sum_n a(\mathbf{r}_j - \mathbf{r}_n) [a^{-1}]_{nj} & \text{if } \mathbf{r}_i \text{ has } \uparrow\text{-spin and } \mathbf{r}_j \text{ is empty in } |\alpha\rangle, \\ 0 & \text{otherwise.} \end{cases} \quad (2.18)$$

where  $\#(i, j)$  is the number of occupied sites between site  $i$  and  $j$ , and  $\mathbf{r}_n$  are the positions of the  $\downarrow$ -spins in  $|\alpha\rangle$ .

In this thesis, I also compute *off-diagonal* matrix elements between a wavefunction projected to different particle numbers,

$$\langle N-2 | c_{i\uparrow} c_{j\downarrow} | N \rangle. \quad (2.19)$$

I am assuming here a wavefunction  $|\psi\rangle$  where the particle number is fluctuating, and  $|N\rangle = P_N |\psi\rangle$ . The main difficulty is to compute the correct normalization of this expectation value. It is easier to normalize it to the wavefunction with *higher* particle number,

$$\frac{\langle N-2 | c_{i\uparrow} c_{j\downarrow} | N \rangle}{\langle N | N \rangle} \simeq \sum_{\{\tilde{\alpha}\}} \frac{\langle N-2 | c_{i\uparrow} c_{j\downarrow} | \tilde{\alpha} \rangle}{\langle N | \tilde{\alpha} \rangle}. \quad (2.20)$$

This matrix element is just the ratio between a determinant with one row and one column *removed*, and the determinant. Using again linear algebra, I get

$$\frac{\langle N-2 | c_{i\uparrow} c_{j\downarrow} | \alpha \rangle}{\langle N | \alpha \rangle} = \begin{cases} [a^{-1}]_{ji} & \text{if } \mathbf{r}_i \text{ has } \uparrow\text{-spin and } \mathbf{r}_j \text{ has } \downarrow\text{-spin in } |\alpha\rangle, \\ 0 & \text{otherwise.} \end{cases} \quad (2.21)$$

In order to compute the same expectation value with normalization to the wavefunction with lower particle number, I need to sample the wavefunction  $|N-2\rangle$  instead,

$$\frac{\langle N | c_{j\downarrow}^\dagger c_{i\uparrow}^\dagger | N-2 \rangle}{\langle N-2 | N-2 \rangle} \simeq \sum_{\{\tilde{\alpha}'\}} \frac{\langle N | c_{j\downarrow}^\dagger c_{i\uparrow}^\dagger | \tilde{\alpha}' \rangle}{\langle N-2 | \tilde{\alpha}' \rangle}. \quad (2.22)$$

In this case, the matrix element is the ratio between a determinant with one row and one column *added*, and the determinant. To compute this, I expand the determinant in the numer-



ator and get

$$\frac{\langle N|c_{j\downarrow}^\dagger c_{i\uparrow}^\dagger|\alpha\rangle}{\langle N-2|\alpha\rangle} = \begin{cases} \sum_{n,m} a(\mathbf{r}_i - \mathbf{r}_n)a(\mathbf{r}_m - \mathbf{r}_j)[a^{-1}]_{mn} & \text{if } |\alpha\rangle \text{ has a hole at } \mathbf{r}_i \text{ and } \mathbf{r}_j \\ 0 & \text{otherwise.} \end{cases} \quad (2.23)$$

The correctly normalized expectation value is then given by the product of these matrix elements<sup>4</sup>

$$\left| \frac{\langle N-2|c_{i\uparrow}c_{j\downarrow}|N\rangle}{\sqrt{\langle N|N\rangle\langle N-2|N-2\rangle}} \right|^2 = \frac{\langle N-2|c_{i\uparrow}c_{j\downarrow}|N\rangle}{\langle N|N\rangle} \frac{\langle N|c_{j\downarrow}^\dagger c_{i\uparrow}^\dagger|N-2\rangle}{\langle N-2|N-2\rangle}. \quad (2.24)$$

Finally, let me note that one can greatly reduce the MC error bars on these expectation values or reduce the simulation time by taking advantage of lattice symmetries. For example, using the translational invariance of the wavefunction, I can write  $\langle n_i n_j \rangle = \frac{1}{L} \sum_q \langle n_{i+q} n_{j+q} \rangle$  which provides  $L$  independent measurements in a single MC walk.

In conclusion, variational Monte Carlo is a numerical method which allows to compute various static correlations in a given wavefunction within small error bars. In Chapter 3, I will present and discuss new results that I obtained within the VMC method.

---

<sup>4</sup>This expectation value may be used as a superconducting order parameter. I will discuss it in the next chapter in more detail. As a by-product of this computation, one can obtain the number  $\frac{\langle N|N\rangle}{\langle N-2|N-2\rangle}$  which is relevant for understanding the particle-number renormalization by the Gutzwiller projector in a grand-canonical wavefunction [41].

### 2.1.3. Gutzwiller approximation

Although VMC provides a scheme to compute static correlations in Gutzwiller-projected RVB wavefunctions to a high precision, it is still a computationally demanding numerical tool. Furthermore, VMC is not able to give any *dynamical* or *temperature dependent* information. For this reason, we may resort to an analytical tool for RVB wavefunctions: the Gutzwiller approximation (GA) [5, 26].

The GA replaces the Gutzwiller projector in the expectation values by a renormalization with a statistical weight factor. Let  $|\psi_0\rangle$  be an unprojected mean-field wavefunction containing states with doubly occupied sites. Using GA, we write the expectation value of an operator  $O$  as

$$\frac{\langle\psi_0|P_d O P_d|\psi_0\rangle}{\langle\psi_0|P_d|\psi_0\rangle} \simeq g_O \frac{\langle\psi_0|O|\psi_0\rangle}{\langle\psi_0|\psi_0\rangle}. \quad (2.25)$$

The Gutzwiller renormalization factor  $g_O$  for the operator  $O$  is obtained by comparing the dimension of the Hilbert space contributing to the processes in the Gutzwiller-projected and the unprojected wavefunction, respectively.

Consider for example the hopping operator  $O = c_{i\uparrow}^\dagger c_{j\uparrow}$ . In the projected Hilbert space, the probability for such a hopping process is

$$\sim \sqrt{\bar{n}_{j\uparrow}(1 - \bar{n}_i)\bar{n}_{i\uparrow}(1 - \bar{n}_j)} \quad (2.26)$$

where  $\bar{n}_i = \langle\psi_0|P_d n_i P_d|\psi_0\rangle$ . On the other hand, in the unprojected Hilbert space, the same probability is

$$\sim \sqrt{\bar{n}_{j\uparrow}^0(1 - \bar{n}_{i\uparrow}^0)\bar{n}_{i\uparrow}^0(1 - \bar{n}_{j\uparrow}^0)} \quad (2.27)$$

with  $\bar{n}_{i\uparrow}^0 = \langle\psi_0|n_{i\uparrow}|\psi_0\rangle$ . The Gutzwiller factor is then written as

$$g_t = \frac{\sqrt{\bar{n}_{j\uparrow}(1 - \bar{n}_i)\bar{n}_{i\uparrow}(1 - \bar{n}_j)}}{\sqrt{\bar{n}_{j\uparrow}^0(1 - \bar{n}_{i\uparrow}^0)\bar{n}_{i\uparrow}^0(1 - \bar{n}_{j\uparrow}^0)}}. \quad (2.28)$$

Considering homogenous and non-magnetic wavefunctions ( $\bar{n}_{i\uparrow} = \bar{n}_{j\downarrow} = \frac{\bar{n}}{2}$ ; which is the case for the wavefunctions considered in this thesis) and assuming that  $\bar{n}_i = \bar{n}_i^0$ , we obtain the well-known result

$$g_t = \frac{1 - \bar{n}}{1 - \bar{n}/2} = \frac{2x}{1 + x}. \quad (2.29)$$

Note that  $g_t$  renormalizes all square operators like  $c^\dagger c$  as well as operators of the form  $c_\uparrow c_\downarrow$ , like (2.5) or (2.19). The Gutzwiller approximation in a grand-canonical wavefunction with

fluctuating particle number is more complicated and becomes particularly problematic in the half-filled limit where the condition  $\bar{n} = \bar{n}^0$  requires careful inspection [5, 41, 42, 43, 44].

The Gutzwiller renormalization factor for the spin-exchange term  $O = \mathbf{S}_i \cdot \mathbf{S}_j$  can be computed in a similar way. For  $S_i^+ S_j^-$  the probability for processes in the projected space is

$$\sim \sqrt{\bar{n}_{i\downarrow} \bar{n}_{j\uparrow} \bar{n}_{j\downarrow} \bar{n}_{i\uparrow}} \quad (2.30)$$

and for the unprojected space it is

$$\sim \bar{n}_{i\downarrow}^0 (1 - \bar{n}_{j\uparrow}^0) \bar{n}_{j\downarrow}^0 (1 - \bar{n}_{i\uparrow}^0). \quad (2.31)$$

For a wavefunction with spin-rotation symmetry,  $S_i^z S_j^z$  has clearly the same renormalization factor. Under the same assumptions as before, the renormalization factor for the spin-exchange term is given by

$$g_S = \frac{\sqrt{\bar{n}_{i\downarrow} \bar{n}_{j\uparrow} \bar{n}_{j\downarrow} \bar{n}_{i\uparrow}}}{\bar{n}_{i\downarrow}^0 (1 - \bar{n}_{j\uparrow}^0) \bar{n}_{j\downarrow}^0 (1 - \bar{n}_{i\uparrow}^0)} = \frac{1}{(1 - \bar{n}/2)^2} = \frac{4}{(1 + x)^2}. \quad (2.32)$$

The Gutzwiller approximation (or more refined versions of it, see e.g. Refs. [42, 43, 45]) may now be used to compute the same static correlations as VMC is able to compute exactly. A more advanced application of the Gutzwiller approximation is the so-called *renormalized mean-field theory* (RMFT) of the  $t$ - $J$  model [26] where the Gutzwiller projectors in the  $t$ - $J$  Hamiltonian are directly replaced by Gutzwiller-renormalization factors,

$$H_{\text{RMFT}} = -gt \sum_{\langle i,j \rangle, \sigma} c_{i\sigma}^\dagger c_{j\sigma} + g_S J \sum_{\langle i,j \rangle} [\mathbf{S}_i \cdot \mathbf{S}_j - \frac{n_i n_j}{4}]. \quad (2.33)$$

As one is working in the unprojected Hilbert space now, the model can be treated by conventional means, e.g. by a self-consistent mean-field decoupling (hence the name RMFT).

## 2.2. Quantum dimer models

### 2.2.1. Introduction

The quantum dimer model (QDM) on the triangular lattice is a further approach that I use in this thesis. The aim of QDMs is to consider low-energy effective models for spin- $\frac{1}{2}$  antiferromagnets. The usual starting point for calculations with Heisenberg systems are the eigenstates of the  $S_i^z$  operators. However, as I discussed earlier in this chapter, under certain circumstances (like geometric frustration or doping) this may not be the best starting point. An alternative to the  $S^z$  eigenstates is provided by the *valence bond* states (see Section 2.1), as proposed by Anderson [12, 46, 47].

After Anderson’s publication on the cuprates in 1987 [12], the research on RVB theory split into two branches. The first direction was mainly motivated by the observation that a projected  $d$ -wave superconductor is the most competitive variational state for the  $t$ - $J$  model on the square lattice [27, 28]. The  $d$ -wave superconductor has gapless points in the spectrum (nodal points) and the singlet amplitude  $a_{\mathbf{k}} = \frac{v_{\mathbf{k}}}{u_{\mathbf{k}}}$  is not analytic at these nodal points. The corresponding amplitude  $a(\mathbf{r})$  is expected to be long-range and so are various correlation functions [48, 49]. This line of research is sometimes summarized under the name of *algebraic spin liquids*. The second branch of research considered RVB wavefunctions which have exponentially short-range singlet bonds, in particular only nearest-neighbor valence bonds,  $a(\mathbf{r}_{nn}) = \pm 1$  and  $a(\mathbf{r})_{|\mathbf{r}|>0} = 0$ . This second type of RVB wavefunctions can be investigated with the help of quantum dimer models.

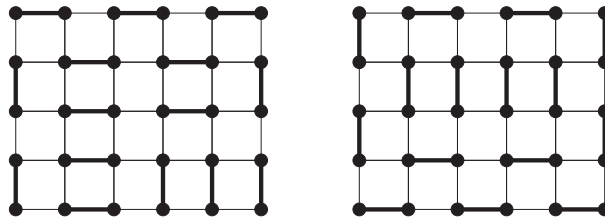


**Figure 2.3.:** Two examples of short-range (nearest-neighbor) close-packed dimer coverings of a square lattice.

A short-range valence-bond spin state of the form<sup>5</sup>  $\prod_{(i,j)} b_{ij}^\dagger |0\rangle$  may be defined by pairing nearest-neighbor sites on a lattice (paired sites = dimers; bold bars in Fig. 2.3). We call such a configuration a *close-packed covering of a lattice by hardcore dimers*. “Close-packed”, because we do not allow empty sites (= holes or monomers) and “hardcore”, because two dimers are not allowed to cover the same lattice site. The spin state corresponding to a dimer

<sup>5</sup>The operator  $b_{ij} = \frac{1}{\sqrt{2}}[c_{i\downarrow}c_{j\uparrow} - c_{i\uparrow}c_{j\downarrow}]$  was introduced in Section 2.1.

covering  $c$  is

$$|\psi_c\rangle = \prod_{(i,j) \in c} b_{ij}^\dagger |0\rangle, \quad (2.34)$$

where the product is over all pairs of sites  $(i, j)$  which are connected by a dimer in  $c$ . These states are normalized,  $\langle \psi_c | \psi_c \rangle = 1$ , but not orthogonal in general. The relation between two dimer coverings can be characterized by their *transition graph*, i.e. their superposition on the lattice. The transition graph of the dimer coverings in Fig. 2.3 is shown in Fig. 2.4. It is obvious that the transition graph of two close-packed dimer coverings consists of closed loops. One can show [50] that the overlap between the corresponding spin states of two close-packed dimer coverings  $c$  and  $c'$  is related to their transition graph by

$$\langle \psi_c | \psi_{c'} \rangle = \pm 2^{\sum_u (1 - l_u)} \quad (2.35)$$

where the sum is over all loops  $u$  in the transition graph and  $l_u$  is the length (number of sites) of the loop.

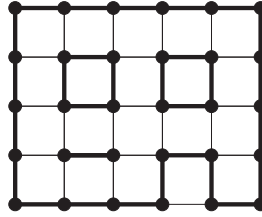


**Figure 2.4.:** The transition graph for the dimer coverings shown in Fig. 2.3. For close-packed dimers, the transition graph consists of closed non-intersecting loops on the lattice.

The dimension of the singlet subspace for  $N$  spins is  $\frac{N!}{(N/2)!(N/2+1)!} \simeq 2^N$  as  $N \rightarrow \infty$  [51]. The number of dimer coverings on a large square lattice with  $N$  sites is<sup>6</sup>  $e^{\frac{G}{\pi}N} \simeq (1.339)^N$  [72]. We see that the space of nearest-neighbor valence-bond (VB) states is considerably smaller than the singlet subspace. Using this valence-bond basis to construct a meaningful low-energy effective Hamiltonian is therefore a strong statement about the spin model (much stronger than the restriction to the singlet sector). A family of spin models which have valence-bond states as exact eigenstates were constructed by Klein [52]. However, the Klein models have complicated interactions and seem relatively far from a simple Heisenberg model on the square or triangular lattice. One may still hope that frustration introduced by further-neighbor interactions, lattice distortions, or weak hole doping stabilizes VB- or RVB-type states.

A realistic spin model which may possess an RVB ground state is the strongly frustrated *Kagomé lattice* antiferromagnet [53, 54]. The recent discovery of *Herbertsmithite*, a material believed to be described by an almost perfect Heisenberg antiferromagnet on the Kagomé lattice, has renewed the interest in this model [55]. However, from recent variational calculations,

<sup>6</sup> $G = 1^{-2} - 3^{-2} + 5^{-2} - \dots$  is *Catalan's constant*.

the RVB ground state is believed to be of algebraic type, i.e. with long-range singlets [56]. Note that it is still far from established if the proposed state captures the true nature of the Kagomé Heisenberg system.

Apart from their usefulness to illustrate fundamental theoretical concepts, proposals have been made to engineer QDMs in mesoscopic devices with the help of Josephson junctions. An interesting application of such devices would be fault-tolerant q-bits in quantum computing [57].

### 2.2.2. Topological degeneracy and topological order

A reason for the interest in quantum dimer models is their capacity to illustrate the relatively novel concept of *topological order*. Traditionally, the different phases of matter are characterized in terms of local order parameters. This viewpoint, pioneered by Landau, has been extremely successful in many branches of physics (e.g. condensed matter, statistical physics, elementary particles, etc.) and forms the basis of the theory of critical phenomena [58]. However, there are examples of phases which cannot be characterized by a local order parameter. The states which appear in the fractional quantum Hall system are such examples. These phases are generally liquid states with gapped excitations. In the absence of a local order parameter, the phase may be characterized by *topological order* as it was suggested by Wen [59, 60]. Apart from the fractional quantum Hall system, no topological phase has been experimentally realized and unambiguously identified in solid state physics. Quantum dimer models are reasonably close to realistic spin systems, yet relatively simple to solve and, most importantly, topological order can rigorously be shown to exist in some cases. QDMs are therefore highly interesting *toy models* to study these topological phases in a wider context of solid state physics.

One characteristic of a topologically ordered phase is that the ground state degeneracy depends on the genus of the underlying space on which the model is defined (the model on e.g. a sphere, torus, cylinder, etc. has a different number of degenerate ground states) [61, 62]. To have topological order, one requires furthermore that (i) the degenerate ground states are all orthogonal and (ii) the ground-state expectation value of any local order parameter is identical in each topological sector (i.e. not only the Hamiltonian, but no local order at all can distinguish between the degenerate ground states) [48, 63].

### 2.2.3. The square-lattice Rokhsar-Kivelson quantum dimer model

The quantum dimer model (QDM) was first formulated by Rokhsar and Kivelson (RK) in their seminal work of 1988 [64]. In this model, the Hilbert space is spanned by dimer coverings which are defined to be orthogonal. Such orthogonal states may formally be constructed for spin models, but here I leave out these details and instead refer to the original work. Let  $c$  denote a (classical) dimer covering. The corresponding vector  $|c\rangle$  satisfies

$$\langle c|c'\rangle = \delta_{cc'}. \quad (2.36)$$

The Hamiltonian in this Hilbert space is defined as

$$H_{\text{RK}} = \sum_{\text{plaquettes}} -J[|\square\rangle\langle\square| + |\square\rangle\langle\square|] + v[|\square\rangle\langle\square| + |\square\rangle\langle\square|]. \quad (2.37)$$

The operator

$$|\square\rangle\langle\square| + |\square\rangle\langle\square|, \quad (2.38)$$

acting on a plaquette (elementary square) of the lattice, returns zero if the plaquette has no parallel dimers; if the plaquette has parallel dimers, then they are rotated by 90 degrees (it “flips” the plaquette). The operator

$$|\square\rangle\langle\square| + |\square\rangle\langle\square| \quad (2.39)$$

returns zero if there are no parallel dimers on the plaquette, and it acts as identity on plaquettes with parallel dimers (the plaquette is “flippable”). As a result, the operator in (2.37) proportional to  $v$  counts the number of flippable plaquettes.

The physical motivation behind the model (2.37) in the framework of Anderson’s RVB construction is the following [64, 65]: a dimer represents two electrons in a real-space Cooper pair. These “pre-formed” pairs may or may not condense. In the close-packed limit, when all sites are occupied by a dimer, the system is insulating. If the dimers are in a liquid phase, it is expected to capture the pseudogap phase of the cuprates. The alternative possibility is that the dimers order and form a crystal. When the density of dimers is reduced and unpaired sites are introduced, then the system becomes conducting. It may even become superconducting if the pairs condense.

At the *RK point* in parameter space, defined by  $J = v > 0$ , the ground state of (2.37) is known exactly. It is the prototype of a short-range RVB (sRVB) wavefunction: the equal-weight superposition of all dimer coverings

$$|\text{sRVB}\rangle = \frac{1}{\sqrt{N_0}} \sum_c |c\rangle \quad (2.40)$$

where  $N_0$  is the total number of coverings. A formal proof may be given by noting that the RK Hamiltonian (2.37) can be written as a sum of (non-commuting) projection operators,

$$H_{\text{RK},J=v} = J\sqrt{2} \sum_{\text{plaquettes}} P_{\square} \quad (2.41)$$

where

$$P_{\square} = \frac{1}{\sqrt{2}} [|\square\rangle - |\square\rangle][\langle\square| - \langle\square|] \quad (2.42)$$

projects to the subspace with parallel dimers on the plaquette superposed with a phase shift  $\pi$ . The eigenvalues of a sum of projectors are clearly non-negative. Applied to the state  $|\text{sRVB}\rangle$ , these projectors all give zero which establishes that  $|\text{sRVB}\rangle$  is a ground state of  $H_{\text{RK},J=v}$ . There are ground state degeneracies, but I defer their discussion to the triangular-lattice quantum dimer model.

There is a lot more to say about the square-lattice quantum dimer model. I will restrict here to some key results only. While very little is known about finite-temperature properties, we have a relatively complete picture of the zero-temperature  $J$ - $v$  phase diagram. In the limit  $\frac{v}{J} \rightarrow -\infty$ , the ground state is a maximally flippable state, the so-called *columnar* state (Fig. 2.5a). In the other limit,  $\frac{v}{J} \rightarrow +\infty$ , the ground state has the minimal number of flippable plaquettes, the so-called *staggered* state (Fig. 2.5c). The ground states for intermediate

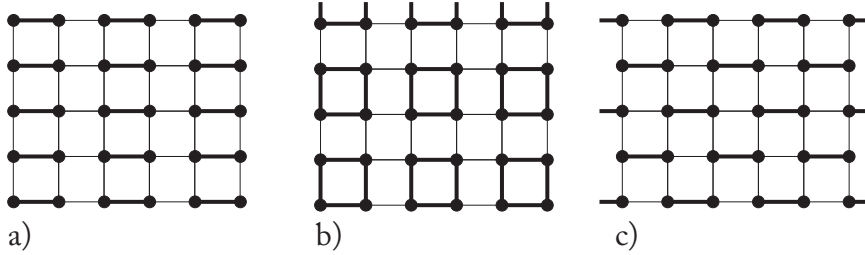


**Figure 2.5.:** a) Columnar dimer state [ $v \rightarrow -\infty$ ], b) plaquette phase [ $0.6J \lesssim v < J$ ], and c) staggered dimer state [ $v > J$ ].

values of  $\frac{v}{J}$  are only known for finite lattices from quantum and Green's function Monte Carlo simulations, exact diagonalization studies [66, 67, 68], and mapping to field theories close to the RK point [69, 70, 71]. These studies suggest an intermediate *plaquette phase* for  $0.6 \lesssim \frac{v}{J} < 1$  where parallel dimers resonate on one out of four plaquettes (Fig. 2.5b).



### 2.2.4. Static and dynamical correlation functions at Rokhsar-Kivelson points

The very special form of the ground state at the RK point as an equal-weight superposition of all dimer coverings facilitates the computation of certain zero-temperature correlation functions. For example, the static correlations for an operator which is diagonal in the dimer basis is

$$\langle sRVB|O|sRVB\rangle = \frac{1}{N_0} \sum_{c,c'} \langle c|O|c'\rangle = \frac{1}{N_0} \sum_c O_c. \quad (2.43)$$

This is simply a correlation function in the classical statistical mechanics of dimer coverings where all coverings have identical weight.

The classical dimer problem on the square lattice has been solved exactly [72, 73], e.g. the dimer-dimer correlation functions are known. For the square lattice, the dimer correlation functions decay algebraically at large distance. This gives further support to the idea that the RK point is a quantum critical point between two ordered phases [74]. On field-theoretic grounds, one expects to find gapless excitations in such a phase. This expectation can be proven to be exact [64, 75]. These results are, however, disappointing from the point of view of a topological RVB liquid. Despite its liquid character and short valence bonds, the square lattice QDM does not provide an example of such a topological phase, at least in its simplest form. For this reason, the search for topological phases concentrated on QDMs on non-bipartite lattices, in particular on the triangular lattice which I will consider next.

Due to the special form of the Hamiltonian (2.37) at the RK point as a sum of projectors, the dynamical correlation functions in imaginary time can be mapped to correlation functions in a classical stochastic process. These correlation functions can then be computed efficiently with classical Monte Carlo algorithms [69, 76, 77, 78, 93].

### 2.2.5. The triangular-lattice Rokhsar-Kivelson quantum dimer model and topological sectors

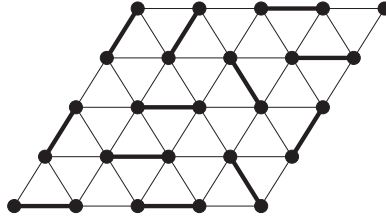


**Figure 2.6.:** A typical dimer covering of the triangular lattice.

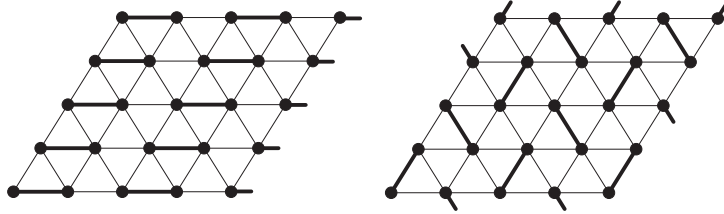


**Figure 2.7.:** Crystalline phases on the triangular lattice. Left: columnar state with maximal number of flippable plaquettes for  $\frac{v}{J} \rightarrow -\infty$ . Right: staggered state with no flippable plaquettes for  $\frac{v}{J} \rightarrow +\infty$ .

Analogously to the square-lattice QDM, the model can be defined on the triangular (or any other) lattice. A typical dimer covering on the triangular lattice is given in Fig. 2.6. Again, we define a minimal quantum Hamiltonian on the space spanned by the dimer coverings, Eq. (2.44). The first term in the Hamiltonian flips parallel dimers on each plaquette of the lattice, the second one counts the plaquettes with parallel dimers. The plaquettes on this lattice are three types of rhombi: right-, up-, and left-pointing.

$$H_{\text{RK}} = \sum_{\nabla, \hat{\sigma}, \Delta} -J[|\Delta\rangle\langle\Delta| + |\hat{\sigma}\rangle\langle\hat{\sigma}|] + v[|\Delta\rangle\langle\Delta| + |\hat{\sigma}\rangle\langle\hat{\sigma}|]. \quad (2.44)$$

Similar to the square lattice, one can prove that the ground state at the RK point ( $J = v$ ) is given by the analog sRVB wavefunction (2.40). The ground state for  $\frac{v}{J} \rightarrow -\infty$  and  $\frac{v}{J} \rightarrow +\infty$  are again crystalline phases, columnar in the first limit and staggered in the second (Fig. 2.7). An intermediate ordered phase with large unit cell (christened “ $\sqrt{12} \times \sqrt{12}$ -phase” by Moessner and Sondhi) was found numerically in the vicinity of  $v \simeq 0$  [79, 80].

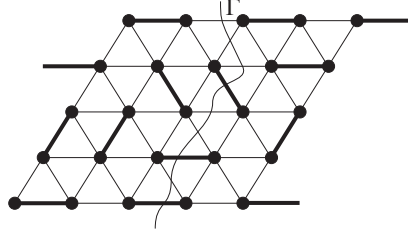


**Figure 2.8.:** A dimer covering on a  $4 \times 4$  lattice with periodic boundary conditions in both directions. The simple closed path  $\Gamma$  winds once around the torus and defines the operator  $\nu_\Gamma = (-1)^{\#\text{ of dimers intersecting } \Gamma}$ .

Let us briefly discuss an important symmetry of this model. Consider a particular dimer covering on, say, a torus (periodic boundary conditions in both space directions). Let us draw a simple closed path  $\Gamma$  which winds once around the torus and which does not cross lattice sites (Fig. 2.8). Consider the number of dimers  $N_\Gamma$  that intersect the path  $\Gamma$ . The operator

$$\nu_\Gamma = (-1)^{N_\Gamma} \quad (2.45)$$

commutes with the Hamiltonian (2.44) and represents therefore a conserved quantity. This is easy to understand since a flipping process of the Hamiltonian can change the number of dimers intersecting  $\Gamma$  in Fig. 2.8 by two only.

Are there as many independent conserved quantities  $\nu_\Gamma$  as there are closed paths  $\Gamma$ ? The answer is of course no. Once a closed path  $\Gamma$  is chosen, it is easy to see that deforming it continuously (i.e. by gluing closed paths which are topologically trivial) only changes the sign of the operator  $\nu_\Gamma$ :

$$\nu_{\Gamma+\Gamma'} = (-1)^{\#\text{ of sites enclosed by } \Gamma'} \nu_\Gamma. \quad (2.46)$$

As a result, we see that there are as many independent conserved quantities  $\nu$  as there are nontrivial closed paths for the topological space on which the dimer model is defined. In the case of a torus, there are two such paths. On a sphere there are none, on a cylinder one, etc. The eigenspaces of the operator  $\nu_\Gamma$  are called *topological sectors*. The triangular-lattice QDM on a torus has four topological sectors.

The presence of topological sectors gives us important information about the ground state degeneracy at the RK point. For the triangular QDM on the torus, the sRVB ground-state wavefunction (2.40) can be replaced by four orthogonal and degenerate ground states,

$$|\text{sRVB}, i\rangle = \frac{1}{\sqrt{N_0^i}} \sum_{c \in V_i} |c\rangle, \quad (2.47)$$

where the sum goes only over the basis vectors spanning the topological sector  $i$ . This degeneracy is one property of a topologically ordered phase. However, it is not a sufficient

condition, one also has to show that all other correlations are independent of the sector. At the RK point, analytical methods are available to compute the correlation functions of the triangular-lattice QDM and topological order has been proven to exist [63, 79]. Furthermore, a finite correlation length for dimer-dimer correlations has been found, which fits well into the phenomenology of a topological liquid. Efficient Monte Carlo methods can be used to study excitations and a gapped spectrum was found [76, 77]. More involved numerical techniques have shown that the ground state is in a topological phase for some extended parameter range  $0.8 \lesssim \frac{v}{J} \leq 1$ . For  $\frac{v}{J} > 1$ , the staggered phase immediately sets in [80].

### 2.2.6. Topological excitations in the dimer liquid

In the last section, I have shown that the ground state in the topological phase of the triangular-lattice QDM is relatively well known. At this point, the natural question arises about the excitations in this state. The exact low-lying eigenstates are not known, but can we understand them at least variationally? Read and Chakraborty [81] and RK [65, 82] have argued that the gapped excitation of such a liquid must be a *topological defect*, i.e. a twist in the phase of the ground state wavefunction.<sup>7</sup> Indeed, this nicely fits in with the field-theoretic scenario of electron fractionalization in the pseudogap phase of the cuprates by Senthil and Fisher [85]. In the Senthil-Fisher proposal, the physical electron splits into a spin- $\frac{1}{2}$  and a spinless charge degree of freedom (the spinon and the holon) which interact via a discrete  $Z_2$  gauge field. This is the analog to one-dimensional models where spin-charge separation is known to occur [24]. Consider now the topological dimer liquid as an effective model for such a  $Z_2$  lattice gauge theory in two dimensions (in its *deconfined phase* where the fractionalization actually takes place [74, 86]). In the dimer model, the spinon mass is assumed to be infinite because this excitation would break a dimer. Apart from the holon excitation, which may be mimicked by introducing *monomers* into the dimer model, there is only the gauge degree of freedom left. The massive excitation in a pure gauge theory without matter fields is a vortex. The vortex in the  $Z_2$  gauge theory is the analog to the topological defect in the QDM. This  $Z_2$ -vortex was baptized *vison* by Senthil-Fisher. I will use the same terminology for the dimer analog.

The vison in the QDM is constructed in the following way [63, 76, 81]. Consider the path  $\Gamma$  that we used to construct the topological sectors, but now terminate it on a plaquette (Fig. 2.9). Of course, on a compact surface there is always a second end of the path. This open path is the precise analog to the string used by Dirac to construct the magnetic monopole [87]. For a single monopole, the Dirac string has to go to infinity (or to terminate at the boundary, for a finite system). On a compact space, monopoles can only exist in pairs.

---

<sup>7</sup>It is interesting to keep in mind a historical motivation for the topological excitation: Read and Chakraborty constructed this excitation for the short-range RVB state on a square lattice. Marshall's sign rule [83] for the ground state of a bipartite Heisenberg model [46, 84] in the presence of a single hole naturally calls for such a phase twist in the wavefunction.

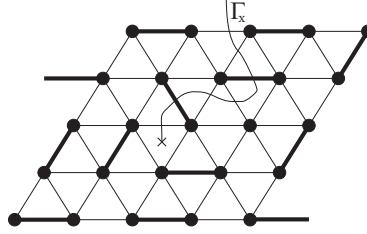


**Figure 2.9.:** The vison-string  $\Gamma_x$  defines the vison operator  $V_x = (-1)^{\# \text{ dimers intersecting } \Gamma_x}$ . The operator  $V_x$  lives on the dual lattice (plaquettes).

The vison operator is defined as

$$V_x = (-1)^{\# \text{ dimers intersecting } \Gamma_x} \quad (2.48)$$

where  $\Gamma_x$  is an open path starting at plaquette  $x$  and going to a reference plaquette. The location of the reference plaquette depends on the boundary condition of the system (it is at the boundary for a finite system, at infinity for the infinite system, or some arbitrary plaquette for a compact system). The corresponding two-vison operator,

$$V_{\Gamma(x,y)} = V_x V_y, \quad (2.49)$$

does not depend on the boundary conditions. Furthermore, it is again obvious that a continuous deformation of the path  $\Gamma(x,y)$ , keeping the endpoints  $x$  and  $y$  fixed, only changes the sign of the operator by the parity of the number of sites crossed,

$$V_{\Gamma'(x,y)} = (-1)^{\# \text{ of sites between } \Gamma \text{ and } \Gamma'} V_{\Gamma(x,y)}. \quad (2.50)$$

It is clear that there is an arbitrariness in the sign of the vison operator for each position on the dual lattice  $x$ . This arbitrariness can be removed by choosing a reference dimer covering and multiplying the vison operator in definition (2.48) by the corresponding value in the reference state [76]. In this way, the vison operator  $V_x$  is displaying the parity of the number of loops in the overlap graph between the dimer covering and the reference covering that wrap around  $x$ . The choice of a reference covering may be called *fixing a  $Z_2$  gauge*, in analogy with the corresponding lattice gauge theory.

The vison operator creates a state which has the physical properties we expect from a vortex. Suppose we break a dimer located far away from the vison into two spinons. Then we move one of the spinons in a large circle around the vison by rearranging the dimers with local moves. After the rearrangement, we pair up the two spinons again into a dimer. During this process, a new loop in the overlap graph between the states before and after the move is created and the wavefunction acquires a sign. For a system containing many visons, the sign only changes if there is an odd number of visons inside the circle.

The state created by applying the vison operator to the ground state,

$$|\text{vison}, x\rangle = V_x |\text{sRVB}\rangle, \quad (2.51)$$

is not a true eigenstate of the RK Hamiltonian. However, it is orthogonal to the ground state and has the desired properties of a vortex. To obtain an exact excitation, the variational state (2.51) should be modified in the vicinity of the vison center  $x$ . However, the global properties of this wavefunction are correct. An important point is that such a *visonlike* excitation cannot be deformed to a local (non-visonlike) excitation by any local rearrangement of dimers. The energy of both types of excitations (non-visonlike and visonlike) can be probed at the RK point by computing the appropriate dynamical correlation functions with classical Monte Carlo [69]. It was found by Ivanov that the gap to visonlike excitations is smaller than the one to non-visonlike excitations [76]. The obtained vison gap is  $\sim 0.1v$ , in accordance with earlier predictions [57], and it was recently confirmed in Ref. [77].

### 2.2.7. Doping quantum dimer models

In the context of the RVB construction, it is very interesting to consider the other degrees of freedom of the  $Z_2$  gauge theory: the spinon and the holon. Is the original intuition of RK correct and do additional holons lead to a condensed superconducting state?

There has recently been renewed interest in quantum dimer-monomer models [88, 89, 90, 91, 92, 93]. Let me just note that two test-monomers are found to be confined in the square-lattice model. However, they are indeed found to be deconfined in the liquid phase of the triangular-lattice QDM [88, 79]. Introducing dynamical holes with the simplest hopping process generically leads to phase separation between crystalline and liquid regions. Interestingly, a uniform superfluid phase was found on the triangular lattice in some region of the RVB phase,  $v \lesssim J$  [92].

The topological sectors for a quantum dimer model can still be defined in the presence of static holes. The operator  $\nu_\Gamma$ , Eq. (2.45), can be defined as before, but the effect of a continuous deformation of the path  $\Gamma$  needs to be adapted. As a consequence, topological defects are present in the system. Energetic considerations for the corresponding spin models suggest that static holes may form bound states with a vortex in some cases [81, 84].

Vortex excitations in the presence of mobile holes pose technical difficulties. As soon as the hole is mobile, the topological sectors get mixed by the dynamics and  $\nu_\Gamma$  is not conserved anymore. As a consequence, it is difficult to define topological defects in such a situation. However, progress can be made in the case of a small hopping amplitude of the hole. The dispersion of a slow hole is strongly affected by the presence of a bound vortex [93], as I will show in Chapter 4.

## Chapter 3.

# Strongly correlated superconductors and their electronic properties

### 3.1. Introduction

In Chapter 2, I have introduced several techniques which can be used to attack the difficult problem of doped Mott insulators. In this chapter, I analyze the problem in the context of the experimental probe of angle-resolved photoemission spectroscopy (ARPES). I apply and extend these theoretical techniques, in order to make progress in the understanding of the spectral properties in the framework Anderson's RVB approach to doped Mott insulators.

The studies starting from Anderson's wavefunctions are intrinsically variational. It may therefore seem difficult to make statements about spectral properties (i.e. about excitations) in such a variational framework. However, in this thesis I am mainly interested in the properties of *low-lying excitations*. At low temperature, the experimentally accessible properties are dominated by such excitations. If translation in space is a symmetry of the Hamiltonian, we may construct variational wavefunctions with a given momentum and minimize its energy. The result is a genuine low-lying variational excitation (as long as it is orthogonal to the variational ground state).

#### 3.1.1. Key experimental technique: angle-resolved photoemission spectroscopy

Angle-resolved photoemission spectroscopy (ARPES) is an experimental technique which has been developed to a high perfection during the last 20 years [29, 30]. In the early years of ARPES, not all experimental results were reproducible. However, the intense effort of the community has improved methods and sample quality to an impressive degree. The popularity of this technique, which is now used by many research groups around the world, is due to its ability to provide momentum-resolved information about the electronic excitations in the solid. Furthermore, ARPES is particularly appropriate to study layered, quasi-two-

dimensional structures which explains the large interest in this technique after the discovery of HTSC.

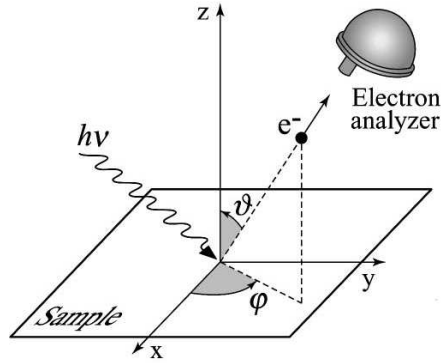


**Figure 3.1.:** The principle of angle-resolved photoemission spectroscopy: An incident photon with energy  $\hbar\nu$  knocks out a valence electron from the surface of the sample. The detected intensity of ejected electrons is proportional to the single-particle spectral function. Picture taken from [30].

Under certain assumptions (mainly the so-called *sudden approximation* in the *step models*, see [29, 30] for details), the intensity of ejected electrons measured in photoemission experiments (see Fig. 3.1) is given by

$$I(\mathbf{k}, \omega) = I_0(\mathbf{k}, \nu) f(\omega) A_\beta(\mathbf{k}, \omega) \quad (3.1)$$

where  $\mathbf{k}$  is the two-dimensional momentum of the electron parallel to the sample surface.  $\omega$  is the energy of the electron with respect to the Fermi energy.  $I_0$  is a kinematic factor which depends on the momentum of the electron, but also on the polarization and frequency of the incident photon. There are experimental methods to remove this factor (normalization to the spectra in a different phase, explicit calculation, selection rules, etc.) which I will not discuss here. The function

$$f(\omega) = \frac{1}{1 + e^{\beta\omega}} \quad (3.2)$$

is the Fermi-Dirac distribution. At zero temperature ( $T = \beta^{-1} \rightarrow 0$ ), photoemission only probes the occupied states with  $\omega < 0$ .  $A_\beta(\mathbf{k}, \omega)$  is the single-particle spectral function, defined as the imaginary part of the retarded Green's function. At zero temperature, it is given



by [29, 30, 95, 96, 97]

$$\begin{aligned}
A(\mathbf{k}, \omega) &= -\frac{1}{\pi} \text{Im} G(\mathbf{k}, \omega + i0^+) \\
&= -\frac{1}{\pi} \text{Im} \left[ \langle \psi_0^N | c_{\mathbf{k}} \frac{1}{\omega - [H - E_0^N] + i0^+} c_{\mathbf{k}}^\dagger | \psi_0^N \rangle + \langle \psi_0^N | c_{\mathbf{k}}^\dagger \frac{1}{\omega + [H - E_0^N] + i0^+} c_{\mathbf{k}} | \psi_0^N \rangle \right] \\
&= \sum_n |\langle \psi_n^{N+1} | c_{\mathbf{k}}^\dagger | \psi_0^N \rangle|^2 \delta(\epsilon_n - \omega) + \sum_m |\langle \psi_m^{N-1} | c_{\mathbf{k}} | \psi_0^N \rangle|^2 \delta(\epsilon_m + \omega). \tag{3.3}
\end{aligned}$$

$|\psi_0^N\rangle$  is the normalized  $N$ -particle ground state of the system with energy  $E_0^N$ . The last line of (3.3) is the so-called *spectral representation*,  $|\psi_n^{N\pm 1}\rangle$  are the eigenstates with  $N\pm 1$  particles, respectively, and  $\epsilon_n$  are the excitation energies. Note that the spin index  $\sigma$  is omitted in expression (3.3). ARPES measurements are not sensitive to the electron spin and I will omit it whenever an expression is valid for both spin orientations.

ARPES measurements must be done at low temperature [5]. The main drawback of (direct) ARPES is its insensitivity to the spectral function at positive energy  $\omega$ , because of the strong cutoff from the Fermi-Dirac distribution in (3.1). The energy-symmetrization of ARPES spectra is a widely applied procedure to fix this issue [29]. Under the assumption that the spectral function is symmetric in  $\omega$ , one may write

$$I^{sym}(\mathbf{k}, \omega) = I(\mathbf{k}, \omega) + I(\mathbf{k}, -\omega) = I_0(\mathbf{k}, \nu) A_\beta(\mathbf{k}, \omega). \tag{3.4}$$

However, the symmetry in energy of the ARPES spectral function is controversial.

An alternative to the *direct* ARPES discussed here (photon in, electron out) is the *inverse* photoemission spectroscopy [30]. In inverse ARPES, electron bombardment of the sample produces emission of light which is then detected (electron in, photon out). The inverse method probes the occupied electron states in the solid and provides information about the spectral function at positive energy. However, inverse spectroscopy has very poor resolution at present and the angle-resolved information is of little use.

## 3.2. Analysis of the spectra within the resonating-valence-bond picture and the $t$ - $J$ model

In the following, I am interested in the spectral properties of a strongly interacting system as described, e.g., by the  $t$ - $J$  model. I suppose that the onsite repulsion  $U$  is very large and consider only the lower Hubbard band where the double occupancy is projected out. The energy range in the projected subspace is restricted to  $|\omega| \lesssim \Omega_U$  where  $\Omega_U \sim U$  is a large cutoff scale. In the case of the cuprates, this cutoff is  $\Omega_U \simeq 1\text{eV}$  [98].

### 3.2.1. Spectral sum rules in the $t$ - $J$ model

In the subspace with less than 2 electrons per site, we may work with Gutzwiller-projected electron operators,

$$\tilde{c}_{i\sigma} = c_{i\sigma}[1 - n_{i\bar{\sigma}}], \quad (3.5)$$

and their Fourier transform,

$$\tilde{c}_{\mathbf{k}\sigma} = \frac{1}{\sqrt{L}} \sum_i \tilde{c}_{i\sigma} e^{-i\mathbf{k}\cdot\mathbf{x}_i}. \quad (3.6)$$

The (anti-)commutation relations are

$$\{\tilde{c}_{i\sigma}, \tilde{c}_{j\sigma}^\dagger\} = \delta_{ij} [1 - n_{i\bar{\sigma}}], \quad (3.7a)$$

$$\{\tilde{c}_{i\sigma}, \tilde{c}_{j\bar{\sigma}}^\dagger\} = \delta_{ij} c_{i\bar{\sigma}}^\dagger c_{i\sigma}, \quad (3.7b)$$

$$\{\tilde{c}_{i\sigma}, \tilde{c}_{j\sigma}\} = 0. \quad (3.7c)$$

The spectral function (3.3) in the lower Hubbard band is given by

$$\begin{aligned} \tilde{A}(\mathbf{k}, \omega) &= -\frac{1}{\pi} \text{Im} \tilde{G}(\mathbf{k}, \omega + i0^+) \\ &= \sum_n |\langle \tilde{\psi}_n^{N+1} | \tilde{c}_{\mathbf{k}}^\dagger | \tilde{\psi}_0^N \rangle|^2 \delta(\tilde{\epsilon}_n - \omega) + \sum_m |\langle \tilde{\psi}_m^{N-1} | \tilde{c}_{\mathbf{k}} | \tilde{\psi}_0^N \rangle|^2 \delta(\tilde{\epsilon}_m + \omega) \end{aligned} \quad (3.8)$$

where the eigenstates and energies are now restricted to the Gutzwiller-projected subspace.

The total (single-particle) spectral weights are defined as

$$Z_{\mathbf{k}}^{\text{tot}-} = \int_{-\infty}^0 \tilde{A}(\mathbf{k}, \omega) d\omega = \sum_m |\langle \tilde{\psi}_m^{N-1} | \tilde{c}_{\mathbf{k}} | \tilde{\psi}_0^N \rangle|^2, \quad (3.9a)$$

$$Z_{\mathbf{k}}^{\text{tot}+} = \int_0^{\infty} \tilde{A}(\mathbf{k}, \omega) d\omega = \sum_n |\langle \tilde{\psi}_n^{N+1} | \tilde{c}_{\mathbf{k}}^\dagger | \tilde{\psi}_0^N \rangle|^2, \quad (3.9b)$$

$$Z_{\mathbf{k}}^{\text{tot}} = Z_{\mathbf{k}}^{\text{tot}+} + Z_{\mathbf{k}}^{\text{tot}-} = \int_{-\infty}^{\infty} \tilde{A}(\mathbf{k}, \omega) d\omega. \quad (3.9c)$$

I will call  $Z^{\text{tot}+}$  the spectral weight on the particle side, or *particle spectral weight*,  $Z^{\text{tot}-}$  the spectral weight on the hole side, or *hole spectral weight*, and  $Z^{\text{tot}}$  the *total spectral weight*. It is clear from the form of  $A(\mathbf{k}, \omega)$  that the spectral weights satisfy  $0 \leq Z^{\text{tot}\pm} \leq 1$ . The following sum rules<sup>1</sup> are straight-forward to find by completeness of the basis  $|\tilde{\psi}_n\rangle$ ,

$$Z_{\mathbf{k}}^{\text{tot}-} = \langle \tilde{\psi}_0^N | \tilde{c}_{\mathbf{k}}^\dagger \tilde{c}_{\mathbf{k}} | \tilde{\psi}_0^N \rangle = \tilde{n}_{\mathbf{k}}, \quad (3.10a)$$

$$Z_{\mathbf{k}}^{\text{tot}+} = \langle \tilde{\psi}_0^N | \tilde{c}_{\mathbf{k}} \tilde{c}_{\mathbf{k}}^\dagger | \tilde{\psi}_0^N \rangle = \frac{1+x}{2} - \tilde{n}_{\mathbf{k}}, \quad (3.10b)$$

and

$$Z_{\mathbf{k}}^{\text{tot}} = \langle \tilde{\psi}_0^N | \{ \tilde{c}_{\mathbf{k}}, \tilde{c}_{\mathbf{k}}^\dagger \} | \tilde{\psi}_0^N \rangle = \frac{1+x}{2}, \quad (3.11)$$

where  $x = 1 - \frac{N}{L}$  is the hole doping. The last Eq. (3.11) follows directly from the commutation relation for projected fermions, Eq. (3.7a). Note that the total spectral weight for *unprojected* fermions is clearly equal to one. The deficiency from unity in the sum rule (3.11) is due to the Gutzwiller projection and the missing weight  $[(1-x)/2]$  is in the upper Hubbard band,  $|\omega| \gtrsim \Omega_U$ . The effect of the projection is strongest in the limit of half filling,  $x \rightarrow 0$ . At large doping ( $x \rightarrow 1$ ), the commutation relations (3.7) tend to a conventional form and the entire spectral weight remains at low energy.

Further statements can be made if we integrate expressions (3.10) over  $\mathbf{k}$ ,

$$\frac{1}{L} \sum_{\mathbf{k}} Z_{\mathbf{k}}^{\text{tot}-} = \frac{1-x}{2}, \quad (3.12a)$$

$$\frac{1}{L} \sum_{\mathbf{k}} Z_{\mathbf{k}}^{\text{tot}+} = x. \quad (3.12b)$$

We arrive at the known result [44, 98] that at half filling, the total spectral weight is entirely on the hole side and given by a constant<sup>2</sup> equal to  $\frac{1}{2}$ . This asymmetry near half filling is a

<sup>1</sup>The corresponding finite-temperature expressions for Eqs. (3.10) are  $\int_{-\infty}^{\infty} f(\omega) \tilde{A}_{\beta}(\mathbf{k}, \omega) = \langle \tilde{c}_{\mathbf{k}}^\dagger \tilde{c}_{\mathbf{k}} \rangle_{\beta}$  and  $\int_{-\infty}^{\infty} [1-f(\omega)] \tilde{A}_{\beta}(\mathbf{k}, \omega) = \langle \tilde{c}_{\mathbf{k}} \tilde{c}_{\mathbf{k}}^\dagger \rangle_{\beta}$ , see [29, 30]. Relation (3.11) is equally valid at finite temperature.

<sup>2</sup>Note that  $Z_{\mathbf{k}}^{\text{tot}-} = \tilde{n}_{\mathbf{k}} = \frac{1}{2}$  and  $Z_{\mathbf{k}}^{\text{tot}+} = 0$  for all  $\mathbf{k}$  as  $x \rightarrow 0$ .

sign of the closeness to a Mott insulator and explains, for example, the *overall* asymmetry observed in the tunneling spectra between negative and positive bias voltage [44, 98]. Note that this (rigorous) asymmetry has nothing to do with the presence or absence of symmetry in the position of the coherence peaks or in their intensity. The question how this spectral weight of a doped Mott insulator is distributed among *coherent quasiparticles* and *incoherent background* is still open. I will discuss and comment on these issues in the remaining part of this chapter.

### 3.2.2. The Gutzwiller-projected BCS state and its excitations

In this section, I specialize to a particular variational ansatz for the low-lying states of the  $t$ - $J$  model: the BCS wavefunction. As explained in Chapter 2, soon after the discovery of high-temperature superconductivity, a ground state of the form of a Gutzwiller-projected BCS wavefunction was suggested because of the natural way it can explain the emergence of superconductivity from a Mott insulator when doping is increased [12].

The BCS Hamiltonian [25] is given by

$$H_{\text{BCS}} = -t \sum_{\mathbf{k}\sigma} \xi_{\mathbf{k}} c_{\mathbf{k}\sigma}^\dagger c_{\mathbf{k}\sigma} + \sum_{\mathbf{k}\sigma} \Delta_{\mathbf{k}} c_{\mathbf{k}\sigma} c_{-\mathbf{k}\bar{\sigma}} + \text{h.c.} \quad (3.13)$$

Its spectrum is described by the Bogoljubov quasiparticle operators,

$$\gamma_{\mathbf{k}\sigma} = u_{\mathbf{k}} c_{\mathbf{k}\sigma} - \sigma v_{\mathbf{k}} c_{-\mathbf{k}\bar{\sigma}}^\dagger \quad (3.14)$$

where

$$u_{\mathbf{k}}^2 = \frac{1}{2} \left[ 1 + \frac{\xi_{\mathbf{k}}}{\sqrt{\xi_{\mathbf{k}}^2 + \Delta_{\mathbf{k}}^2}} \right] = 1 - v_{\mathbf{k}}^2. \quad (3.15)$$

The ground-state wavefunction of the BCS Hamiltonian is

$$|\text{BCS}\rangle = \prod_{\mathbf{k}} \frac{\gamma_{-\mathbf{k}\bar{\sigma}} \gamma_{\mathbf{k}\sigma}}{v_{\mathbf{k}}} |0\rangle = \prod_{\mathbf{k}} [u_{\mathbf{k}} + v_{\mathbf{k}} c_{\mathbf{k}\uparrow}^\dagger c_{-\mathbf{k}\downarrow}^\dagger] |0\rangle, \quad (3.16)$$

where  $|0\rangle$  is the vacuum for the electron operators.

I construct now a simple variational wavefunction for the  $t$ - $J$  model by Gutzwiller-projecting the BCS ground state and also projecting it to a fixed number of particles  $N$ ,

$$|N\rangle \propto P_N P_d |\text{BCS}\rangle. \quad (3.17)$$

The state (3.17) was found to have very low variational energy when a  $d$ -wave BCS wavefunction of the form  $\xi_{\mathbf{k}} = -2t[\cos k_x + \cos k_y] - \mu$ ,  $\Delta_{\mathbf{k}} = \Delta[\cos k_x - \cos k_y]$  is chosen, and

$\mu/t$  and  $\Delta/t$  are used as variational parameters [27, 28, 34]. However, in this section I will discuss the BCS wavefunctions without specializing to the  $d$ -wave case.

Gutzwiller-projected quasiparticle excitations of the form

$$|\mathbf{k}\sigma, N\rangle \propto P_N P_d \gamma_{\mathbf{k}\sigma}^\dagger |\text{BCS}\rangle \quad (3.18)$$

have been discussed in the literature at least since the early work of Zhang *et al.* [26]. They enjoy renewed attention in this century after the work of Paramakanti *et al.* [6, 33, 97, 98, 99, 100, 101, 102]. Let me first discuss some general properties of these excitations.

### General properties of Gutzwiller-projected BCS quasiparticles

Note that there are several natural candidates for single-particle spin- $\frac{1}{2}$  excitations. Before Gutzwiller projection, we have

$$\gamma_{\mathbf{k}\sigma}^\dagger |\text{BCS}\rangle \propto c_{\mathbf{k}\sigma}^\dagger |\text{BCS}\rangle \propto c_{-\mathbf{k}\bar{\sigma}} |\text{BCS}\rangle. \quad (3.19)$$

Clearly, these wavefunctions are also proportional after Gutzwiller projection. More quasiparticles can be constructed by applying the operators after the projection. However, it turns out that the only non-proportional excitation is

$$c_{\mathbf{k}\sigma} P_d |\text{BCS}\rangle. \quad (3.20)$$

These two excitations,  $P_d c |\text{BCS}\rangle$  and  $c P_d |\text{BCS}\rangle$ , are linearly independent candidates for spin- $\frac{1}{2}$  excitations, orthogonal to the ground state  $P_d |\text{BCS}\rangle$ . In this thesis, I am exploring the first type of excitation,  $P_d c |\text{BCS}\rangle$ . The second excitation was considered in detail in a recent publication by Tan *et al.* [103].

Consider the normalized ground-state wavefunction

$$|N\rangle \propto P_N P_d |\text{BCS}\rangle \quad (3.21)$$

and suppose that the (normalized) coherent one-particle excitations have the form

$$|\mathbf{k}\sigma, N \pm 1\rangle \propto P_{N \pm 1} P_d c_{\pm \mathbf{k}\sigma}^\dagger |\text{BCS}\rangle. \quad (3.22)$$

In this case, the zero-temperature spectral function (3.8) is

$$A(\mathbf{k}, \omega) = |\langle N+1, \mathbf{k}\sigma | c_{\mathbf{k}\sigma}^\dagger | N \rangle|^2 \delta(\epsilon_{\mathbf{k}}^+ - \omega) + |\langle N-1, \mathbf{k}\sigma | c_{\mathbf{k}\sigma} | N \rangle|^2 \delta(\epsilon_{\mathbf{k}}^- + \omega) + A_{\mathbf{k}}^{\text{inc}}(\omega) \quad (3.23)$$

where  $\epsilon_{\mathbf{k}}^{\pm}$  are the variational energies of the excitations,<sup>3</sup>

$$\epsilon_{\mathbf{k}}^{\pm} = \langle N \pm 1, \mathbf{k}\sigma | H | \mathbf{k}\sigma, N \pm 1 \rangle - \langle N | H | N \rangle \quad (3.24)$$

and  $A_{\mathbf{k}}^{\text{inc}}$  is the *incoherent part* of the spectral function.<sup>4</sup> The prefactors in (3.23) are the *spectral weights* of the quasiparticle (3.22) or the *coherent spectral weights*,

$$Z_{\mathbf{k}}^{+} = |\langle N + 1, \mathbf{k}\sigma | c_{\mathbf{k}\sigma}^{\dagger} | N \rangle|^2, \quad (3.25a)$$

$$Z_{\mathbf{k}}^{-} = |\langle N - 1, \mathbf{k}\sigma | c_{\mathbf{k}\sigma} | N \rangle|^2. \quad (3.25b)$$

The coherent spectral weights can be brought to a simpler form. For clarity, I will drop the particle-number projector and the spin indices in the following. Using the simple relation  $P_d c P_d = c P_d$ , the particle spectral weight can be written as  $Z^{+} = \frac{|\langle P c P c^{\dagger} \rangle|^2}{\langle P \rangle \langle c P c^{\dagger} \rangle} = \frac{\langle c P c^{\dagger} \rangle}{\langle P \rangle}$ . Commuting the projected operators by using (3.7a), one finds<sup>5</sup>

$$Z_{\mathbf{k}}^{+} = \frac{1+x}{2} - \langle N | c_{\mathbf{k}\sigma}^{\dagger} c_{\mathbf{k}\sigma} | N \rangle. \quad (3.26)$$

Comparing (3.26) with the general result, Eq. (3.10b), we see that this excitation has a spectral weight which is *entirely coherent on the particle side*, i.e.

$$A_{\mathbf{k}}^{\text{inc}}(\omega) = 0 \text{ for } \omega > 0. \quad (3.27)$$

As a corollary, it is clear that  $Z_{\mathbf{k}}^{+} = Z_{\mathbf{k}}^{\text{tot}+} \propto x$  when  $x \rightarrow 0$ . Furthermore, I can derive the following exact relation for the hole spectral weight. Using an alternative representation for the excitation [see (3.19)], one may write  $Z^{-} = \frac{|\langle c P c P \rangle|^2}{\langle P \rangle \langle c P c^{\dagger} \rangle} = \frac{|\langle P c c P \rangle|^2}{\langle P \rangle \langle c P c^{\dagger} \rangle} = \frac{\langle P c c P \rangle^2}{|\langle P \rangle|^2 Z^{+}}$  and therefore we have proven that

$$Z_{-\mathbf{k}}^{+} Z_{\mathbf{k}}^{-} = |\langle \mathbf{k}\sigma, N - 1 | c_{-\mathbf{k}\bar{\sigma}} c_{\mathbf{k}\sigma} | \mathbf{k}\sigma, N + 1 \rangle|^2. \quad (3.28)$$

Interestingly, this relation also holds for the unprojected BCS state (where  $Z_{\mathbf{k}}^{+} = |u_{\mathbf{k}}|^2$  and  $Z_{\mathbf{k}}^{-} = |v_{\mathbf{k}}|^2$ ).

The right-hand side of (3.28) can be used as a superconducting order parameter for a finite system [104, 27]. This is a natural choice, since the off-diagonal long-range order which defines the superconducting coherence of a state [33], namely

$$\Phi_{ij}^{SC} = \lim_{r \rightarrow \infty} \langle c_{i\sigma} c_{j\bar{\sigma}} c_{i+r\sigma}^{\dagger} c_{j+r\bar{\sigma}}^{\dagger} \rangle, \quad (3.29)$$

<sup>3</sup>I have omitted here a possible *width*  $\Gamma_{\mathbf{k}}^{\pm}$  of the quasiparticle. This omission is not relevant for the following discussion.

<sup>4</sup>This terminology implies that we think of  $A_{\mathbf{k}}^{\text{inc}}$  as a smooth function of  $\omega$  without singularities. The corresponding *incoherent spectral weights* are defined as  $Z^{\text{inc}\pm} = \pm \int_0^{\pm\infty} A^{\text{inc}}(\omega) d\omega = Z^{\text{tot}\pm} - Z^{\pm}$ .

<sup>5</sup>Relation (3.26) was published recently by S. Yunoki [97].

implies finiteness of the matrix element  $\langle cc \rangle$ .<sup>6</sup>

It is clear from the general sum-rule in a Gutzwiller-projected Hilbert space [Eqs. (3.10) and (3.11)] that the coherent spectral weight of the quasiparticle is bounded,

$$Z_{\mathbf{k}}^- \leq Z_{\mathbf{k}}^{\text{tot}-} = n_{\mathbf{k}}, \quad (3.30a)$$

$$Z_{\mathbf{k}} = Z_{\mathbf{k}}^- + Z_{\mathbf{k}}^+ \leq Z_{\mathbf{k}}^{\text{tot}} = \frac{1+x}{2}. \quad (3.30b)$$

We have also explicitly proven these inequalities for this excitation in the publication [102]. In fact, it was recently shown by Tan *et al.* [103] that the basis for elementary excitations in the projected Hilbert space is complete when the second excitation,  $c|N\rangle$ , is included. That is, the total hole spectral weight of these two excitations sum up to  $n_{\mathbf{k}}$ . The new excitation constructed by these authors for a  $d$ -wave superconductor produces a strong coherence peak at high energy ( $\omega \simeq -3t \simeq -1\text{eV}$ ). On physical grounds, however, such an excitation is questionable. A further coherent excitation which takes up the entire intensity seems to be inconsistent with ARPES experiments, where a part of the low-energy spectral intensity is incoherent, especially in the antinodal region (see, e.g., Ref. [121]).

### Gutzwiller approximation for the quasiparticle spectral weights

Before proceeding with the numerical evaluation of the spectral weights, it is interesting to consider their values in the Gutzwiller approximation (GA; see Section 2.1.3). A careful derivation of the simplest GA for electronic excitations in strongly correlated superconductors was recently published by Edegger *et al.* [41] and Fukushima *et al.* [42], including also Hubbard-model corrections in [101]. I will give here very heuristic arguments for the  $t$ - $J$  model, which are nevertheless in complete agreement with the mentioned calculations.

The particle spectral weights can be brought to the form of hopping matrix elements. As already discussed,  $Z^+ = \frac{\langle cPc^\dagger \rangle}{\langle P \rangle}$ . This is exactly the hole-hopping term which is renormalized by  $g_t = \frac{2x}{1+x}$  in the renormalized mean-field theory [26]. Similarly, one can show that  $Z^- = \frac{|\langle c^\dagger cP \rangle|^2}{\langle c^\dagger P c \rangle \langle P \rangle}$ . According to the general principles of the Gutzwiller approximation [6], we expect that all these matrix elements are renormalized by the factor  $g_t$  with respect to the same expectation values without Gutzwiller-projector. It follows that

$$Z_{\mathbf{k}}^+ \simeq g_t [1 - n_{\mathbf{k}}^0] = g_t u_{\mathbf{k}}^2, \quad (3.31a)$$

$$Z_{\mathbf{k}}^- \simeq g_t n_{\mathbf{k}}^0 = g_t v_{\mathbf{k}}^2, \quad (3.31b)$$

where  $n_{\mathbf{k}}^0 = \langle c_{\mathbf{k}}^\dagger c_{\mathbf{k}} \rangle$  is the momentum distribution in the unprojected wavefunction. Accordingly, the off-diagonal matrix elements [right-hand side of (3.28) or (3.29)] are renormalized

<sup>6</sup>The inverse statement is not true in general. In Section 3.3, I will show that it holds in the special case of a  $d$ -wave superconductor.

by the same factor,<sup>7</sup>

$$\frac{\langle P_d c_{-\mathbf{k}\bar{\sigma}} c_{\mathbf{k}\sigma} P_d \rangle}{\langle P_d \rangle} \simeq g_t \langle c_{-\mathbf{k}\bar{\sigma}} c_{\mathbf{k}\sigma} \rangle = g_t \sigma u_{\mathbf{k}} v_{\mathbf{k}}. \quad (3.32)$$

Let me discuss these Gutzwiller-approximate results near half filling. The GA suggests that  $Z^+ \propto Z^- \propto \langle PccP \rangle \propto x$  as  $x \rightarrow 0$ . Note that these results are perfectly consistent with the two exact relations, (3.26) and (3.28). Furthermore, the total coherent spectral weight within GA is a constant equal to  $g_t$ . This is consistent with the exact sum rule (3.11), i.e.  $Z_{\mathbf{k}} = Z_{\mathbf{k}}^+ + Z_{\mathbf{k}}^- \simeq g_t [u_{\mathbf{k}}^2 + v_{\mathbf{k}}^2] = \frac{2x}{1+x} \leq Z_{\mathbf{k}}^{\text{tot}} = \frac{1+x}{2}$ .

$Z^+ \propto x$  is expected, since the total particle spectral weight  $Z^{\text{tot}+}$  is known to vanish with this power near half filling [see (3.12b)]. However, the GA result  $Z^- \propto x$  is not evident on general grounds, since the total hole spectral weight  $Z^{\text{tot}-}$  is finite at half filling. In Section 3.3, I will discuss the numerical results for the coherent spectral weights which I obtained by the variational Monte Carlo method. Although my results indicate a decrease with doping of the hole spectral weight, the decrease seems to be less strong than what is suggested by the GA. Such a particle-hole asymmetry near half filling was confirmed in recent publications [105, 106]. Note that it has recently been claimed by Fukushima in [43] that he can reproduce this particle-hole asymmetry within a variant of the GA in the grand-canonical ensemble.

As I discussed in Chapter 2, the property  $\langle PccP \rangle \propto x^\alpha$  with  $\alpha > 0$  is an important conceptual ingredient which motivated Anderson's RVB construction. The GA suggests that  $\alpha = 1$ . Spanu *et al.* [107] have recently argued that the power  $\alpha$  may actually be smaller than unity. Note that the particle-hole asymmetry that I find near half filling is related to the power  $\alpha$  of the vanishing of the superconducting order, as it is evident from the exact formula (3.28). Clearly, we must have  $\alpha \geq \frac{1}{2}$ . In the extreme limit  $\alpha = \frac{1}{2}$ , the hole spectral weight is finite at half filling ( $Z^- \propto x^{2\alpha-1}$ ). I have not found any proof or disproof of a finite coherent hole spectral weight at half filling, or any further bound on the value of  $\alpha$ . The possibility of a  $\mathbf{k}$ -dependent exponent  $\alpha$  was discussed in Ref. [105].

The limit  $x \rightarrow 0$  discussed here is relevant if we view it as a model of the phase when superconductivity vanishes, at the underdoped end of the superconducting dome (and not at half filling). This region of the phase diagram is sometimes called the *spin-gap phase* [7]. The ARPES intensities in this region of the phase diagram are very broad and the presence or absence of well-defined coherent quasiparticle peaks is a matter of ongoing debate. From the narrower viewpoint of a variational approach to the  $t$ - $J$  model, this discussion is less relevant. In the half-filled limit, magnetic correlations become important and the energy of the pure BCS wavefunction can be lowered significantly by introducing antiferromagnetic and

<sup>7</sup>Here, we make the important assumption that the average particle number in the Gutzwiller-projected and in the unprojected wavefunction are the same. This is not the case near half filling for simple BCS wavefunctions in the grand-canonical ensemble, where the particle number is allowed to fluctuate. This leads to subtle issues with the Gutzwiller approximation in the grand-canonical ensemble which I will not discuss here. See Refs. [41, 43, 44].



staggered-flux order parameters in the mean-field Hamiltonian, Eq. (3.13) [34]. For a realistic modeling of the cuprates at half filling, it would be necessary to construct spin and charge excitations in such states.<sup>8</sup>

### 3.2.3. Effective Fermi surface for the coherent quasiparticle

The Fermi surface (FS;  $\mathbf{k}_F$ ) of a metal is defined as the locus in the Brillouin zone (BZ) with gapless charge excitations. Equivalently, one defines the FS as the points in the BZ where the one-particle normal Green's function [see (3.3)] diverges at the Fermi energy<sup>9</sup> [108],

$$G(\mathbf{k}_F, \omega = 0) \rightarrow \pm\infty. \quad (3.33)$$

In the absence of single-particle excitations at the Fermi energy (e.g. in the case of a superconductor), the definition of the Fermi surface is extended to the *Luttinger surface* [109, 110]. The Luttinger surface is defined as the locus in the BZ where the Green's function at  $\varepsilon_F$  changes sign, i.e.

$$G(\mathbf{k}_F, \omega = 0) \rightarrow 0, \pm\infty. \quad (3.34)$$

In the following, I will use the term Fermi surface in the more general sense of a Luttinger surface.

It has been emphasized recently in Refs. [111, 112] that an unambiguous experimental determination of the Fermi surface in superconducting cuprates is difficult. The following definitions of the Fermi surface are most commonly used in experiments [29, 30]:

- *locus of minimal gap* - This is either determined from the experimental dispersion or from the maximum in the spectral intensity at the Fermi energy,  $A(\mathbf{k}, \omega = 0)$ .
- *maximum gradient method* - The momentum distribution may be determined experimentally from  $n_{\mathbf{k}} = \int f(\omega)A(\mathbf{k}, \omega) d\omega$ . The experimental FS is then defined as the point on a cut in the BZ where  $\partial_{\mathbf{k}}n_{\mathbf{k}}$  is maximal.
- *half- $n_{\mathbf{k}}$*  - The locus of points where  $n_{\mathbf{k}} = \frac{1}{2}$ .
- *normal-state FS* - The sample may be heated up above  $T_c$  (or  $T^*$  in the underdoped region) and the location of gapless excitations can be found.

I will not further explore the issues related to the determination of the experimental FS. Note, however, that the various definitions of the FS usually agree within the experimental uncertainties. Furthermore, within conventional *s*-wave BCS theory with small gap parameter  $\Delta$ , the various experimental definitions of the FS coincide with the *underlying Fermi surface* in

<sup>8</sup>See also Section 3.4, where I model the pseudogap phase with more complicated mean-field states, however without taking into account the Gutzwiller constraint exactly.

<sup>9</sup>Here and in the following, I choose  $\varepsilon_F = E_{N+1}^0 - E_N^0$  as origin for  $\omega$ .

the BCS theory [111], defined as

$$\xi_{\mathbf{k}_F} = 0, \quad (3.35)$$

where  $\xi_{\mathbf{k}}$  is the normal dispersion in the BCS Hamiltonian, (3.13).

In the context of the variational quasiparticle excitation discussed in this thesis, we may write the single-particle Green's function as

$$G(\mathbf{k}, \omega) = \frac{Z_{\mathbf{k}}^+}{\omega - \epsilon_{\mathbf{k}}^+} + \frac{Z_{\mathbf{k}}^-}{\omega + \epsilon_{\mathbf{k}}^-} + G_{\mathbf{k}}^{\text{inc}}(\omega), \quad (3.36)$$

where the  $G_{\mathbf{k}}^{\text{inc}}(\omega)$  is the smooth incoherent background and  $\epsilon_{\mathbf{k}}^{\pm}$  are the variational excitation energies given in (3.24). Neglecting the incoherent background and under the assumption of a symmetric dispersion  $\epsilon_{\mathbf{k}}^- = \epsilon_{\mathbf{k}}^+$ , the Luttinger condition (3.34) becomes

$$Z_{\mathbf{k}_F}^+ = Z_{\mathbf{k}_F}^-. \quad (3.37)$$

This motivates our definition of the *effective Fermi surface* as the points in the BZ which satisfy relation (3.37). Note that the assumption  $\epsilon_{\mathbf{k}}^- = \epsilon_{\mathbf{k}}^+$  is not evident close to half filling. However, Yunoki *et al.* [99] have found a symmetric quasiparticle dispersion in the case of a *d*-wave superconductor,<sup>10</sup> which gives support to this assumption. Note also that in the case of an unprojected BCS superconductor, where  $Z_{\mathbf{k}}^+ = u_{\mathbf{k}}^2$  and  $Z_{\mathbf{k}}^- = v_{\mathbf{k}}^2$ , the effective FS and the underlying FS coincide. This is even the case in the strong-coupling approach within the GA, where  $Z_{\mathbf{k}}^+ = g_t u_{\mathbf{k}}^2$  and  $Z_{\mathbf{k}}^- = g_t v_{\mathbf{k}}^2$ . Putting aside the correctness of the assumption of a symmetric dispersion and the negligence of the incoherent background, a deviation of the effective Fermi surface (3.37) from the underlying one (3.35) indicates a departure from conventional BCS theory and a breakdown of the simplest version of the Gutzwiller approximation.

<sup>10</sup>These authors apply an additional Jastrow factor to the variational ground state and excitations.

### 3.3. Spectral weight of a Gutzwiller-projected $d$ -wave superconductor

The main results of this section have been published in [102].

#### 3.3.1. Introduction

Shortly after the discovery of superconductivity in copper-oxide compounds [2], Anderson proposed a Gutzwiller-projected BCS wavefunction which would describe the superconducting ground state of high-temperature superconductors [12]. The variational approach to superconducting cuprates based on Anderson's original proposal has since had a lot of success, while the strong Coulomb repulsion and the nonperturbative nature of the problem make other approaches extremely difficult. Interest in projected wavefunctions as variational ground states for cuprate superconductors was initiated by several research groups in the late 80's [27, 28] and has led to considerable activity in the field. The Gutzwiller-projected wavefunctions show a large overlap with exact ground states on small clusters and have low variational energies for the  $t$ - $J$  model [104, 113]. Furthermore, several experimental properties of the cuprates like the zero-temperature phase diagram and  $d$ -wave pairing symmetry are extremely well predicted within this approach [6, 33].

Due to considerable progress of the experimental technique of angle-resolved photoemission spectroscopy (ARPES) on cuprates, more and more high-quality data on the low-lying spectral properties of these compounds have been made available in recent years [29, 30]. Experimentally, the low-energy excitations of superconducting cuprates are known to resemble BCS quasiparticles (QPs) [119]. It is therefore interesting to theoretically explore the wavefunction of projected QP excitations and compare them to unprojected BCS QPs. The most apparent differences are the doping dependency of the nodal Fermi velocity and the renormalization of the nodal QP spectral weight and of the current carried by QPs [33, 97, 99, 100, 101]. In this section, we further analyze the properties of the superconducting ground state and the QP excitations with the variational Monte Carlo technique (VMC) [27]. We calculate the equal-time Green's functions, both normal and anomalous, in the Gutzwiller-projected state and derive from them the QP spectral weights for addition and removal of an electron at zero temperature. The main conclusion of our study is that, due to a nontrivial interplay of superconductivity and strong Coulomb repulsion (Gutzwiller projection), the coherent electron and hole spectral weights are renormalized differently. A natural way to describe this asymmetry is to define the "effective Fermi surface" as the locus of points where the electron and the hole spectral weights are equal. Thus defined Fermi surface acquires an additional outward bending in the antinodal region as compared to the original underlying Fermi surface. This bending is a signature of a deviation from the BCS theory and may be responsible for the geometry of the Fermi surface observed in ARPES experiments. The validity of Luttinger's rule [109] in strongly interacting and superconducting materials

has recently been questioned experimentally and theoretically [29, 30, 111, 112]. Our findings provide further indication of its inapplicability in strongly correlated superconductors.

The remaining part of Section 3.3 is organized as follows. Section 3.3.2 contains the definition of the model and the wavefunctions used in our calculations. In Section 3.3.3, I describe our results on the QP spectral weights. Section 3.3.4 is devoted to the calculation of the equal-time anomalous Green's function. Finally, Section 3.3.5 discusses the “effective Fermi surface” and its deviation from the underlying Fermi surface.

### 3.3.2. The model

In the tight-binding description, the cuprates are modeled by electrons hopping on a square lattice. The appropriate model is the  $t$ - $J$  Hamiltonian:

$$H_{t-J} = -t \sum_{\langle i,j \rangle, \sigma} P_d c_{i\sigma}^\dagger c_{j\sigma} P_d + J \sum_{\langle i,j \rangle} (\mathbf{S}_i \cdot \mathbf{S}_j - \frac{n_i n_j}{4}) \quad (3.38)$$

acting in the Hilbert space with less than two electrons per site. Here  $n_{i\sigma} = c_{i\sigma}^\dagger c_{i\sigma}$ ,  $\mathbf{S}_i = \frac{1}{2} \sum_{\sigma, \sigma'} c_{i\sigma}^\dagger \boldsymbol{\sigma}_{\sigma\sigma'} c_{i\sigma'}$ ,  $c_{i\sigma}^\dagger$  is the electron creation operator in the Wannier state at site  $i$ , and  $\boldsymbol{\sigma}$  are the Pauli matrices. The no-double occupancy is preserved by the Gutzwiller projector  $P_d = \prod_i [1 - n_{i\uparrow} n_{i\downarrow}]$ .

The  $t$ - $J$  model can be viewed as the large- $U$  limit of the one-band Hubbard model, neglecting the 3-site-hopping term. Provided that the model is analytic in  $t/U$ , doubly occupied sites can be re-introduced perturbatively to recover the full Hilbert space of the Hubbard model [15, 33]. Although the inclusion of these corrections present no major difficulty, we choose to neglect them here. In most quantities, only small corrections arise from finite double occupancy [33, 100], which makes this approach to the large- $U$  Hubbard model consistent. Furthermore, it has been argued that the  $t$ - $J$  model is in fact more appropriate than the one-band Hubbard model in describing the CuO<sub>2</sub> planes [16].

We consider the usual variational ground state [27],

$$|\Psi_N\rangle = P_N P_d |d\text{-BCS}(\Delta, \mu)\rangle, \quad (3.39)$$

where  $P_N$  is the particle number projector on the subspace of  $N$  electrons. We will denote  $L$  the total number of sites. Both particle number and number of sites are even.  $|d\text{-BCS}\rangle$  is the ground state of the BCS mean field Hamiltonian with nearest-neighbor hopping and  $d$ -wave pairing symmetry on the square lattice:  $|d\text{-BCS}\rangle = \prod_{\mathbf{k}} [u_{\mathbf{k}} + v_{\mathbf{k}} c_{\mathbf{k}\uparrow}^\dagger c_{-\mathbf{k}\downarrow}^\dagger] |0\rangle \propto \prod_{\mathbf{k}, \sigma} \gamma_{\mathbf{k}\sigma} |0\rangle$ .  $\gamma_{\mathbf{k}\sigma} = u_{\mathbf{k}} c_{\mathbf{k}\sigma} - \sigma v_{\mathbf{k}} c_{-\mathbf{k}\bar{\sigma}}^\dagger$ ,  $u_{\mathbf{k}}^2 = \frac{1}{2} (1 + \frac{\xi_{\mathbf{k}}}{E_{\mathbf{k}}}) = 1 - v_{\mathbf{k}}^2$ ,  $E_{\mathbf{k}} = \sqrt{\xi_{\mathbf{k}}^2 + \Delta_{\mathbf{k}}^2}$ ,  $\xi_{\mathbf{k}} = -2(\cos k_x + \cos k_y) - \mu$ ,  $\Delta_{\mathbf{k}} = \Delta(\cos k_x - \cos k_y)$ . The wavefunction (3.39) has two free parameters:  $\Delta$  and  $\mu$ . These variational parameters are chosen to minimize the energy of the  $t$ - $J$  Hamiltonian

(3.38) for the experimentally relevant value  $t = 3J$  and for every doping level. I use the optimized parameters from [34].

The following ansatz is used for the excited states [6, 26, 33, 97, 99, 100, 101],

$$|\Psi_{N,\mathbf{k},\sigma}\rangle = P_N P_d \gamma_{\mathbf{k}\sigma}^\dagger |d\text{-BCS}\rangle. \quad (3.40)$$

In the following, the normalized versions of (3.39) and (3.40) will be denoted by  $|N\rangle$  and  $|\mathbf{k}\sigma, N\rangle$ , respectively:

$$|N\rangle = \|\Psi_N\|^{-1} |\Psi_N\rangle, \quad (3.41a)$$

$$|\mathbf{k}\sigma, N\rangle = \|\Psi_{N,\mathbf{k},\sigma}\|^{-1} |\Psi_{N,\mathbf{k},\sigma}\rangle. \quad (3.41b)$$

The RVB wavefunction (3.39) implements both strong electron correlations and superconductivity.<sup>11</sup> It is known to have a considerable overlap with the true ground state of the  $t$ - $J$  model at non-zero hole doping on small clusters [113, 104, 114, 115]. There is also numerical support from exact diagonalization studies indicating well-defined BCS-like QPs as low-energy excitations of the  $t$ - $J$  model [116]. Therefore, the excited trial states (3.40) are expected to be close to the true excitations of the  $t$ - $J$  model. However, here we are more interested in the physical content of the proposed wavefunctions than in their closeness to the eigenstates of a particular Hamiltonian.

---

<sup>11</sup>As an alternative to the canonical formulation in Eqs. (3.39) and (3.40), one can work in the grand-canonical ensemble, without the particle-number projector, but with an additional fugacity factor [41, 44]. Here, the canonical scheme is chosen for numerical convenience, as it is commonly done in most VMC studies.

### 3.3.3. Quasiparticle spectral weights

As I discussed in Section 3.2.2, the coherent<sup>12</sup> spectral weights are defined as the overlap between the bare electron or hole added ground state and the QP excitations of the model,

$$Z_{\mathbf{k}}^{\pm} = |\langle \mathbf{k}\sigma, N \pm 1 | c_{\mathbf{k}\sigma}^{\pm} | N \rangle|^2. \quad (3.42)$$

The particle spectral weight can be calculated from the relation [97]

$$Z_{\mathbf{k}}^+ = \frac{1+x}{2} - n_{\mathbf{k}}, \quad (3.43)$$

where  $n_{\mathbf{k}}$  is the momentum distribution (equal-time normal Green's function),

$$n_{\mathbf{k}} = \langle N | c_{\mathbf{k}\sigma}^{\dagger} c_{\mathbf{k}\sigma} | N \rangle, \quad (3.44)$$

and  $x = 1 - \frac{N}{L}$  is the hole concentration.

The hole spectral weight can also be calculated from ground-state expectation values,<sup>13</sup> with the help of the relation derived in Section 3.2.2,

$$Z_{\mathbf{k}}^+ Z_{\mathbf{k}}^- = |\Phi_{\mathbf{k}}|^2, \quad (3.45)$$

where  $\Phi_{\mathbf{k}}$  is the superconducting order parameter (equal-time anomalous Green's function),

$$\Phi_{\mathbf{k}} = \langle N - 1 | c_{\mathbf{k}\uparrow} c_{-\mathbf{k}\downarrow} | N + 1 \rangle. \quad (3.46)$$

Further, we define the total (coherent) spectral weight as

$$Z_{\mathbf{k}} = Z_{\mathbf{k}}^+ + Z_{\mathbf{k}}^-. \quad (3.47)$$

The main contribution to  $Z_{\mathbf{k}}$  is given by  $Z_{\mathbf{k}}^+$  outside the Fermi surface and by  $Z_{\mathbf{k}}^-$  inside. As I discussed in Section 3.2.2, the weights must satisfy the upper bounds  $Z_{\mathbf{k}} \leq \frac{1+x}{2}$  and  $Z_{\mathbf{k}}^- \leq n_{\mathbf{k}}$ .

Numerically, I compute the spectral weight  $Z_{\mathbf{k}}^-$  by first computing  $Z_{\mathbf{k}}^+$  and  $\Phi_{\mathbf{k}}$ , and then using relation (3.45). The disadvantage of this method is large error bars around the center of the Brillouin zone where both  $Z_{\mathbf{k}}^+$  and  $\Phi_{\mathbf{k}}$  are small.<sup>14</sup> However, the precision is sufficient to establish that the total coherent spectral weight  $Z_{\mathbf{k}}$  is a smooth function of  $\mathbf{k}$  and has no singularity at the nodal point. In order to avoid the singular points along the nodal direction of a  $d$ -wave superconductor, I use periodic boundary conditions in one, and antiperiodic boundary

<sup>12</sup>Throughout this section, the coherent (quasiparticle) spectral weight is discussed; the word ‘‘coherent’’ is sometimes omitted in the following.

<sup>13</sup>Note that I am assuming wavefunctions with conserved parity in this section, i.e.  $Z_{\mathbf{k}}^{\pm} = Z_{-\mathbf{k}}^{\pm}$ .

<sup>14</sup>Recently performed calculations of  $Z_{\mathbf{k}}^-$  by direct sampling of the excited states are free from this problem [106, 117].

conditions in the other direction. More technical details on the Monte Carlo algorithm can be found in Section 2.1.2.

In Figs. 3.2 and 3.3, I plot the spectral weights  $Z_{\mathbf{k}}^+$ ,  $Z_{\mathbf{k}}^-$ , and  $Z_{\mathbf{k}}$  along the contour  $0 \rightarrow (0, \pi) \rightarrow (\pi, \pi) \rightarrow 0$  in the Brillouin zone for different doping levels. Figure 3.6 shows the contour plots of  $Z_{\mathbf{k}}$  in the region of the Brillouin zone where our method produces small error bars.<sup>15</sup> From these data, we can make the following observations.

- (i) In the case of an unprojected BCS wavefunction, the total spectral weight is constant and unity over the Brillouin zone. Within the Gutzwiller approximation, the total weight is a constant equal to  $\frac{2x}{1+x}$ . Taking the Gutzwiller projection into account exactly, we see that for low doping ( $x \simeq 3\%$ ), the spectral weight is reduced by a factor up to 20 (which is in qualitative agreement with the GA). The renormalization is asymmetric in the sense that the electronic spectral weight  $Z_{\mathbf{k}}^+$  is more reduced than the hole spectral weight  $Z_{\mathbf{k}}^-$ . The total spectral weight is not constant, in disagreement with the GA. For higher doping ( $x \simeq 23\%$ ), the spectral-weight reduction is much smaller. The electron-hole asymmetry decreases and the total weight is closer to the GA predictions.
- (ii) Since there is no electron-hole mixing along the zone diagonal, the spectral weights  $Z_{\mathbf{k}}^+$  and  $Z_{\mathbf{k}}^-$  have a discontinuity at the nodal point. The data show that the total weight is continuous across the nodal point. Strong correlation does not affect this feature of uncorrelated BCS theory. Recently, it has been shown in Ref. [105] that the total spectral weight of the Gutzwiller-projected (non-superconducting) Fermi sea is continuous across the Fermi surface. This is consistent with our result.

In Ref. [119], the coherent spectral weights of a slightly overdoped sample of Bi2223 were measured along the cut  $(\pi, 0) \rightarrow (\pi/2, \pi/2)$  and an almost constant total spectral weight was reported in this experiment. It can be seen from Fig. 3.6 that the total spectral weight is approximately constant along this cut, so the experimental result agrees well with this property of the quasiparticle excitation.

An anisotropy of the ARPES intensity along the experimental FS (the so-called nodal-antinodal dichotomy) was reported in a series of experiments [120, 121]. Experimentally, the spectral weight measured in the anti-nodal region is suppressed in underdoped cuprates, while it is large in the optimally doped and overdoped region. Usually, this effect is associated with formation of some charge or spin order, static or fluctuating one. From Fig. 3.6 we see that a similar (but weaker) tendency can be observed in the framework of Gutzwiller-projected

<sup>15</sup>Our VMC results show qualitative agreement with the hole spectral weight reported in Ref. [101] where the authors used the Gutzwiller approximation to calculate the same quantity in the large-U Hubbard model. It should be noted, however, that the asymmetry we find near half filling cannot be explained within the standard Gutzwiller approximation. In a recent publication, Fukushima [43] proposes an extended Gutzwiller approximation scheme. The author claims that his scheme can reproduce the asymmetry in our VMC results. Our results are consistent with other recent VMC calculations [100, 105, 106, 118, 103] and earlier calculations of  $Z_{\mathbf{k}}^+$  in Ref. [33].

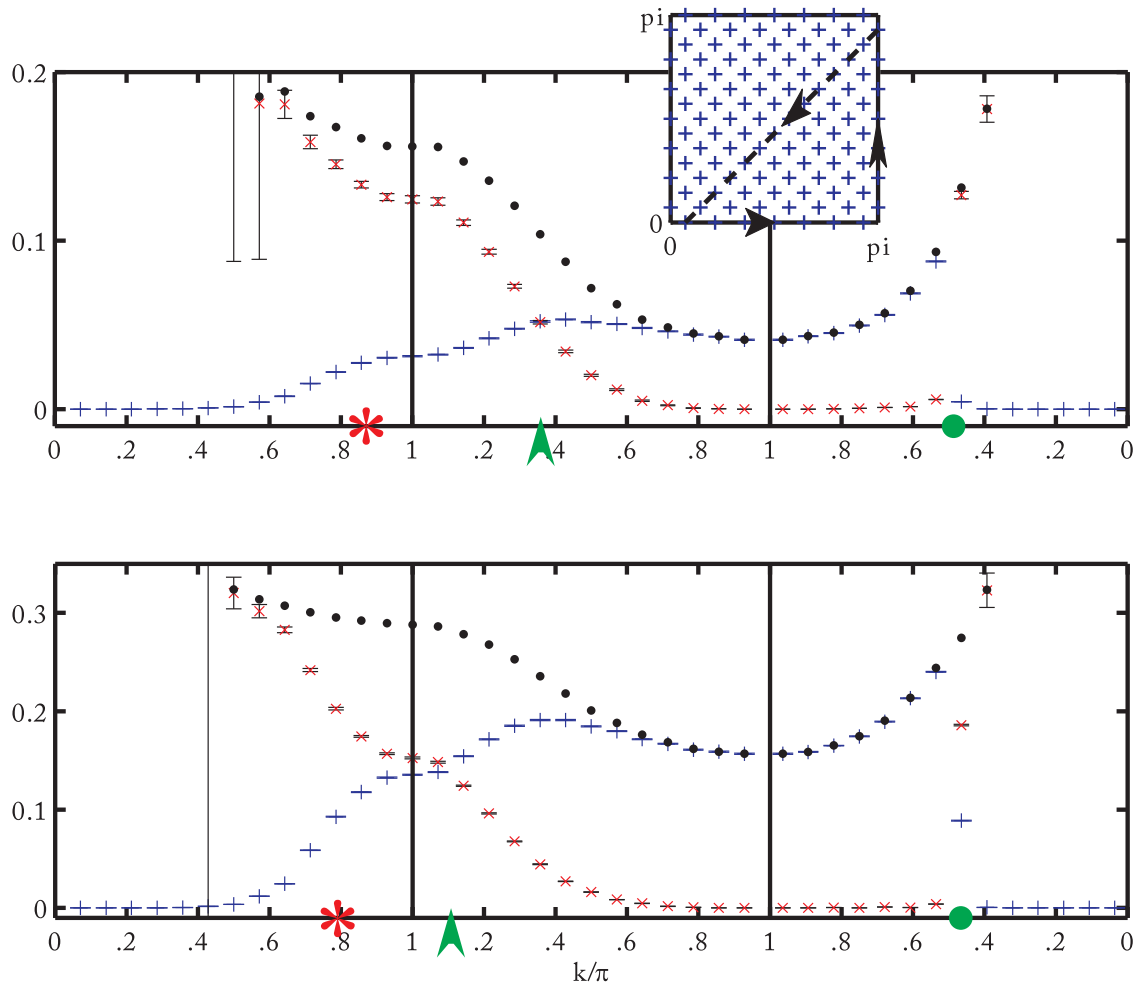


**Figure 3.2.:** QP spectral weights for 6 holes (upper plot,  $x \simeq 3\%$ ) and 22 holes (lower plot,  $x \simeq 11\%$ ) on 196 sites. The spectral weights are plotted along the contour  $0 \rightarrow (0, \pi) \rightarrow (\pi, \pi) \rightarrow 0$  (shown in inset). Plus signs (+, blue) denote the particle spectral weight  $Z_{\mathbf{k}}^+$ , crosses ( $\times$ , red) denote the hole spectral weight  $Z_{\mathbf{k}}^-$ , error bars are shown. Solid dots (black) denote their sum, the total coherent spectral weight  $Z_{\mathbf{k}}$ , error bars not shown. On the horizontal axis, the red star (\*) denotes the intersection with the underlying Fermi surface along the  $0 \rightarrow (0, \pi)$  direction; the thick green dot is the nodal point.  $Z_{\mathbf{k}}^+$  and  $Z_{\mathbf{k}}^-$  jump at the nodal point, while  $Z_{\mathbf{k}}$  is continuous. The intersection with the effective Fermi surface (see Section 3.3.5) is marked by an green arrowhead. On the diagonal (last segment),  $k$  is given in units of  $\sqrt{2}$ .

quasiparticle excitations.<sup>16</sup> However, the experimentally observed effect is much stronger and a claim that the nodal-antinodal dichotomy can be explained within this framework would be too hasty.

<sup>16</sup>If we use the effective FS defined here to compare with the experimental one.



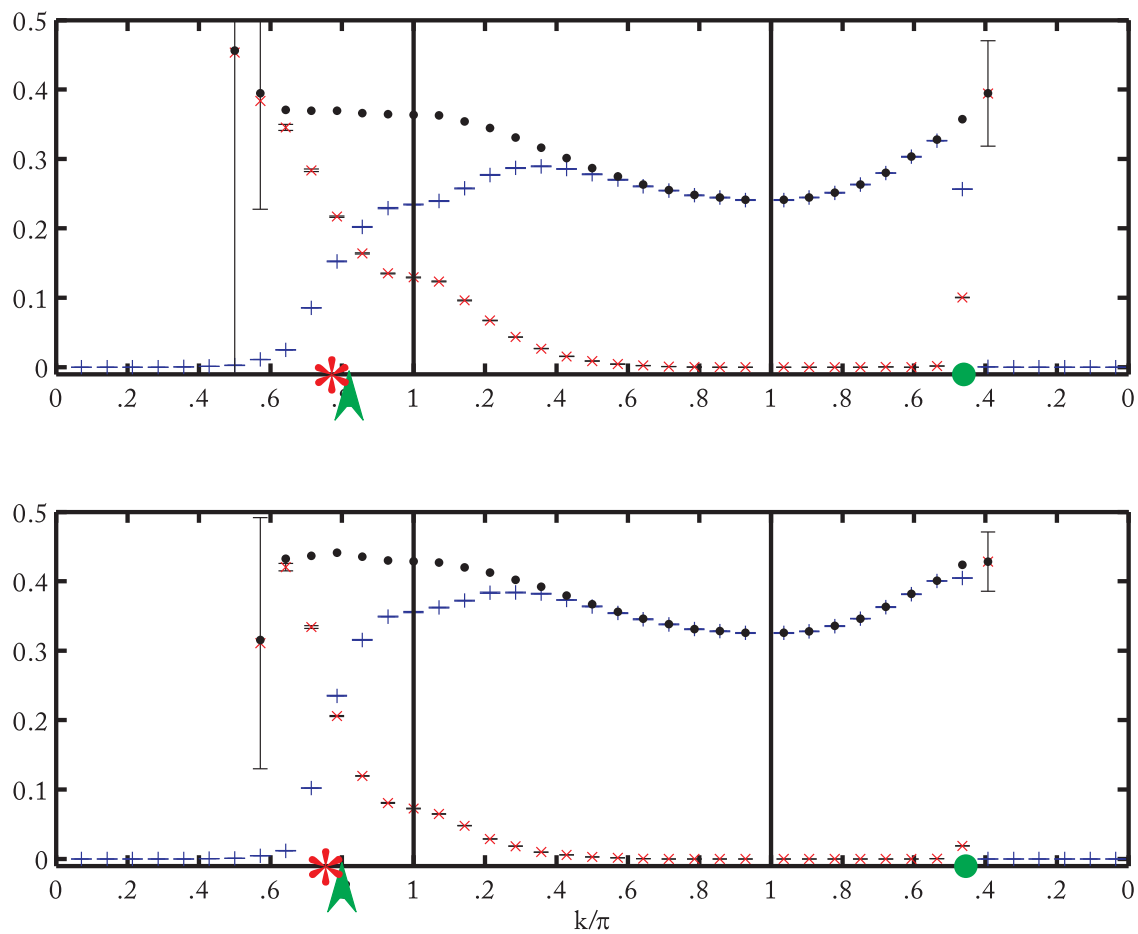


**Figure 3.3.:** Same plot as Fig. 3.2 of the QP spectral weights for 34 holes (upper plot,  $x \simeq 17\%$ ) and 46 holes (lower plot,  $x \simeq 23\%$ ) on 196 sites.

### 3.3.4. Superconducting order parameter

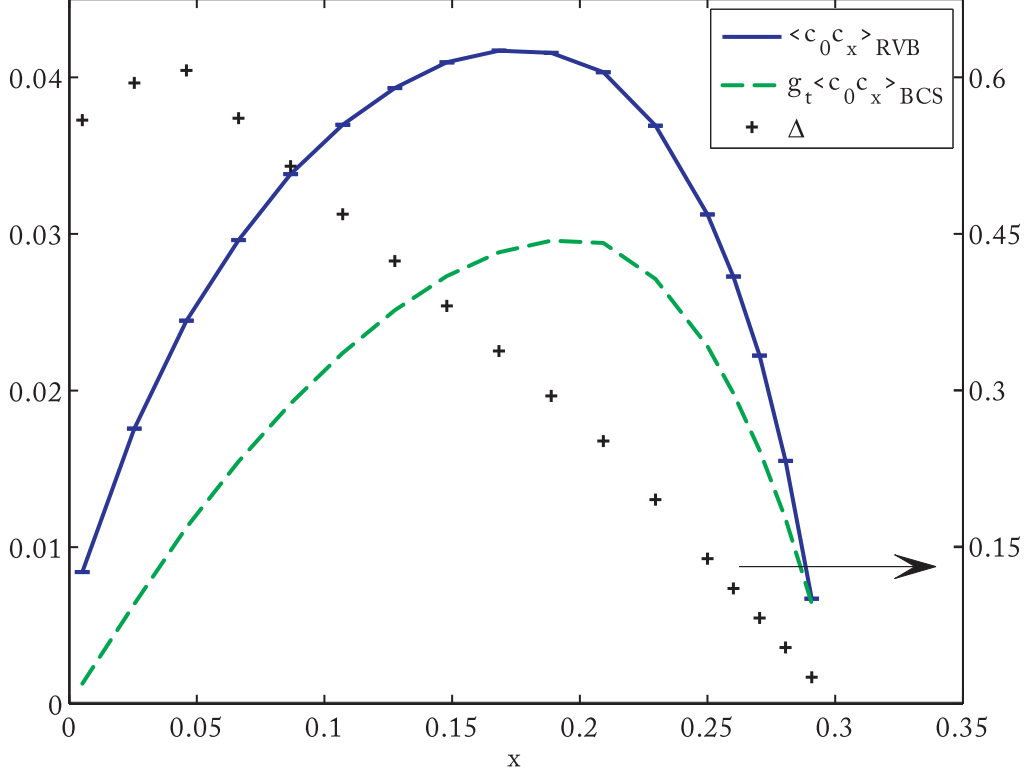


**Figure 3.4.:** Doping dependency of the nearest-neighbor superconducting order parameter  $\Phi_{ij}$  (calculated in the  $14 \times 14$  system). The error bars are smaller than the symbol size. The same quantity calculated in the Gutzwiller approximation is also shown for comparison (green dashed line). The variational parameter  $\Delta$  is shown with the scale on the right.

In Fig. 3.4, I plot the nearest-neighbor superconducting correlation  $\Phi_{ij}$  [the Fourier transform of  $\Phi_{\mathbf{k}}$  defined in (3.46)] as a function of doping. This curve shows close quantitative agreement with the result of Ref. [33], where the authors extracted the superconducting order parameter from the long-range asymptotics of the nearest-neighbor pairing correlator,  $\Phi^{SC} = \lim_{r \rightarrow \infty} \langle c_0 c_1 c_r^\dagger c_{r+1}^\dagger \rangle$ . With the method employed here, I find the same qualitative and quantitative conclusions as previous authors [27, 33]: vanishing of superconductivity at half filling  $x \rightarrow 0$  and at the superconducting transition on the overdoped side  $x_c \simeq 0.3$ .<sup>17</sup>

<sup>17</sup>It is interesting to note that I observe a sensitive dependency of the superconducting order parameter on the variational parameter  $\mu$  at high doping (as  $\Delta \rightarrow 0$ ). This results from projecting to the particle-number tail of an almost normal state ( $\Delta \simeq 0$ ), if the value of  $\mu$  is far away from the Fermi-sea chemical potential. Remarkably, the optimal variational value of  $\mu$  approaches the Fermi-sea chemical potential as  $\Delta \rightarrow 0$  [34]. In the Gutzwiller-projected Fermi sea,  $\mu$  can no longer be treated as a variational parameter, but is fixed by the particle-number constraint. (The variational parameter  $\mu$  *must not* be confused with the physical chemical potential.)

The optimal doping is close to  $x_{opt} \simeq 0.18$ . In the same plot, I also show the commonly used Gutzwiller approximation where the unprojected expectation value is renormalized by the factor  $g_t = \frac{2x}{1+x}$  [6]. The Gutzwiller approximation underestimates the correct value by approximately 25%.

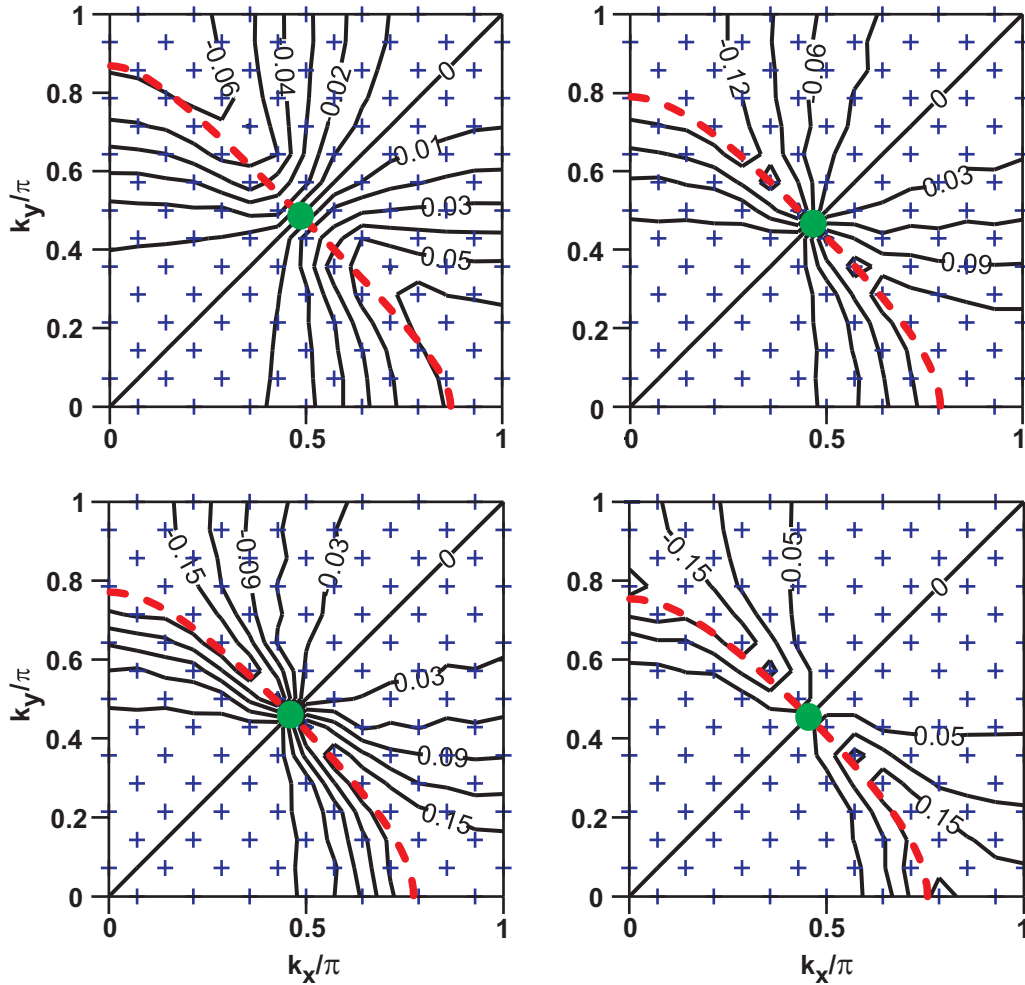


**Figure 3.5.:** Pairing correlation  $\Phi_{\mathbf{k}}$  in the Brillouin zone at different doping levels:  $x \simeq 3\%$  (upper left), 11% (upper right), 17% (lower left) and 23% (lower right) in a  $14 \times 14$  system with periodic-antiperiodic boundary conditions. The dashed red line is the unprojected, underlying Fermi surface.

In Fig. 3.5, I show contour plots of the superconducting order parameter  $\Phi_{\mathbf{k}}$  for four values of doping. It resembles qualitatively the unprojected  $d$ -wave pairing amplitude, but is somewhat distorted due to the particle-hole asymmetry (see discussion in the previous and the following sections).

## 3.3.5. Fermi surface

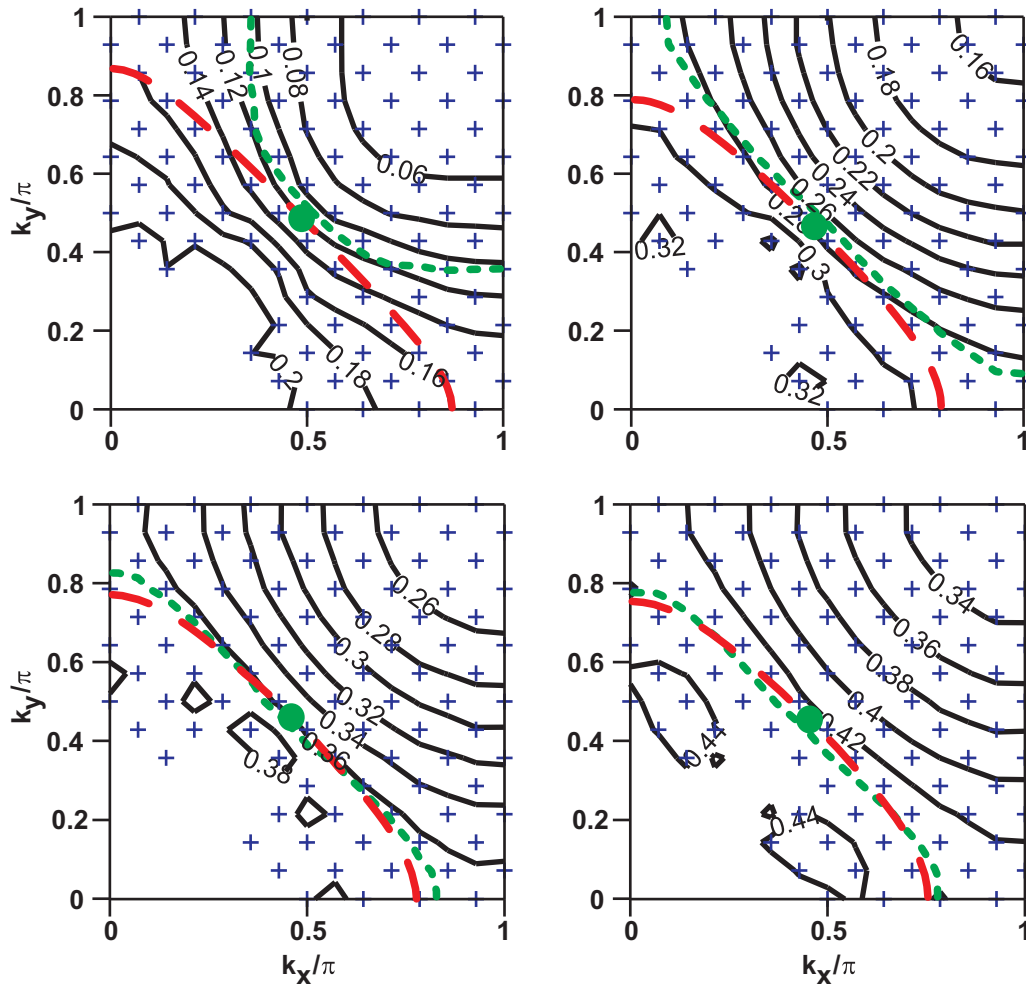


**Figure 3.6.:** Contour plots of the total QP spectral weight  $Z_k$  (black lines). The underlying FS (long-dashed red line) and effective FS (short-dashed green line) are also shown. The doping levels are  $x \simeq 3\%$  (top left),  $11\%$  (top right),  $17\%$  (bottom left) and  $23\%$  (bottom right). The + signs indicate points where we can compute the values within small error bars.

As discussed in Section 3.2.3, the *effective FS* is defined as the locus  $Z_{\mathbf{k}_F}^+ = Z_{\mathbf{k}_F}^-$ . In Fig. 3.6, I plot the underlying and the effective FS which were obtained by VMC calculations. The contour plot of the total QP weight is also shown in this figure. It is interesting to note the following points.

- (i) In the underdoped region, the effective FS is open and bent outwards (hole-like FS). In the overdoped region, the effective FS closes and embraces more and more the underlying one with increasing doping (electron-like FS).
- (ii) Luttinger's rule [109] for the effective FS is clearly violated in the underdoped region, i.e. the area enclosed by this FS is not conserved by the interaction; it is larger than the one enclosed by the underlying Fermi surface.
- (iii) In the optimally doped and overdoped region, the total spectral weight is approximately constant along the effective FS, within error bars. In the highly underdoped region, we observe a small concentration of the spectral weight around the nodal point ( $\simeq 20\%$ ).

A large “hole-like” FS in underdoped cuprates has been reported in ARPES experiments by several groups [120, 122, 123]. The effective FS that I find here agrees with these experimental results.

It should be noted that a negative next-nearest hopping  $t'$  would lead to a similar FS curvature as I find in the underdoped region. I would like to emphasize that the original  $t$ - $J$  Hamiltonian as well as the variational states do not contain any  $t'$ . Our results show that the outward curvature of the FS is due to strong Coulomb repulsion, without need of  $t'$ . Next-nearest hopping terms in the microscopic description of the cuprates may not be necessary to explain the FS curvature found in ARPES experiments. Remarkably, if the next-nearest hopping  $t'$  is included in the variational ansatz (and not in the original  $t$ - $J$  Hamiltonian), a finite and negative  $t'$  is generated, as it was shown by Himeda and Ogata [124]. Apparently, in this case the underlying FS has the tendency to adjust to the effective FS. A similar bending of the FS was also reported in the recent analysis of the current carried by Gutzwiller-projected quasiparticles [100]. A high-temperature expansion of the momentum distribution  $n_{\mathbf{k}}$  of the  $t$ - $J$  model was done in Ref. [125] where the authors find a violation of Luttinger's rule and a hole-like curvature of the FS. Our findings provide further evidence along this line.

A natural question is the role of superconductivity in the unconventional bending of the FS. In the limit  $\Delta \rightarrow 0$ , the variational states are Gutzwiller-projected excitations of the Fermi sea and the spectral weights are step-functions at the (underlying) FS. In a recent paper [105] it was shown that  $\lim_{\mathbf{k} \rightarrow \mathbf{k}_F^+} Z_{\mathbf{k}}^+ = \lim_{\mathbf{k} \rightarrow \mathbf{k}_F^-} Z_{\mathbf{k}}^-$  for the Gutzwiller-projected Fermi sea, which means that the underlying and the effective FS coincide in that case. This suggests that the “hole-like” FS results from a nontrivial interplay between strong correlation and superconductivity. We lack a qualitative explanation of this effect. However, it may be a consequence of the proximity of the system to the non-superconducting “staggered-flux” state [34, 126] or to antiferromagnetism [49, 33] near half-filling.

## 3.4. An SU(2) approach to the pseudogap phase

The results presented in this section have been submitted for publication [127].

### 3.4.1. Introduction

The most unusual and debated feature of high-temperature superconductivity (HTSC) is the pseudogap (PG) phase, the high-temperature phase in the underdoped region of the phase diagram between the destruction of superconductivity at  $T_c$  and the pseudogap temperature  $T^*$  [128, 129]. While the zero-temperature phase diagram of HTSC is relatively well understood, there is currently much experimental and theoretical interest in the intermediate-temperature PG phase. In this phase, several surprising experimental features show up: e.g. the ARPES spectra show a state which is partially gapped on the experimental Fermi surface [29, 30, 130, 131, 132, 133, 134].

Theoretically, the low-temperature physics of HTSC is well described by variational wavefunctions of the  $t$ - $J$  model [3, 4, 5, 6, 26, 27, 113, 135]. The antiferromagnetic parent state at half filling is destroyed as doping is increased. Due to the gain of spin-exchange energy in the Gutzwiller-projected state, a  $d$ -wave mean-field order is favored away from half filling. The characteristic dome for the superconducting order can be reproduced variationally [33, 102]. Low-lying Gutzwiller-projected quasiparticle excitations reproduce well many experimental features [33, 97, 98, 99, 102, 106, 118, 136]. The main disadvantage of the variational approach is that it is a zero-temperature theory and cannot easily be extended to finite temperature or to high-energy excitations [5].

Many years ago, it was noticed that there is a redundant description of Gutzwiller-projected fermionic wavefunctions exactly at half filling, parameterized by local SU(2) rotations [137, 138]. Away from half filling, this redundancy is lifted. Later, Wen and Lee *et al.* proposed a slave-boson field theory, where this redundancy is promoted to a dynamical SU(2) gauge theory away from half filling [139, 140, 141]. The advantage of the SU(2) slave-boson approach is that it incorporates strong correlations when gauge fluctuations around the mean-field saddle points are included. Integrating over all gauge-field configurations in this approach enforces the Gutzwiller constraint  $n_i < 2$ . The slave-boson mean-field theory is then not restricted to low temperatures.

The SU(2) approach to the  $t$ - $J$  model predicts that a state with staggered magnetic fluxes through the plaquettes of the square lattice is close in energy to the  $d$ -wave superconductor at low doping [126, 139, 140]. In fact, a staggered local SU(2) rotation on nearest-neighbor sites transforms the  $d$ -wave superconductor (SC) into the staggered-flux (SF) state. These two states are identical at half filling. At small doping, one expects the local symmetry to be weakly broken, and the SU(2) rotation provides a route to construct a low-lying non-superconducting variational state of the weakly doped  $t$ - $J$  model. This led to the proposal by Wen and Lee

that the pure SF state should be realized inside vortex cores of HTSC [126]. Indeed, it was confirmed numerically that the Gutzwiller-projected SF state is a very competitive variational state for the  $t$ - $J$  model [34]. Further support for the SU(2) approach came from the discovery of SF correlations in the Gutzwiller-projected  $d$ -wave superconductor [142].

In this work, we restrict ourselves to the so-called “staggered  $\theta$ -mode” which interpolates between the SC and the SF states [143]. As the temperature is increased through  $T_c$  in the underdoped compounds, vortices proliferate and eventually destroy the phase coherence. In order to form energetically inexpensive vortices in the superconductor, the order parameter rotates to the SF state inside the cores. However, in contrast to vortex cores, we do not expect a pure SF state to be realized in the bulk. The PG state should be viewed as a thermal average over different intermediate states between the SF and the SC state, parameterized by appropriate SU(2) rotations.

In the superconducting phase at low temperature, it is sufficient to include Gaussian fluctuations away from the superconducting state. In this framework, Honerkamp and Lee found that coupling to the Gaussian  $\theta$ -mode strongly depletes the antinodal quasiparticles [144]. This is in contrast to zero temperature, where Gutzwiller-projected excitations show rather weak reduction of spectral weight in the antinodal region as I have shown in Section 3.3. At temperatures between  $T_c$  and  $T^*$ , strong fluctuations towards the SF state are expected to affect the electronic spectral functions even more. In the present work, we are interested in the electron spectral intensities in the pseudogap region, i.e. in the presence of large fluctuations of the order parameter between the SC and the SF states.

Our model bears some similarity to the  $\sigma$ -model approach for the SU(2) gauge theory of the  $t$ - $J$  model, introduced by Lee *et al.* [3, 140]. In contrast to these authors, we do not use a self-consistent mean-field treatment, but we consider an effective model with input from Gutzwiller-projected variational wavefunctions of the  $t$ - $J$  model.

A complementary study was conducted by Honerkamp and Lee who considered SU(2)-fluctuations in an inhomogeneous vortex liquid [145]. These authors computed the density of states and helicity modulus, and found that a dilute liquid of SF vortices would account for the large Nernst signal observed in the pseudogap phase [146]. In the present work, we are particularly interested in the implications of the fluctuating-staggered-flux scenario for the ARPES spectra.

Finally, let us note that our model concerns the low-energy spectra of cuprate superconductors,  $|\omega| \lesssim 200$  meV. The interesting high-energy anomalies ( $|\omega| \simeq 0.4 - 1$  eV) which were discovered in recent experimental [147, 148] and theoretical [103] works are not in the scope of the current discussion.

The remaining part of Section 3.4 is organized in the following way. In Section 3.4.2, we introduce the model and describe the observable (the spectral function) that we want to study. In Section 3.4.3, we give a detailed account on the spectra of the pure (unaveraged)

states. Finally, in Section 3.4.4 we present our results for the averaged spectral functions and in Section 3.4.5 we discuss the experimental implications.

### 3.4.2. The model

The local SU(2) rotation for the  $t$ - $J$  model [3] is conveniently written using spinon doublets in the usual notation,  $\psi^\dagger = (c_\uparrow, c_\downarrow^\dagger)$ . In terms of these doublets, the SF state is defined by the mean-field Hamiltonian  $H_{SF} = \sum_{\langle i,j \rangle} \psi_i^\dagger U_{ij}^{SF} \psi_j - \mu \sum_i \psi_i^\dagger \sigma_3 \psi_i$  where  $U_{ij}^{SF} = -\chi \sigma_3 - i \Delta (-)^{i_x+j_y}$ ,  $\sigma_\alpha$  are the Pauli matrices, and the sum  $\langle i, j \rangle$  is taken over pairs of nearest-neighbor sites of the square lattice. In this work, we restrict ourselves to the following SU(2) rotation,  $U_{ij} \rightarrow g_i^\dagger U_{ij} g_j$ , with  $g_j = e^{i(-)^j \frac{\theta}{2} \sigma_1}$ . Note that for  $\theta = \frac{\pi}{2}$ , the SF Hamiltonian is rotated to a  $d$ -wave superconductor,  $U_{ij}^{SF} \rightarrow U_{ij}^{SC} = -\chi \sigma_3 + \Delta (-)^{i_x+j_x} \sigma_1$ . The intermediate states for general  $\theta$  contain both  $d$ -wave pairing and staggered fluxes through the plaquettes of the square lattice.

We now consider the mean-field Hamiltonian at the intermediate values of  $\theta$  between 0 and  $\pi$ :

$$H_{MF}(\theta) = \sum_{\langle i,j \rangle} \psi_i^\dagger g_i^\dagger(\theta) U_{ij}^{SF} g_j(\theta) \psi_j^\dagger - \chi' \sum_{\langle\langle i,j \rangle\rangle} \psi_i^\dagger \sigma_3 \psi_j - \mu \sum_i \psi_i^\dagger \sigma_3 \psi_i. \quad (3.48)$$

As usual, the chemical potential  $\mu$  is added to enforce the desired average particle number. We have also added a phenomenological next-nearest-neighbor hopping  $\chi'$ . Note that the parameters  $\chi$ ,  $\chi'$ , and  $\Delta$  of the Hamiltonian (3.48) are the effective parameters describing the variational ground state and quasiparticle spectrum of the  $t$ - $J$  model, for the physically relevant values  $t \simeq 3J$ . For example, the hopping  $\chi$  only weakly depends on doping (at small doping) and is approximately given by  $\chi \simeq \frac{t}{3} \simeq 100$  meV [33, 99, 101]. At 10% doping,  $\Delta/\chi$  decreases slightly from  $\sim 0.25$  in the SC state to  $\sim 0.2$  in the SF state<sup>18</sup> [34].

The value of the next-nearest-neighbor hopping is taken to be  $\chi' = -0.3\chi$ , to mimick the experimental Fermi surface observed in cuprates. Earlier studies of Gutzwiller-projected wavefunctions suggest that such an effective next-nearest-neighbor hopping may appear in the underdoped region as a consequence of strong correlations, even in the absence of the term in the physical Hamiltonian (see Section 3.3 and Refs. [102, 124]). Note that we keep this term unrotated in (3.48).

<sup>18</sup>For the numerical averaging, we interpolate the order parameter  $\Delta$  in  $s = \cos\theta$  as  $\Delta(s) = \sqrt{\Delta_{s=1}^2 s^2 + \Delta_{s=0}^2 (1-s^2)}$ . From the variational procedure in Ref. [34], at  $t = 3J$  and 10% doping, the SF and SC variational values of the order parameter are not exactly identical:  $\Delta_{s=1} \simeq 0.2$  and  $\Delta_{s=0} \simeq 0.25$ , respectively. This weak dependency of the order parameter on  $s$  is not important for the main conclusions of our study.



In our model, physical quantities at finite temperature are given by an appropriate functional integral over the mean-field parameters  $U_{ij}$ , weighted by a free energy which is almost flat in the directions parameterized by  $g_j$ . As indicated earlier, we restrict our study to staggered SU(2) rotations parameterized by the angle  $\theta$ . At the same time, we neglect the amplitude fluctuations of the order parameter  $\Delta$ , since the energy scale associated with these fluctuations is high – of the order of  $T^*$ , in our approach. On the other hand, the energy scale  $\varepsilon_c = E_{SF} - E_{SC}$ , responsible for the  $\theta$ -fluctuations, is much lower – at 10% doping it is estimated as  $\varepsilon_c \simeq 0.02J \simeq 30K$  (per lattice site) from variational Monte Carlo calculations [34].

The free energy describing classical fluctuations of  $\theta$  can be written in terms of a  $\theta$ -dependent “condensation energy” (of order  $\varepsilon_c$ ) and a gradient term  $\rho(\nabla\theta)^2$  [145]. We assume a situation where the resulting correlation length  $\xi = \sqrt{\rho/\varepsilon_c}$  is much larger than one lattice spacing.<sup>19</sup> In this case, the characteristic temperature, below which the condensation energy selects the superconducting state over the staggered-flux one, is  $T_c \sim \rho/\ln \xi$  (the same scale determines the temperature of the Kosterlitz-Thouless-type transition).<sup>20</sup> For temperatures above that scale but below  $\rho$ ,

$$\rho/\ln \xi < T < \rho, \quad (3.49)$$

the order parameter slowly varies in space and takes all possible values related by SU(2) rotations. Therefore, in this temperature range, we can approximate the classical fluctuations by an equal-weight statistical average over the uniform states with all possible values of  $\theta$ . The corresponding integration measure for  $\theta$  is  $\int_0^1 d(\cos \theta)$ , inherited from the invariant measure on SU(2).

We calculate the spectral function  $A_{\mathbf{k}}^\theta(\omega) = -\frac{1}{\pi} \text{Im} G(\mathbf{k}, \omega + i\Gamma)$  where  $G$  is the single-particle Green’s function<sup>21</sup> of  $H_{MF}$ , Eq. (3.48). Note that  $\omega$  is measured with respect to the Fermi energy throughout Section 3.4. As explained above, the spectra in the pseudogap phase are modeled by the averages of this spectral function over the order-parameter space,  $A_{\mathbf{k}}(\omega) = \int_0^1 d(\cos \theta) A_{\mathbf{k}}^\theta(\omega)$ . The spectral functions of the pure states [ $A_{\mathbf{k}}^\theta(\omega)$ ] are sums of delta functions. After averaging, the spectral functions acquire an intrinsic width. In addition, we introduce a lifetime broadening  $\Gamma$  to make the figures more readable.

<sup>19</sup>For simplicity, we do not distinguish between the two stiffnesses: for  $\theta$  and for the superconducting phase.

We assume them to be of the same order and much larger than  $\varepsilon_c$ . This assumption does not fully agree with earlier numerical calculations with Gutzwiller-projected wavefunctions (where the superfluid stiffness was estimated of the same order as  $\varepsilon_c$ ) [34], but is consistent with the experimental estimates of  $\xi$  of order 5-10 lattice spacings. See, e.g., S. H. Pan *et al.*, Phys. Rev. Lett. **85**, 1536 (2000) or I. Maggio-Aprile *et al.*, *ibid.* **75**, 2754 (1995).

<sup>20</sup>Y. Okwamoto, J. Phys. Soc. Japan **53**, 2434 (1984); A. S. T. Pires, Phys. Rev. B **50**, 9592 (1994).

<sup>21</sup>Note that the unit cell for  $H_{MF}$  [Eq. (3.48)] contains two sites. Therefore, one may define the normal Green’s function as a  $2 \times 2$  matrix. However, for comparison with the ARPES intensity, we are considering here the Green’s function  $G(t) = i\theta(t) \langle \{c_{\mathbf{k}}(t), c_{\mathbf{k}}^\dagger(0)\} \rangle$  which corresponds to the sum over all entries of the matrix Green’s function. Since  $H_{MF}$  is a quadratic model,  $G(\mathbf{k}, \omega)$  (and its spectral function) is independent of temperature. The intensity measured in direct photoemission at finite temperature is given by this spectral function times the Fermi distribution, see Sect. 3.1.1.

### 3.4.3. Pure states

In order to understand the averaged spectral function, we first outline how the intermediate states evolve as  $s = \cos \theta$  is increased from  $s = 0$  (SC state) to  $s = 1$  (SF state). In Fig. 3.8, we plot the FS (more precisely the Luttinger surface)<sup>22</sup> and the spectral intensity at the Fermi energy. As the parameter  $s$  is increased from 0, the BCS FS gradually deforms to the well-known pocket around  $(\frac{\pi}{2}, \frac{\pi}{2})$  of the SF state. However, the points on the SC FS where it crosses the diagonal  $(\pi, 0)$ - $(0, \pi)$  do not move as  $s$  is changed. We will call them *SU(2)-points*, because at these points, the full SU(2) symmetry is intact even away from half filling. We will comment more on this later. As we increase  $s$ , the SC gap, symmetric with respect to the Fermi level, decreases and closes at  $s = 1$  [ $\Delta_{SC} = 2(\cos k_x - \cos k_y) \Delta \sqrt{1 - s^2}$ ]. At the same time, the SF gap opens on the diagonal  $(\pi, 0)$ - $(0, \pi)$  at the energy  $\omega \simeq -\tilde{\mu}$  [we define  $\tilde{\mu} = \mu - 2\chi' \cos k_x \cos k_y$ ]. The SF gap value is  $\Delta_{SF} \simeq 2(\cos k_x - \cos k_y) \Delta s$ . The spectral weight is transferred among the four bands and all of them gain intensity in the intermediate states. However, in most parts of the zone, there is only a single strong band.

The SU(2)-points we mentioned in the last paragraph belong in fact to SU(2)-surfaces (see illustration in Fig. 3.7) where  $\tilde{\mu} = 0$ . On these surfaces, the full SU(2) symmetry is intact even away from half filling, in the sense that the mean-field spectra are degenerate and independent of  $s = \cos \theta$  [if we neglect the weak dependency  $\Delta(s)$ ].

A schematic plot of the band structure and an illustration of the spectral-weight transfer as we go from the SC to the SF state is shown in Figs. 3.9, 3.10, and 3.11 on cuts parallel to the nodal direction  $(0, 0)$ - $(\pi, \pi)$ . The behaviour is qualitatively similar for all parallel cuts. The strong weights stay on the respective bands as they continuously move, except in a small stripe between the diagonal  $(0, \pi)$ - $(\pi, 0)$  and the SC FS, outside the SF pocket (Regions II and III in Fig. 3.7). In Region II ( $\tilde{\mu} < 0$ ), the strong SC band at positive energy transfers some of its weight to the SF band at negative energy (see Fig. 3.10). Here, the midpoint of the SF bands lies at positive energy. In Region III ( $\tilde{\mu} > 0$ ), the strong SC band at negative energy transfers its weight to the SF band at positive energy (see Fig. 3.11). The midpoint of the SF bands is now shifted below the Fermi energy.

<sup>22</sup>Known subtleties and discrepancies in the various definitions of the experimental FS [111, 112] are not in the scope of this discussion; here, we use the theoretically well-defined Luttinger surface where the mean-field Green's function changes sign,  $G(\mathbf{k}_F, 0) = 0, \pm\infty$  [110]. The Green's function described in Footnote ?? is used.

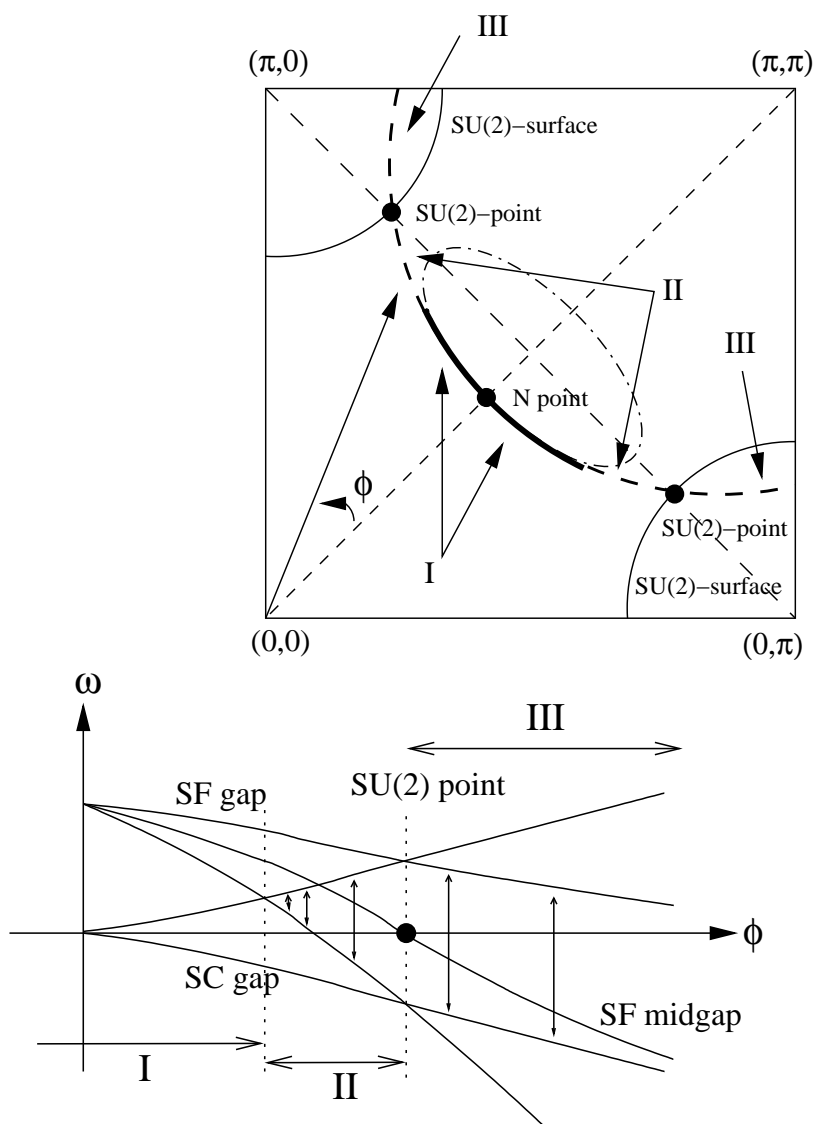


**Figure 3.7.:** Schema of the different regions of the Fermi surface. The SC and SF gaps open near the node (N-point) where they are small and do not overlap. The Fermi surface appears as a gapless arc in Region I. In Region II, the two gaps start to overlap and form an effective gap which is shifted upwards in energy (vertical arrows). The effective gap comes down in energy as we go towards the antinode in Region II. Exactly at the SU(2)-points on the diagonal  $(0, \pi)$ - $(\pi, 0)$ , the effective gap is symmetric. Beyond the SU(2)-points (Region III), the midgap is shifted below the Fermi energy.

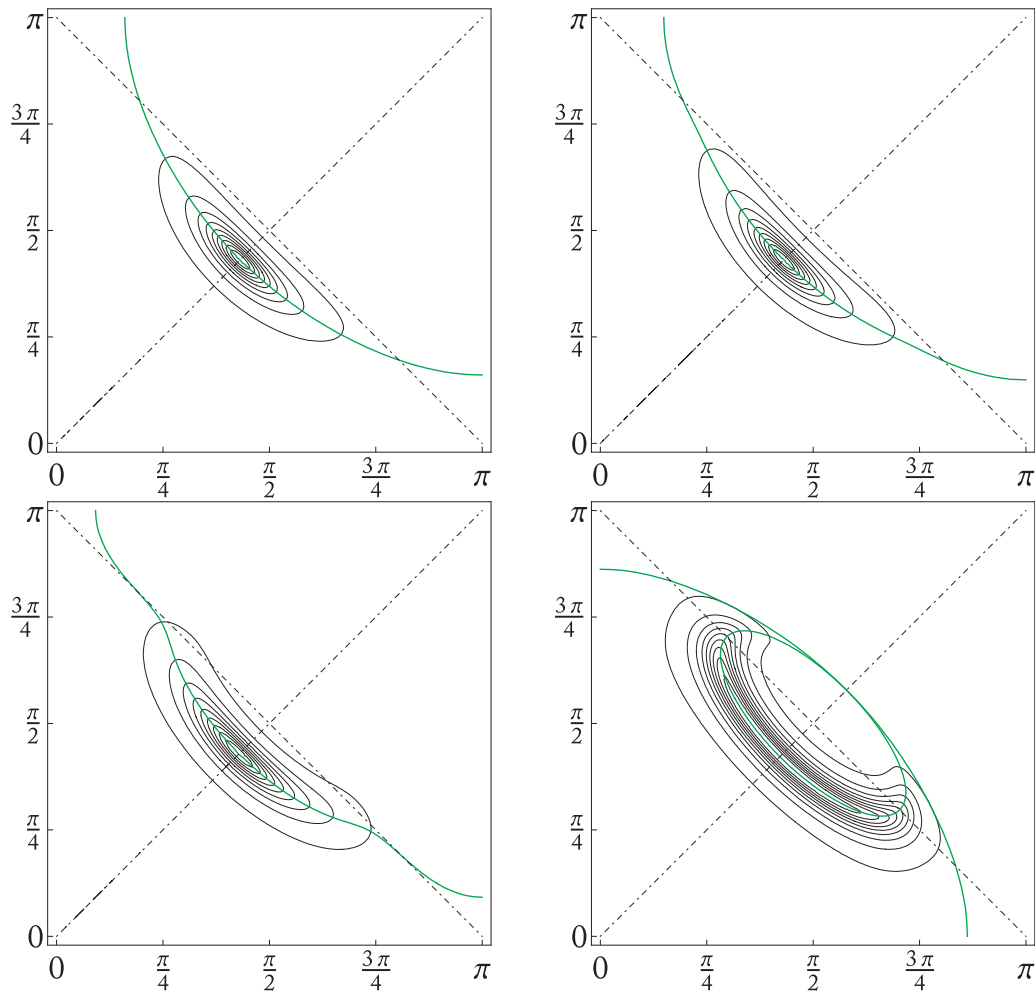


**Figure 3.8.:** Contour plot of the spectral intensity at the Fermi energy for the pure states. Doping is 10% and we use a lifetime broadening  $\Gamma = 0.2\chi$ . The solid line (green) represents the location of the Fermi surface where the Green's function changes sign. From upper left to lower right, we have  $\cos \theta = 0, \frac{1}{3}, \frac{2}{3}, 1$ . The upper-left plot shows the spectrum of the  $d$ -wave superconductor, the lower-right plot displays the pure staggered-flux state.

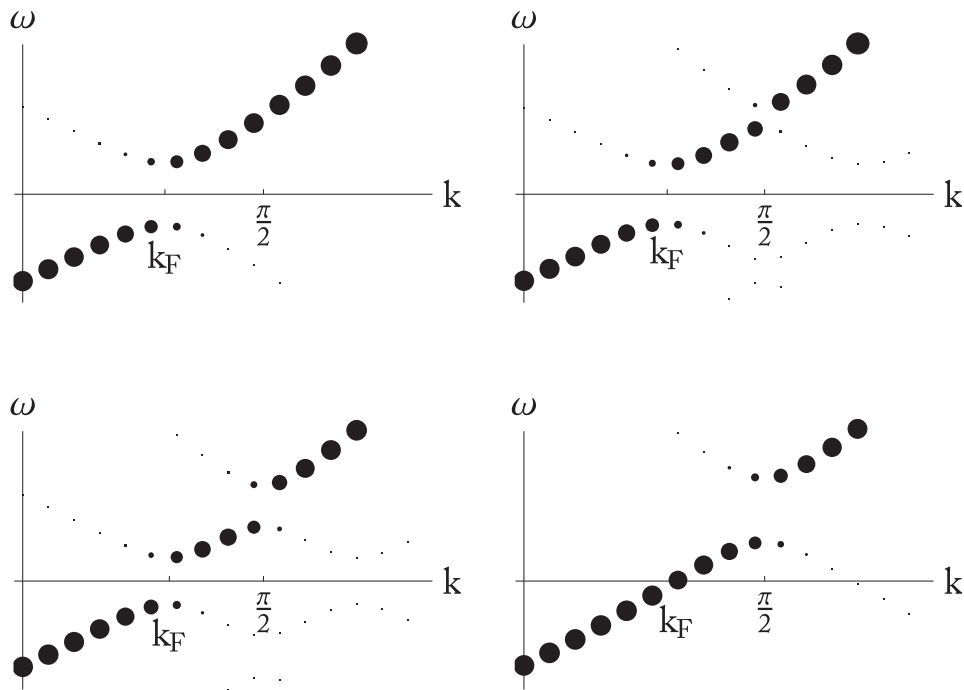


**Figure 3.9.:** Schematic evolution of the spectra along a cut parallel to the nodal direction, inside the pocket (through Region I in Fig. 3.7, e.g. cut  $b$  in Fig. 3.12). The dot size is proportional to the spectral intensity. From upper left to lower right, we have  $\cos \theta = 0, \frac{1}{3}, \frac{2}{3}, 1$ . Upper left is the superconducting state, lower right is the staggered-flux state.

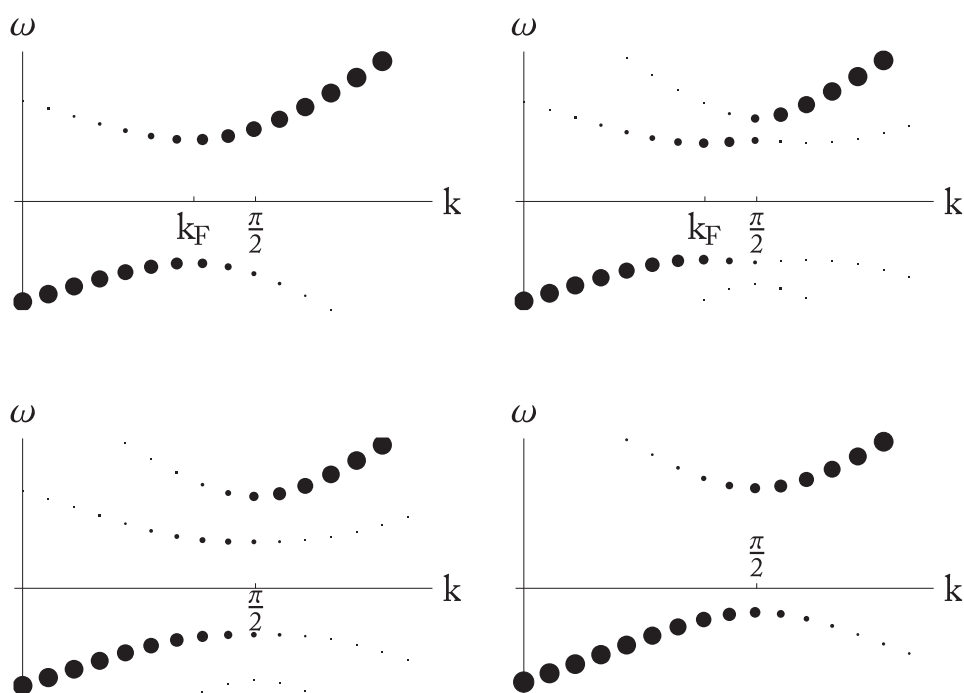


**Figure 3.10.:** Same plot as in Fig. 3.9, but for a cut outside the pocket (through Region II in Fig. 3.7, e.g. cut  $c$  in Fig. 3.12).

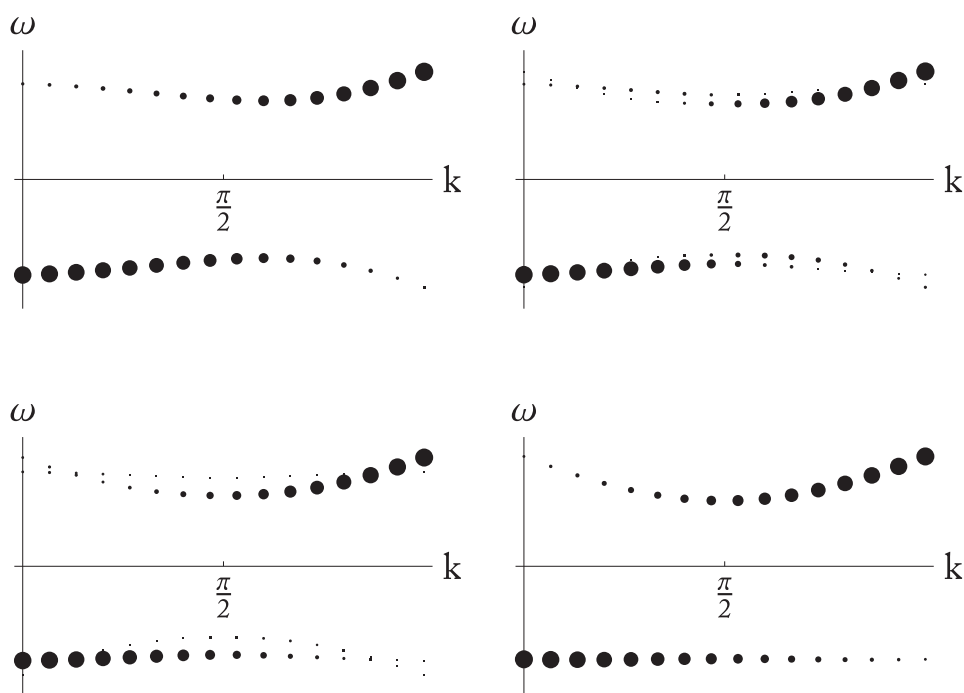


**Figure 3.11.:** Same plot as in Fig. 3.9, but for a cut outside the SU(2)-point (through Region III in Fig. 3.7, e.g. cut  $d$  in Fig. 3.12).

### 3.4.4. Averaged state

The gap considerations in the last section help now to understand the spectral properties of the averaged pseudogap state. If we neglect the weak dependency  $\Delta(s)$ , the average gaps in the pocket region (Region I in Fig. 3.7) may be estimated as  $\langle \Delta_{SC} \rangle \simeq \frac{\pi}{2} \Delta (\cos k_x - \cos k_y)$  and  $\langle \Delta_{SF} \rangle \simeq \Delta (\cos k_x - \cos k_y)$ . In the region outside the pocket, the midgap energy of an effective gap is approximately given by  $-\frac{1}{2} \tilde{\mu}$ . If we are strict with the definition of the effective gap and only consider the truly excitation-free region, then we come to a picture with a gapless arc in Region I and an opening of an effective gap when the two gaps start to overlap in Region II. This effective gap opens above the Fermi energy and comes down as we move towards  $(\pi, 0)$ . At the SU(2)-point, it is symmetric around the Fermi energy. Moving further out in Region III, we find an effective gap with midgap below the Fermi energy (see Fig. 3.7).

In Fig. 3.12, we plot the averaged spectral intensity at the Fermi energy,  $A_{\mathbf{k}}(0)$ , with a quasiparticle lifetime broadening of  $\Gamma = 0.2\chi$ . The “turn in” of the Fermi surface at the pocket edge, which is typical for the pure SF pocket (see lower-right plot in Fig. 3.8), was used in Ref. [149] as an argument against the staggered-flux state since this feature is not seen in experiments. We see here that this “turn in” is completely washed out by the averaging (fluctuations towards the SC state). The “Fermi arc” of the averaged state (arc of high intensity at the Fermi energy; see Fig. 3.12) is clearly bent towards the SC Fermi surface.

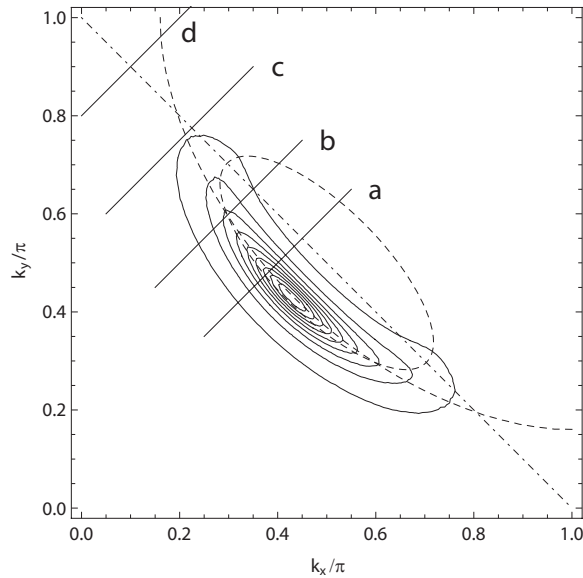


**Figure 3.12.:** Averaged spectral intensity at the Fermi energy,  $A_{\mathbf{k}}(0)$ . Doping is 10% and we use a lifetime broadening  $\Gamma = 0.2\chi$ . The dashed lines are the Fermi surfaces of the SF and SC states, respectively. The full spectra on the cuts  $a$  to  $c$  are given in Figs. 3.13 to 3.16.

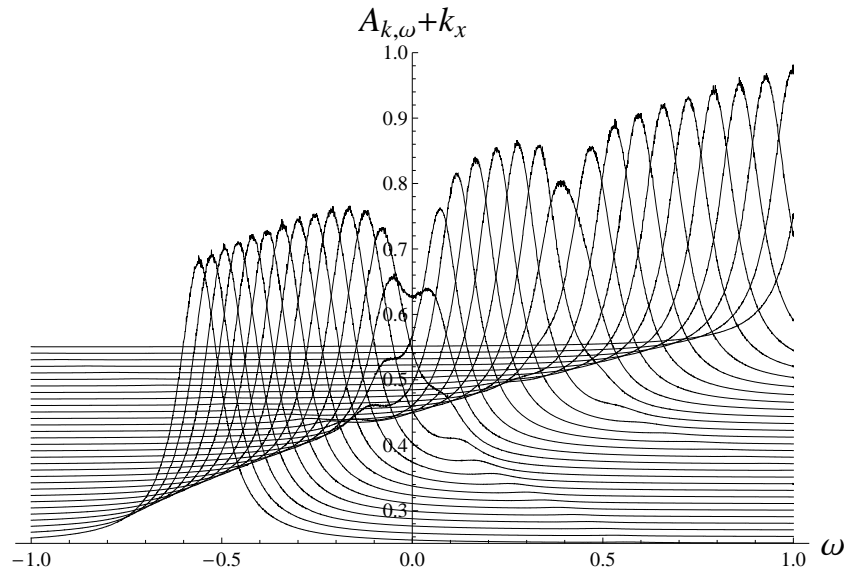


**Figure 3.13.:** Averaged spectral intensity along a cut in the BZ parallel to the nodal direction, cut  $a$  in Fig. 3.12. The spectra are set off in  $y$ -direction by  $k_x$  (in units of  $\pi$ ). We use a lifetime broadening  $\Gamma = 0.12\chi$ . The parameters used are  $\Delta(s) = \sqrt{(0.2s)^2 + 0.25^2(1 - s^2)}$  and doping is 10%. The energy is given in units of  $2\chi \simeq 200$  meV, the intensities are in arbitrary units. The Fermi energy is at  $\omega = 0$ .

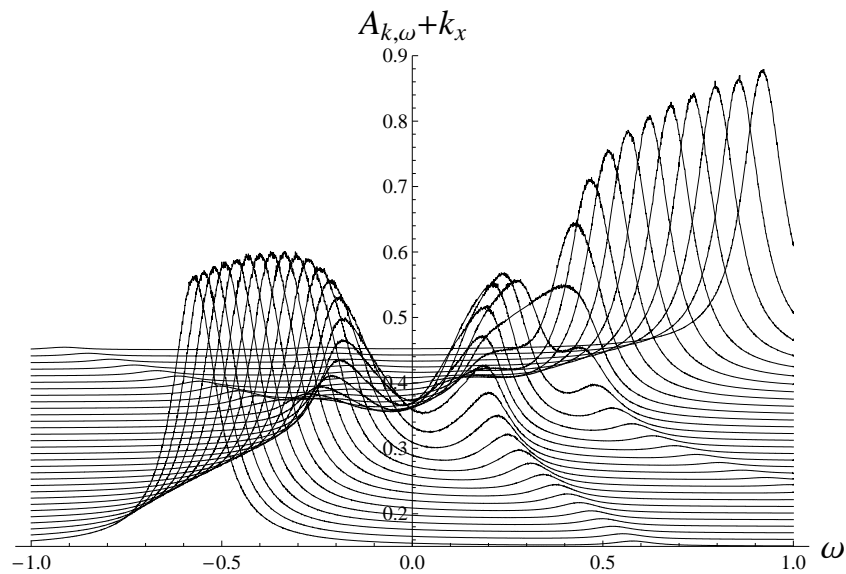


**Figure 3.14.:** Same plot as in Fig. 3.13 but on cut  $b$  in Fig. 3.12.



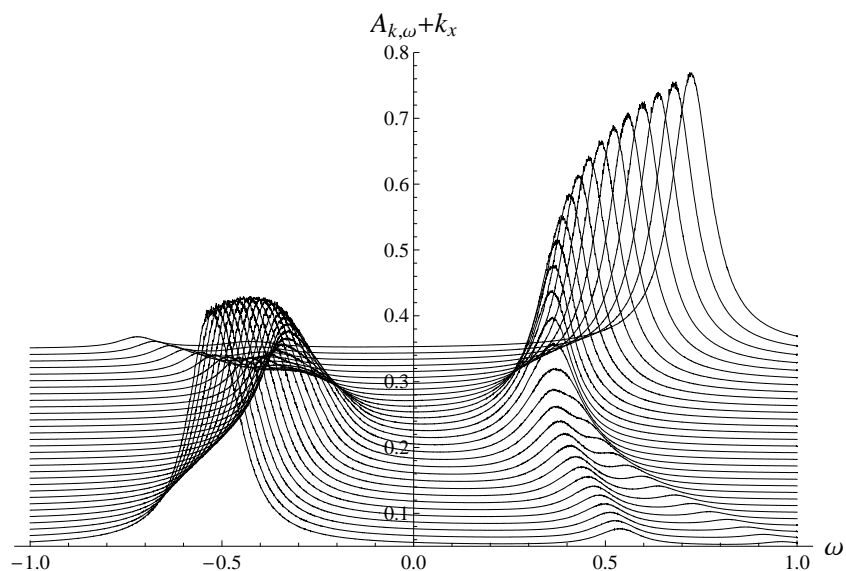


**Figure 3.15.:** Same plot as in Fig. 3.13 but on cut  $c$  in Fig. 3.12. An asymmetric effective gap with midgap above the Fermi energy is formed.

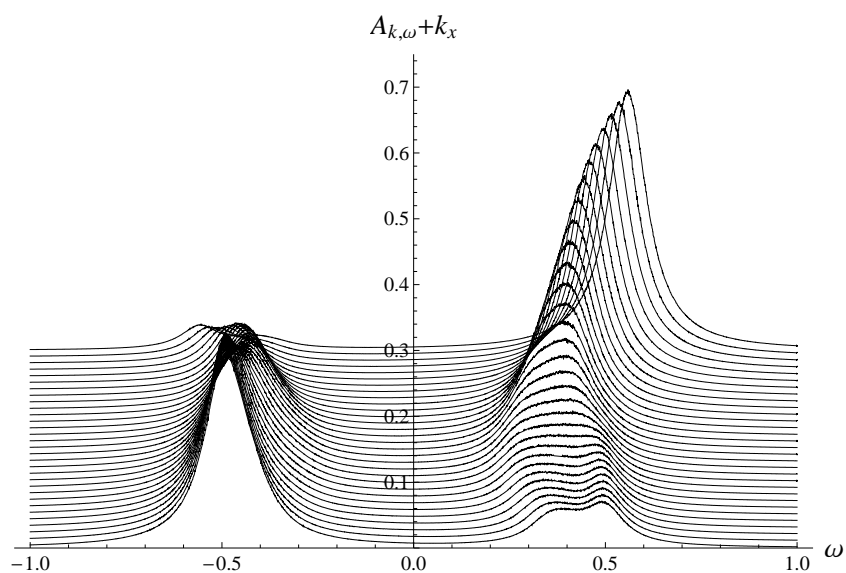


**Figure 3.16.:** Same plot as in Fig. 3.13 but on cut  $d$  in Fig. 3.12. An asymmetric effective gap with midgap below the Fermi energy is formed.

The averaged spectra on the cuts  $a$  to  $d$  in Fig. 3.12 are shown in Figs. 3.13 to 3.16. In addition to the intrinsic width of the averaged state, we have chosen a lifetime broadening of  $\Gamma = 0.12\chi$  in these plots. From the averaged spectral intensities we can confirm what was already anticipated from the pure states:

- (i) In the region near the node, one can see a small symmetric suppression of intensity coming from the superconducting gap centered at the Fermi energy and a very small suppression coming from the staggered-flux gap centered above the Fermi energy. These “gaps” are easily washed out by broadening effects (see Figs. 3.13 and 3.14) and may give rise to a Fermi arc.
- (ii) Outside the arc, the (pseudo-)gap opens asymmetrically, with midgap first above the Fermi energy (Fig. 3.15). Closer to the BZ boundary, as we cross the SU(2)-point, the gap becomes asymmetric with midgap below the Fermi energy (Fig. 3.16). At the SU(2)-point the gap is exactly symmetric (see illustration in Fig. 3.7).
- (iii) The backbending spectra at the edges of the two gaps lead to a doubling of the bands in some locations of the BZ (see Figs. 3.14 and 3.15). This band-doubling only happens for weak branches and at positive energy.

Finally, let us emphasize that the asymmetry we find in this work is in the location of the two pseudogap coherence peaks with respect to the Fermi energy. A different asymmetry in the renormalization of the coherent spectral weights in the superconducting state at low doping has been reported in recent variational Monte Carlo calculations, where the Gutzwiller constraint  $n_i < 2$  is taken into account exactly (see Section 3.3 and Refs. [102, 103, 105]). We expect that such a spectral-weight asymmetry is also present in our model (if one includes the Gutzwiller projection), but a confirmation would require an extensive numerical work.

### 3.4.5. Experimental implications

The intensity measured in ARPES experiments is given by  $I(\mathbf{k}, \omega) = I_0(\mathbf{k})f(\omega)A_{\mathbf{k}}(\omega)$  where  $f(\omega)$  is the Fermi-Dirac function at a given temperature and  $I_0$  is the ARPES matrix element (see Section 3.1.1). It is experimentally very challenging to construct unbiased methods to measure the spectral function at positive energy ( $\omega > 0$ ) since the measurement must be done at sufficiently low temperatures. Energy-symmetrization of the ARPES spectra [29, 30] is a widely applied procedure, although it uses the assumption of a symmetric spectral function [ $A_{\mathbf{k}}(\omega) = A_{\mathbf{k}}(-\omega)$ ]. Using this assumption, the Fermi-Dirac function can be removed from the experimental intensity,  $I^{sym}(\mathbf{k}, \omega) = I(\mathbf{k}, \omega) + I(\mathbf{k}, -\omega) = I_0(\mathbf{k})A_{\mathbf{k}}(\omega)$ . However, there is no *a priori* reason for the cuprate spectrum to be symmetric in energy. As the staggered-flux scenario analyzed in this section shows, the assumption may be wrong in the pseudogap phase of the cuprates.

The most striking prediction of our model, the formation of a staggered-flux gap above the Fermi energy, is difficult to verify directly in ARPES experiments, because this effect only appears at positive energy, around  $\omega \simeq 100$  meV. On the other hand, our more subtle prediction, the combination of superconducting and staggered-flux gaps into a single asymmetric gap, appearing in the anti-nodal region of cuprates may well be within with current experimental reach. However, it is clear that any energy symmetrization procedure inevitably destroys such signs in the ARPES spectra. A careful explicit removal of temperature- and device-dependent factors from the ARPES intensity will be extremely important in order to detect these effects. We hope that our work will stimulate experimental and theoretical effort in this direction.



## Chapter 4.

# Single hole and vortex excitation in the doped Rokhsar-Kivelson quantum dimer model on the triangular lattice

The main results of this chapter have been published in [93]. For an introduction to quantum dimer models, see Section 2.2.

We consider the quantum dimer model on the triangular lattice doped with mobile holes. We choose the simplest form of the hole-hopping term which involves rearrangement of one dimer. The Hamiltonian reads

$$\begin{aligned} H_{\text{RK+hole}} &= \sum_{\nabla, \hat{\nabla}, \nabla} [-J(|\nabla\rangle\langle\nabla| + |\hat{\nabla}\rangle\langle\hat{\nabla}|) + v(|\nabla\rangle\langle\hat{\nabla}| + |\hat{\nabla}\rangle\langle\nabla|)] \\ &\quad + \sum_{\Delta, \nabla} [-t(|\Delta\rangle\langle\Delta| + |\nabla\rangle\langle\nabla|) + 2u|\Delta\rangle\langle\nabla|] \\ &= H_{\text{RK}} + H_t, \end{aligned} \tag{4.1}$$

where the first sum is performed over all three orientations of rhombi and the second sum is over both up and down triangles and over all three possible positions of the hole on the triangle.

We consider the model [Equation (4.1)] at the RK point,  $J = v = 1$ , in the sector with a single hole. At  $t = u \geq 0$ , the Hamiltonian has the usual “supersymmetric” properties of the RK point: Its ground state is exactly known and given by the equal-amplitude superposition of all possible states [64], and the quantum mechanics can be mapped onto a classical stochastic dynamics in imaginary time [69]. We further consider the hole term  $H_t$  as a perturbation in  $t \ll 1$ ,  $u \ll 1$ . To simplify the formulas, we assume  $u = t \geq 0$ , but our results are extendable to  $u \neq t$ .

In the unperturbed Hamiltonian  $H_{\text{RK}}$ , the position of the hole  $x$  is a static parameter. We consider the hole on the infinite lattice (or, equivalently, on a large finite lattice far from the boundary). In such a setup there are two degenerate ground states of  $H_{\text{RK}}$  for each hole

position. They correspond to two disconnected (topological) sectors  $\mathcal{H}_x^\pm$  of the Hilbert space, characterized by the values  $\pm 1$  of the vison operator

$$V_x = (-1)^{\# \text{ of dimers intersecting } \Gamma_x}, \quad (4.2)$$

for some path  $\Gamma_x$  connecting the hole position  $x$  to infinity (in a finite system to the boundary) [81, 84]. The corresponding ground states are given by the sums over all dimer coverings in the respective topological sector and are denoted as  $\psi_0^\pm(x)$ . Note that while the labeling  $\pm$  of the two sectors  $\mathcal{H}_x^\pm$  depends on the choice of the path  $\Gamma_x$ , the sectors themselves do not. Changing the path  $\Gamma_x$  amounts to possible interchanges  $\mathcal{H}_x^+ \leftrightarrow \mathcal{H}_x^-$  and, therefore,  $\psi_0^+(x) \leftrightarrow \psi_0^-(x)$ . This ambiguity reflects the  $Z_2$  degree of freedom in labeling the topological sectors, and it will play an important role in the motion of the hole with a trapped vison. Technically, this  $Z_2$  gauge may be fixed by specifying (arbitrarily), for each  $x$ , a reference dimer covering which belongs to  $\mathcal{H}_x^+$ .

The two topological sectors  $\mathcal{H}_x^\pm$  differ by the parity of the dimer intersection at infinity and hence are indistinguishable by any local operator (since all correlation functions are short-ranged in the RK model on the triangular lattice [79, 63]). Therefore, for excitations obtained from the ground states by local operators (in the vicinity of  $x$ ), one can establish a one-to-one linear mapping between the states in  $\mathcal{H}_x^+$  and in  $\mathcal{H}_x^-$ . Taking odd and even combinations of the corresponding states  $\psi^+(x) \pm \psi^-(x)$ , we obtain the decomposition of the Hilbert space into even and odd sectors  $\mathcal{H}_x^{e,o}$ . Those even and odd sectors correspond to the non-vison and vison sectors of excitations, respectively, introduced in Ref. [76].

The key observation for our discussion is that the Hamiltonian [Equation (4.1)] preserves the decomposition into  $\mathcal{H}_x^{e,o}$  at every point  $x$ . While it is obviously true for  $H_{RK}$  and the potential part of  $H_t$ , one can also easily check that the hopping part of  $H_t$  does not have matrix elements between  $\mathcal{H}_x^e$  and  $\mathcal{H}_{x'}^o$  for neighboring sites  $x$  and  $x'$ . Hence, the excitations of the moving hole can also be classified into two branches: the non-vison branch [contained in  $\oplus_x \mathcal{H}_x^e$ ] and the vison branch [contained in  $\oplus_x \mathcal{H}_x^o$ ]. This splitting into even (non-vison) and odd (vison) branches is a generic feature of any perturbative mixing of topological sectors in quantum dimer models.

## 4.1. Non-vison excitation branch

The energy spectrum of the non-vison branch can be calculated to first order in the perturbative expansion in  $H_t$ . We can fix the phases of all RK ground states  $\psi_0^e(x) = \psi_0^+(x) + \psi_0^-(x)$  by taking the linear combination of all dimer coverings with the amplitude one (up to normalization). Then, the problem of the moving hole maps onto the tight-binding model with the hopping amplitude

$$t_1 = -\langle \psi_0^e(x) | H_t | \psi_0^e(x') \rangle \quad (4.3)$$

for nearest-neighbor  $x$  and  $x'$  (here and in the following we always assume normalized states). This amplitude may be converted into an expectation value in the RK model with a static hole,

$$t_1 = 2t \langle \psi_0(x) | \Delta \rangle \langle \Delta | \psi_0(x) \rangle = 2t \frac{N_3}{N_1}, \quad (4.4)$$

where  $N_1$  and  $N_3$  are the numbers of dimer coverings with one site and one three-site triangle removed, respectively. The ratio  $\frac{N_3}{N_1}$  is well defined in the limit of the infinite system and can be computed numerically with a suitable method. We have calculated this coefficient with a Monte Carlo simulation similar to that in Refs. [63] and [76] (using clusters of toroidal geometry with up to  $17 \times 17$  sites), with the result  $\frac{N_3}{N_1} = 0.229 \pm 0.001$ .

Taking into account the potential term in  $H_t$  and performing the Fourier transformation in  $x$ , the dispersion of the hole without a vison takes the form

$$E_{\mathbf{k}} = -2t_1 (\cos k_1 + \cos k_2 + \cos k_3 - 3), \quad (4.5)$$

where  $k_1$ ,  $k_2$ , and  $k_3$  are the projections of the vector  $\mathbf{k}$  on the three lattice directions (with  $k_1 + k_2 + k_3 = 0$ ).

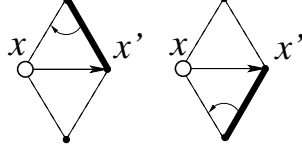


**Figure 4.1.:** These two types of hopping processes set opposite correspondences between the sectors  $\mathcal{H}_x^\pm$  and  $\mathcal{H}_{x'}^\pm$ , and therefore cancel each other in (4.6).

## 4.2. Vison excitation branch

The hopping of a hole with a trapped vison is more complicated. The phases of the odd-sector ground states,  $\psi_0^o(x) = \psi_0^+(x) - \psi_0^-(x)$ , cannot be synchronized invariantly for all  $x$ , which reflects the frustration of the vison motion [76]. The freedom of the  $Z_2$  gauge [the paths  $\Gamma_x$  in (4.2) or, equivalently, the reference dimer configuration for each  $x$ ] corresponds to the choice of the overall sign for the states in  $\mathcal{H}_x^o$ .

Regardless of the chosen  $Z_2$  gauge, the hopping amplitude vanishes to first order,

$$\langle \psi_0^o(x) | H_t | \psi_0^o(x') \rangle = 0 \quad (4.6)$$

for nearest-neighbors  $x$  and  $x'$ . This can be seen as the cancellation of the two types of hopping processes from  $x$  to  $x'$ , corresponding to two possible dimer flips (Fig. 4.1). Each of those dimer flips maps each of  $\mathcal{H}_x^\pm$  into one of  $\mathcal{H}_{x'}^\pm$ . The change in topological sector depends on the chosen gauge, but the correspondence between the two sectors  $\mathcal{H}_x^\pm$  and the two sectors  $\mathcal{H}_{x'}^\pm$  is opposite for the two types of flips. As a result, the corresponding processes connecting two ground states  $\psi_0^o(x)$  and  $\psi_0^o(x')$  exactly cancel each other.<sup>1</sup>

A nontrivial hopping appears only to higher order in perturbation theory for some trajectories. The second-order hopping amplitude

$$t_2 = \sum_{x', n \neq 0} \frac{1}{E_n} \langle \psi_0^o(x) | H_t | \psi_n^o(x') \rangle \langle \psi_n^o(x') | H_t | \psi_0^o(x'') \rangle \quad (4.7)$$

involves excitations  $\psi_n^o(x')$  of  $H_{RK}$  with energies  $E_n$ .

Similarly to the cancellation of the nearest-neighbor hopping amplitude to first order in perturbation, one can show the cancellation to second order of the hopping processes  $x \rightarrow x' \rightarrow x''$  connecting nearest-neighbor and next-nearest-neighbor sites [processes (a) and (b) in Fig. 4.2]. One can verify that, in those cases, processes symmetric with respect to the line  $xx''$  exactly cancel each other.

---

<sup>1</sup>For an explicit derivation, see [94].



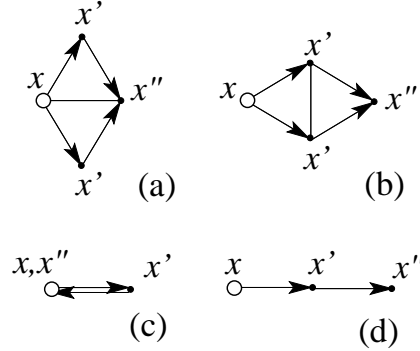


**Figure 4.2.:** The two trajectories of the hole exactly cancel each other in the second order of the perturbation theory [Equation (4.7)] for (a) nearest-neighbor and (b) next-nearest-neighbor hoppings. The non-vanishing second-order terms are (c) on-site and (d) next-next-nearest-neighbor hoppings.

The only nontrivial hopping in the second order occurs for trajectories  $x \rightarrow x' \rightarrow x''$  involving two links along the same direction [i.e., for the on-site energy correction and for the next-next-nearest-neighbor hopping, processes (c) and (d) in Fig. 4.2]. The corresponding next-next-nearest-neighbor hopping amplitude [Fig. 4.2(d)] to second order in perturbation [Equation (4.7)] may be expressed via dynamic correlation functions in the RK model with a static hole at position  $x'$ ,

$$\begin{aligned}
 t_2 &= \int_0^\infty d\tau \langle \psi_0^o(x) | H_t e^{-\tau H_{RK}} H_t | \psi_0^o(x'') \rangle \\
 &= t^2 \int_0^\infty d\tau I(\tau),
 \end{aligned} \tag{4.8}$$

where

$$I(\tau) = \langle \psi_0(x') | P_{xx'} e^{-\tau H_{RK}} P_{x'x''} | \psi_0(x') \rangle \tag{4.9}$$

and

$$\begin{aligned}
 P_{xx'} &= |\Delta\rangle\langle\Delta| - |\nabla\rangle\langle\nabla| \\
 P_{x'x''} &= |\nabla\rangle\langle\nabla| - |\Delta\rangle\langle\Delta|.
 \end{aligned} \tag{4.10}$$

The dynamic correlation function  $I(\tau)$  is well defined in the limit of infinite system size and does not depend on the topological sector in this limit. It may be computed with a classical Monte Carlo method as in Ref. [76]. Using clusters of toroidal geometry and up to  $17 \times 17$  sites, we find  $\int_0^\infty d\tau I(\tau) = -1.51 \pm 0.08$  (observe that it is negative).

Note that the sign of  $t_2$  in (4.8) corresponds to a particular relative gauge choice at points  $x$  and  $x''$ : the reference dimer coverings at  $x$  and  $x''$  are connected by two dimer flips on

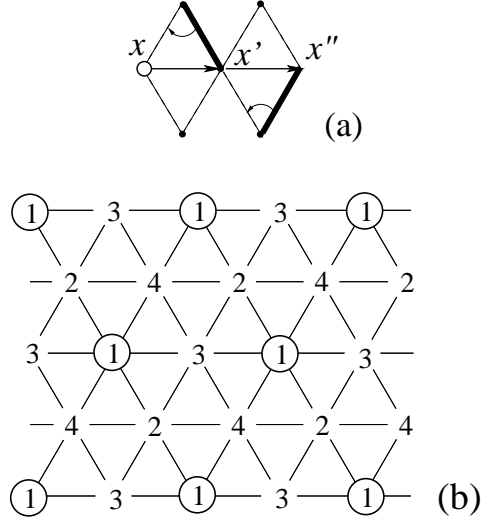


**Figure 4.3.:** (a) We fix the relative gauge at the next-next-nearest-neighbor sites by relating the reference configurations in  $\mathcal{H}_x^+$  and  $\mathcal{H}_{x''}^+$  via two consecutive dimer flips on opposite sides of the line  $xx'x''$ . (b) The four sublattices connected by the hopping of the vison-hole bound state. This composite excitation can only hop by multiples of two lattice periods.

opposite sides of the line  $xx'x''$  (Fig. 4.3). One can show that this local gauge convention for any two sites separated by two lattice periods can be consistently extended to a global gauge on the sublattice of such sites (with the period of this sublattice equals twice that of the original lattice). There are four such sublattices (Fig. 4.3), and the hole-vison excitation hops on each of them independently, without a possibility to cross over to another sublattice. The resulting dispersion relation is that of the tight-binding model with the doubled lattice constant and the hopping amplitude given by (4.8),

$$E_{\mathbf{k}}^{(v)} = -2t_2(\cos 2k_1 + \cos 2k_2 + \cos 2k_3) + \varepsilon_0. \quad (4.11)$$

The on-site energy  $\varepsilon_0$  is equal to that in the non-vison sector in (4.5). To leading order in  $t$ , it is given by  $\varepsilon_0 = 6t_1$ .

The hole-vison excitations with dispersion (4.11) are quadruply degenerate (by sublattice) for each value of  $\mathbf{k}$  in the Brillouin zone of the doubled lattice. While we have explicitly demonstrated this degeneracy to second order, it can be extended to all orders of perturbation theory. In fact, this degeneracy is determined by the symmetries of the original Hamiltonian [Equation (4.1)] in the vison sector and can thus be promoted from a perturbative argument to the exact spectrum. The exact degeneracy can be proven using the translational invariance of the Hamiltonian, together with the symmetry under point inversion (rotation by  $\pi$ ) and time reversal (see Appendix A). Physically, this degeneracy can be understood as the cancellation of virtual processes for the flux-carrying excitation on the frustrated triangular lattice.

Finally, let us note that, while our derivation of the vison-hole spectrum was formally done at the RK point, its form and degeneracy are the same in the whole liquid phase away from the RK point (estimated to extend to the region  $0.8 \lesssim \frac{v}{J} \leq 1$  in Ref. [80]), provided the hole hopping is small. Only the numerical coefficients in the hopping amplitudes  $t_1$  and  $t_2$  are modified in this case. Furthermore, our results equally apply when more than one hole is present in the system as long as the holes are sufficiently far apart and do not interact with each other.

### 4.3. Summary

In this chapter, we have calculated the dispersion of a single mobile hole in the RVB liquid phase of the doped RK quantum dimer model on the triangular lattice. We find two branches of excitations: one for the bare hole and the other for a hole-vison bound state. The effective motion of the hole-vison state is strongly modified by the  $Z_2$  flux associated with the vison. Interference effects due to lattice frustration reduce the bandwidth of this type of excitation and lead to additional degeneracies. These are general properties which should be observed in any doped  $Z_2$  RVB liquid on frustrated lattices.

In our specific model [Equation (4.1)], the energy of a *static* ( $t = 0$ ) vison-hole bound state equals that of a hole without a vison. In other words, the vison does not cost any energy if placed in a hole (while in the bulk, its energy is a finite fraction of  $J$ , see Ref. [76]). In the limit of a small hopping amplitude  $t$ , the energy of a static excitation is split, with the bandwidth proportional to  $t$  for the bare hole and to  $\frac{t^2}{J}$  for the hole-vison bound state. As a result, the two branches intersect each other, with the minimum of energy (the ground state) corresponding to the hole without a vison. For some  $\mathbf{k}$  in a region close to the boundary of the Brillouin zone, the vison-hole bound state is lower in energy than the bare hole. In a more general quantum dimer model (or in other RVB-type systems), however, one may imagine the situation where the hole-vison bound state constitutes the ground state (in our dimer model, this may be achieved, for example, by adding ring exchange of dimers around a hole). In such a case, the doped holes spontaneously generate visons, which, in turn, may lead to further interesting effects, e.g., the modification of the statistics of holes [81, 84].



# Appendix A.

## Nonperturbative proof of the 4-fold degeneracy of the vison branch

From perturbative arguments (see Chapter 4) one can understand that the vison-hole bound state can only hop by two sites on a straight line. All the other processes cancel due to vison interference effects. The vison hopping processes that connect the different sublattices cancel each other to all orders in perturbation theory and, as a result, the vison branch is four-fold degenerate. The perturbative argument observes that hopping between different sublattices has always a mirror process and the closed loop in the overlap graph necessarily contains an odd number of sites. For such loops, one can show that the phase is always  $-1$ , hence the interference and cancelation of the two paths.<sup>1</sup>

In this appendix, I want to show that this four-fold degeneracy of the vison branch carries over to the non-perturbative spectrum.

We proceed by showing that the space group representation of the vison must be at least 4 dimensional. By symmetry of the Hamiltonian under the space-group transformations, it follows that the 4 basis states are degenerate in energy and that the exact (non-perturbative) spectrum has this 4-fold degeneracy.

Consider the following symmetry generators of the QDM Hamiltonian on the triangular lattice  $H_{\text{RK+hole}}$  [Equation (2.44)]:

$$T_1 = \text{translation in } x\text{-direction}, \quad (\text{A.1a})$$

$$T_2 = \text{translation in } y\text{-direction}, \quad (\text{A.1b})$$

$$R = \text{rotation around the origin by } \pi, \quad (\text{A.1c})$$

$$C = \text{time reversal}. \quad (\text{A.1d})$$

---

<sup>1</sup>In fact, for finite systems on a torus, the four topological sectors mix due to vison motion around the torus. Since, for a system with a single hole, the lattice must contain an odd number of sites. However, this splitting is exponentially suppressed with system size.

One can see that the space-group operations acting on a state in the vison-hole sector obey the following commutation relations:

$$T_1 T_2 = -T_2 T_1 \quad (\text{A.2a})$$

$$(RT_i)^2 = -1. \quad (\text{A.2b})$$

Let  $|\psi_1\rangle$  be an eigenstate of  $H_{\text{RK+hole}}$ ,  $T_1$ , and  $(T_2)^2$ , with

$$T_1 |\psi_1\rangle = e^{i\phi_1} |\psi_1\rangle \quad (\text{A.3})$$

and

$$(T_2)^2 |\psi_1\rangle = e^{i2\phi_2} |\psi_1\rangle. \quad (\text{A.4})$$

It is clear from (A.2a) that  $|\psi_2\rangle = T_2 |\psi_1\rangle$  is an eigenvector of  $T_2$  with eigenvalue  $-e^{i\phi_1}$ :

$$T_1 |\psi_2\rangle = T_1 T_2 |\psi_1\rangle = -T_2 T_1 |\psi_1\rangle = -e^{i\phi_1} |\psi_2\rangle. \quad (\text{A.5})$$

It follows that  $|\psi_1\rangle$  and  $|\psi_2\rangle$  are linearly independent and, therefore, the translations are at least 2 dimensional when acting on vison states. To complete the matrix representation of  $T_2$ , we have:  $T_2 |\psi_2\rangle = (T_2)^2 |\psi_1\rangle = e^{i2\phi_2} |\psi_1\rangle$ .

We proceed by defining the states  $|\psi_3\rangle = RC|\psi_1\rangle$  and  $|\psi_4\rangle = T_2 |\psi_3\rangle = T_2 RC|\psi_1\rangle$ . Using (A.2) we can again show that these are eigenstates of  $T_1$ :

$$T_1 |\psi_3\rangle = T_1 RC|\psi_1\rangle = -R(T_1)^{-1} C|\psi_1\rangle = -R e^{i\phi_1} C|\psi_1\rangle = -e^{i\phi_1} |\psi_3\rangle \quad (\text{A.6})$$

$$T_1 |\psi_4\rangle = T_1 T_2 |\psi_3\rangle = -T_2 T_1 |\psi_3\rangle = e^{i\phi_1} |\psi_4\rangle. \quad (\text{A.7})$$

In order to show that the 4 states  $|\psi_1\rangle$ ,  $|\psi_2\rangle$ ,  $|\psi_3\rangle$ , and  $|\psi_4\rangle$  are linearly independent, we still need to prove that  $|\psi_2\rangle$  and  $|\psi_3\rangle$ , and  $|\psi_1\rangle$  and  $|\psi_4\rangle$  are not proportional. We show this by contradiction. Suppose  $|\psi_3\rangle = a|\psi_2\rangle$ . It follows that  $|\psi_1\rangle = \bar{a} C R T_2 |\psi_1\rangle = |a|^2 (R T_2)^2 |\psi_1\rangle = -|a|^2 |\psi_1\rangle$ , which is impossible (we have used the fact that  $R T_2$  commutes with complex conjugation). The linear independence of  $|\psi_1\rangle$  and  $|\psi_4\rangle$  can be proven analogously.

We have proven that the space-group matrix representation acting on vison states are 4 dimensional. Their explicit form is

$$\begin{aligned}
 T_1 &= e^{i\phi_1} \begin{pmatrix} 1 & 0 & 0 & 0 \\ 0 & -1 & 0 & 0 \\ 0 & 0 & -1 & 0 \\ 0 & 0 & 0 & 1 \end{pmatrix}, T_2 = e^{i\phi_2} \begin{pmatrix} 0 & e^{i\phi_2} & 0 & 0 \\ e^{-i\phi_2} & 0 & 0 & 0 \\ 0 & 0 & 0 & e^{i\phi_2} \\ 0 & 0 & e^{-i\phi_2} & 0 \end{pmatrix}, \\
 RC &= \begin{pmatrix} 0 & 0 & 1 & 0 \\ 0 & 0 & 0 & -e^{-2i\phi_2} \\ 1 & 0 & 0 & 0 \\ 0 & -e^{2i\phi_2} & 0 & 0 \end{pmatrix}.
 \end{aligned} \tag{A.8}$$

Since these generators are symmetries of the Hamiltonian, we have proven that the exact single hole-vison spectrum is 4-fold degenerate on the triangular lattice.









# Bibliography

- [1] J. Bardeen, L. N. Cooper, and J. R. Schrieffer, *Theory of Superconductivity*, Phys. Rev. **108**, 1175 (1957).
- [2] J. G. Bednorz and K. A. Müller, *Possible High  $T_c$  Superconductivity in the BaLaCuO System*, Z. Phys. B **64**, 189 (1986).
- [3] P. A. Lee, *From HTSC to quantum spin liquids: progress in strong correlation physics*, Rep. Prog. Phys. **71**, 012501 (2008); P. A. Lee, N. Nagaosa, and X.-G. Wen, *Doping a Mott insulator: Physics of HTSC*, Rev. Mod. Phys. **78**, 17 (2006).
- [4] M. Ogata and H. Fukuyama, *The  $t$ - $J$  model for the oxide HTSC*, Rep. Prog. Phys. **71**, 036501 (2008).
- [5] B. Edegger, V. N. Muthukumar, and C. Gros, *Gutzwiller-RVB theory on HTSC: Results from RMFT and VMC calculations*, Adv. Phys. **56**, 927 (2007).
- [6] P. W. Anderson, P. A. Lee, M. Randeria, M. Rice, N. Trivedi and F. C. Zhang, *The physics behind high-temperature superconducting cuprates: the 'plain vanilla' version of RVB*, J. Phys. Cond. Mat. **16**, R755 (2004).
- [7] M. R. Norman and C. Pepin, *The electronic nature of high temperature cuprate superconductors*, Rep. Prog. Phys. **66**, 1547 (2003).
- [8] <http://hoffman.physics.harvard.edu/research/SCintro.php>; see also H. Takahashi: JPSJ Online-News and Comments [Jun. 10, 2008].
- [9] W. H. Weber, C. R. Peters, and E. M. Logothetis, *Raman studies of lanthanum curate superconductors*, J. Opt. Soc. Am. B **6**, 455 (1989).
- [10] D. Vaknin *et al.*, *Antiferromagnetism in  $La_2CuO_{4-y}$* , Phys. Rev. Lett. **58**, 2802 (1987).
- [11] P. W. Anderson, *The Theory of Superconductivity in High- $T_c$  Cuprate Superconductors*, Princeton University Press (1997).
- [12] P. W. Anderson, *Resonating Valence Bond State in  $La_2CuO_4$  and Superconductivity*, Science **235**, 1196 (1987).

- [13] J. Hubbard, Proc. Roy. Soc. A **240**, 539 (1957); J. Hubbard, *ibid.* **243**, 336 (1958); J. Hubbard, *Electron correlations in narrow energy bands*, *ibid.* **276** 238 (1963); J. Hubbard, *ibid.* **277**, 237 (1964); J. Hubbard, *ibid.* **281**, 401 (1964).
- [14] N. F. Mott, *Metal-Insulator Transition*, Rev. Mod. Phys. **40**, 677 (1968).
- [15] P. Fazekas, *Lecture Notes on Electron Correlations and Magnetism*, World Scientific Publishing, Singapore (1999).
- [16] F. C. Zhang and T. M. Rice, *Effective Hamiltonian for the superconduction Cu oxides*, Phys. Rev. B, **37**, 3759(R) (1988).
- [17] W. von der Linden, *A Quantum Monte Carlo approach to many-body physics*, Phys. Rep. **220**, 53 (1992).
- [18] N. D. Mermin and H. Wagner, *Absence of Ferromagnetism or Antiferromagnetism in One- or Two-Dimensional Isotropic Heisenberg Models*, Phys. Rev. Lett. **17**, 1133 (1966).
- [19] P. C. Hohenberg, *Existence of Long-Range Order in One and Two Dimensions*, Phys. Rev. **158**, 383 (1967).
- [20] S. Coleman, *There are no Goldstone bosons in two dimensions*, Commun. Math. Phys. **31**, 259 (1973).
- [21] P. W. Anderson, *Resonating valence bond: a new kind of insulator?*, Mat. Res. Bull. **8**, 153 (1973).
- [22] L. Pauling, *A resonating-valence-bond-theory of metals and intermetallic compounds*, Proc. Roy. Soc. London, A **196**, 343 (1949); *A theory of ferromagnetism*, Proc. N. A. S. **39**, 551 (1953).
- [23] H. Bethe, *Zur Theorie der Metalle. I. Eigenwerte und Eigenfunktionen der linearen Atomkette*, Z. Phys. **71**, 205 (1931).
- [24] T. Giamarchi, *Quantum Physics in One Dimension*, Oxford University Press, 2004.
- [25] J. R. Schrieffer, *Theory of Superconductivity*, Westview Press (1964).
- [26] F. C. Zhang, C. Gros, T. M. Rice, and H. Shiba, *A renormalized Hamiltonian approach to a resonant valence bond wavefunction*, Sup. Sci. Tech. **1**, 36 (1988).
- [27] C. Gros, *Superconductivity in correlated wave functions*, Phys. Rev. B **38** (R), 931 (1988); C. Gros, *Physics of Projected Wavefunctions*, Ann. Phys. (NY) **189**, 53 (1989).
- [28] H. Yokoyama and H. Shiba, *Variational Monte-Carlo studies of Superconductivity in Strongly Correlated Electron Systems*, J. Phys. Soc. Jpn. **57**, 2482 (1988); *Variational Monte-Carlo Studies of Hubbard Model*, *ibid.* **56**, 3582 (1987); *ibid.* **56**, 1490 (1987).

- [29] J. C. Campuzano, M. R. Norman, and M. Randeria, *Photoemission in the high temperature superconductors* in *The Physics of Superconductors*, edited by K. H. Bennemann and J. B. Ketterson (Springer, Berlin, 2004), Vol. II, pp. 167-273.
- [30] A. Damascelli, Z. Hussain, and Z.-X. Shen, *Angle-resolved photoemission studies of the cuprate superconductors*, *Rev. Mod. Phys.* **75**, 473 (2003).
- [31] D. J. Van Harlingen, *Phase-sensitive tests of the symmetry of the pairing state in the high-temperature superconductors – Evidence for  $d_{x^2-y^2}$  symmetry*, *Rev. Mod. Phys.* **67**, 515 (1998).
- [32] C. C. Tsuei and J. R. Kirtley, *Pairing symmetry in cuprate superconductors*, *Rev. Mod. Phys.* **72**, 969 (2000).
- [33] A. Paramekanti, M. Randeria, and N. Trivedi, *Projected Wave Functions and High Temperature Superconductivity*, *Phys. Rev. Lett.* **87**, 217002 (2001); A. Paramekanti, M. Randeria, and N. Trivedi, *High- $T_c$  superconductors: A variational theory of the superconducting state*, *Phys. Rev. B* **70**, 054504 (2004); M. Randeria, A. Paramekanti, and N. Trivedi, *Nodal quasiparticle dispersion in strongly correlated d-wave superconductors*, *ibid.* **69**, 144509 (2004).
- [34] D. A. Ivanov and P. A. Lee, *SF normal state in the weakly doped t-J model*, *Phys. Rev. B* **68**, 132501 (2003); D. A. Ivanov, *AF and phase separation in the t-J model at the low doping: A variational study*, *Phys. Rev. B* **70**, 104503 (2004).
- [35] M. Capello, F. Becca, M. Fabrizio, S. Sorella, and E. Tosatti, *Variational Description of Mott Insulators*, *Phys. Rev. Lett.* **94**, 026406 (2005).
- [36] D. Eichenberger and D. Baeriswyl, *Superconductivity and antiferromagnetism in the two-dimensional Hubbard model: A variational study*, *Phys. Rev. B* **76**, 180504(R) (2007).
- [37] R. B. Laughlin, *Gossamer Superconductivity*, *Phil. Mag.* **86**, 1165 (2006); arXiv:cond-mat/0209269.
- [38] F. C. Zhang, *Gossamer Superconductor, Mott Insulator, and RVB State in Correlated Electron Systems*, *Phys. Rev. Lett.* **90**, 207002 (2003).
- [39] W. Krauth, *Statistical Mechanics: Algorithms and Computations*, Oxford University Press (2006).
- [40] D. Ceperley and G. V. Chester, *Monte Carlo simulation of a many-fermion study*, *Phys. Rev. B* **16**, 3081 (1977).
- [41] B. Edegger, N. Fukushima, C. Gros, and V. N. Muthukumar, *Particle number renormalization in nearly half-filled Mott Hubbard superconductors*, *Phys. Rev. B* **72**, 134504 (2005).

- [42] N. Fukushima, N. Edegger, V. N. Muthukumar, and C. Gros, *Evaluation of matrix elements in partially projected wave functions*, Phys. Rev. B **72**, 144505 (2005).
- [43] N. Fukushima, *Grand-canonical Gutzwiller approximation for magnetic inhomogeneous systems*, Phys. Rev. B **78**, 115105 (2008).
- [44] P. W. Anderson and N. P. Ong, *Theory of asymmetric tunneling in the cuprate superconductors*, J. Phys. Chem. Solids **67**, 1 (2006).
- [45] M. Ogata and A. Himeda, *Superconductivity and Antiferromagnetism in an Extended Gutzwiller Approximation to the  $t$ - $J$  Model: Effect of Double-Occupancy Exclusion*, J. Phys. Soc. Japan **72**, 374 (2003).
- [46] S. Liang, B. Douçot, and P. W. Anderson, *Some New Variational Resonance-Valence-Bond-Type Wave Functions for the Spin- $\frac{1}{2}$  Antiferromagnetic Heisenberg Model on a Square Lattice*, Phys. Rev. Lett. **61**, 365 (1988).
- [47] P. Fazekas, P. W. Anderson, *On the ground state properties of the anisotropic triangular antiferromagnet*, Phil. Mag. **30**, 423 (1974).
- [48] D. A. Ivanov and T. Senthil, *Projected wave functions for fractionalized phases of quantum spin liquids*, Phys. Rev. B **66**, 115111 (2002).
- [49] D. A. Ivanov, *Resonating-valence-bond structure of Gutzwiller-projected superconducting wave functions*, Phys. Rev. B **74**, 24525 (2006).
- [50] B. Sutherland, *Systems with resonating-valence-bond ground states: Correlations and excitations*, Phys. Rev. B **37**, 3786(R) (1988).
- [51] F. Bloch, *Bemerkung zur Elektronentheorie des Ferromagnetismus und der elektrischen Leitfähigkeit*, Z. Phys. **57**, 545 (1929).
- [52] D. J. Klein, *Exact ground states for a class of antiferromagnetic Heisenberg models with short-range interactions*, J. Phys. A **15**, 661 (1982).
- [53] R. R. P. Singh and D. A. Huse, *Ground state of the spin-1/2 kagome-lattice Heisenberg antiferromagnet*, Phys. Rev. B **76**, 180407(R) (2007).
- [54] F. Mila, *Low-Energy Sector of the  $S = 1/2$  Kagome Antiferromagnet*, Phys. Rev. Lett. **81**, 2356 (1998).
- [55] J. S. Helton, K. Matan, M. P. Shores, E. A. Nytko, B. M. Bartlett, Y. Yoshida, Y. Takano, A. Suslov, Y. Qiu, J.-H. Chung, D. G. Nocera, and Y. S. Lee, *Spin Dynamics of the Spin-1/2 Kagome Lattice Antiferromagnet  $\text{ZnCu}_3(\text{OH})_6\text{Cl}_2$* , Phys. Rev. Lett. **98**, 107204 (2007).

- [56] Y. Ran, M. Hermele, P. A. Lee, X. G. Wen, *Projected wavefunction study of Spin-1/2 Heisenberg model on the Kagome lattice*, Phys. Rev. Lett. **98**, 117205 (2007); *Properties of an algebraic spin liquid on the kagome lattice*, Phys. Rev. B **77**, 224413 (2008).
- [57] L. B. Ioffe, M. V. Feigelman, A. Ioselevich, D. A. Ivanov, M. Troyer, and G. Blatter, *Topologically protected quantum bits using Josephson junction arrays*, Nature (London) **415**, 503 (2002).
- [58] J. Cardy, *Scaling and Renormalization in Statistical Physics*, Cambridge University Press, Cambridge, UK (1996).
- [59] X. G. Wen, Phys. Rev. B **40**, 7387(R) (1989); *ibid.* **44**, 2664 (1991); X. G. Wen and Q. Niu, *Ground-state degeneracy of the fractional quantum Hall states in the presence of a random potential and on high-genus Riemann surfaces*, *ibid.* **41**, 9377 (1990); X. G. Wen, *Chiral Luttinger liquid and the edge excitations in the fractional quantum Hall states*, *ibid.* **41**, 12838 (1990); X. G. Wen, *Topological orders in rigid states*, Int. J. Mod. Phys. B **4**, 239 (1990).
- [60] X.-G. Wen, *Quantum Field Theory of Many-body Systems: From the Origin of Sound to an Origin of Light and Electrons*, Oxford University Press (2004).
- [61] M. Oshikawaa and T. Senthil, *Fractionalization, Topological Order, and Quasiparticle Statistics*, Phys. Rev. Lett. **96**, 060601 (2006).
- [62] M. Oshikawaa, Y. B. Kimb, K. Shtengel, C. Nayak, and S. Tewarig, *Topological degeneracy of non-Abelian states for dummies*, Ann. Phys. (NY) **322**, 1477 (2007).
- [63] A. Ioselevich, D. A. Ivanov, and M. V. Feigelman, *Ground-state properties of the Rokhsar-Kivelson dimer model on the triangular lattice*, Phys. Rev. B **66**, 174405 (2002).
- [64] D. S. Rokhsar and S. A. Kivelson, *Superconductivity and the Quantum Hard-Core Dimer Gas*, Phys. Rev. Lett. **61**, 2376 (1988).
- [65] S. A. Kivelson, D. S. Rokhsar, and J. P. Sethna, *Topology of the resonating valence-bond state: Solitons and high- $T_c$  superconductivity*, Phys. Rev. B **35**, 8865 (1987).
- [66] S. Sachdev, *Spin-Peierls ground states of the quantum dimer model: A finite-size study*, Phys. Rev. B **40**, 5204 (1989).
- [67] P. W. Leung, K. C. Chiu, and K. J. Runge, *Columnar dimer and plaquette resonating-valence-bond orders in the quantum dimer model*, Phys. Rev. B **54**, 12938 (1996).
- [68] O. F. Sylåsen, *Plaquette phase of the square-lattice quantum dimer model: Quantum Monte Carlo calculations*, Phys. Rev. B **73**, 245105 (2006).
- [69] C. L. Henley, *Form classical to quantum dynamics at the RK points*, J. Phys. Condens. Matter **16**, 891 (2004); *Relaxation Time for a Dimer Covering with Hight Representation*, J. Stat. Phys. **89**, 483 (1997).

- [70] R. Moessner, S. L. Sondhi, E. Fradkin, *Short-ranged resonating valence bond physics, quantum dimer models, and Ising gauge theories*, Phys. Rev. B **65**, 024504 (2001).
- [71] E. Fradkin, D. A. Huse, R. Moessner, V. Oganesyan, S. L. Sondhi, *Bipartite Rokhsar-Kivelson points and Cantor deconfinement*, Phys. Rev. B **69**, 224415 (2004).
- [72] P. W. Kasteleyn, *Dimer statistics and Phase Transitions*, J. Math. Phys. **4**, 287 (1963).
- [73] M. E. Fisher, *Statistical Mechanics of Dimers on a Plane Lattice*, Phys. Rev. **124**, 1664 (1961); M. E. Fisher and J. Stephenson, *ibid.* **132**, 1411 (1963).
- [74] E. Ardonne, P. Fendley, and E. Fradkin, *Topological order and conformal quantum critical points*, Ann. Phys. (NY) **310**, 493 (2004).
- [75] R. Moessner and S. L. Sondhi, *Three-dimensional resonating-valence-bond liquids and their excitations*, Phys. Rev. B **68**, 184512 (2003).
- [76] D. A. Ivanov, *Vison gap in the Rokhsar-Kivelson dimer model on the triangular lattice*, Phys. Rev. B **70**, 94430 (2004).
- [77] A. M. Läuchli, S. Capponi and F. F. Assaad, *Dynamical dimer correlations at bipartite and non-bipartite Rokhsar-Kivelson points*, J. Stat. Mech. P01010 (2008).
- [78] F. Miserez, *Quantum Dimer Model - Dynamical correlations and Supersymmetric Dimer-Fermion model*, M. Sc. Thesis, Institute of Theoretical Physics, Ecole Polytechnique Fédérale de Lausanne, 2008.
- [79] R. Moessner and S. L. Sondhi, *Resonating Valence Bond Phase in the Triangular Lattice Quantum Dimer Model*, Phys. Rev. Lett. **86**, 1881 (2001); P. Fendley, R. Moessner, and S. L. Sondhi, *Classical dimers on the triangular lattice*, Phys. Rev. B **66**, 214513 (2002).
- [80] A. Ralko, M. Ferrero, F. Becca, D. Ivanov, and F. Mila, *Zero-Temperature Properties of the Quantum Dimer Model on the Triangular Lattice*, Phys. Rev. B **71**, 224109 (2005); *Dynamics of the quantum dimer model on the triangular lattice: Soft modes and local resonating valence-bond correlations*, *ibid.* **74**, 134301 (2006); *Crystallization of the resonating valence bond liquid as vortex condensation*, *ibid.* **76**, 140404(R) (2007).
- [81] N. Read and B. Chakraborty, *Statistics and excitations of the resonating-valence-bond state*, Phys. Rev. B **40**, 7133 (1989).
- [82] S. A. Kivelson, D. S. Rokhsar, and J. P. Sethna, *2e or not 2e: Flux quantization in the Resonating Valence Bond State*, Europhys. Lett. **6**, 353 (1988).
- [83] W. Marshall, *Antiferromagnetism*, Proc. Roy. Soc. (London) **A232**, 48 (1955).
- [84] S. A. Kivelson, *Statistics of holons in the quantum hard-core dimer gas*, Phys. Rev. B **39**, 259 (1989).



- [85] T. Senthil and M. P. A. Fisher, *Z<sub>2</sub> gauge theory of electron fractionalization in strongly correlated systems*, Phys. Rev. B **62**, 7850 (2000); *Fractionalization, topological order, and cuprate superconductivity*, *ibid.* **63**, 134521 (2001).
- [86] Ch. Mudry and E. Fradkin, *Separation of spin and charge quantum numbers in strongly correlated systems*, Phys. Rev. B **49**, 5200 (1994).
- [87] P. A. M. Dirac, *Quantized Singularities in the Electromagnetic Field*, Proc. Roy. Soc. London A **133**, 60 (1931).
- [88] O. F. Syljuåsen, *Continuous-time diffusion Monte Carlo method applied to the quantum dimer model*, Phys. Rev. B **71**, 020401(R) (2005).
- [89] D. Poilblanc, F. Alet, F. Becca, A. Ralko, F. Trouselet, and F. Mila, *Doping quantum dimer models on the square lattice*, Phys. Rev. B **74**, 014437 (2006).
- [90] C. Castelnovo, C. Chamon, Ch. Mudry, and P. Pujol, *Zero-temperature Kosterlitz-Thouless transition in a two-dimensional quantum system*, Ann. Phys. (NY) **322**, 903 (2007).
- [91] S. Papanikolaou, E. Luijten, and E. Fradkin, *Quantum criticality, lines of fixed points, and phase separation in doped two-dimensional quantum dimer models*, Phys. Rev. B **76**, 134514 (2007).
- [92] A. Ralko, F. Mila, and D. Poilblanc, *Phase Separation and Flux Quantization in the Doped Quantum Dimer Model on Square and Triangular Lattices*, Phys. Rev. Lett. **99**, 127202 (2007).
- [93] H. Ribeiro, S. Bieri, and D. A. Ivanov, *Single hole and vortex excitations in the doped Rokhsar-Kivelson quantum dimer model on the triangular lattice*, Phys. Rev. B **76**, 172301 (2007).
- [94] H. Ribeiro, *Resonating-Valence-Bond Dimer Liquids With Mobile Holes*, M. Sc. Thesis, Institute of Theoretical Physics, Ecole Polytechnique Fédérale de Lausanne, 2007.
- [95] J. W. Negele and H. Orland, *Quantum many-particle systems*, Westview Press (1998).
- [96] D. Baeriswyl and N. Macris, *Méthodes à N corps en matière condensée*, lecture notes, Troisième Cycle de la physique en Suisse Romande, EPFL (2001).
- [97] S. Yunoki, *Coherent inverse photoemission spectrum for Gutzwiller projected superconductors*, Phys. Rev. B **72**, 092505 (2005).
- [98] M. Randeria, R. Sensarma, N. Tirvedi, and F.-Ch. Zhang, *Particle-Hole Asymmetry in Doped Mott Insulators: Implications for Tunneling and Photoemission Spectroscopies*, Phys. Rev. Lett. **95**, 137001 (2005).

- [99] S. Yunoki, E. Dagotto, and S. Sorella, *Role of Strong Correlation on the Recent Angle-Resolved Photoemission Spectroscopy Experiments on Cuprate Superconductors*, Phys. Rev. Lett. **94**, 037001 (2005).
- [100] C. P. Nave, D. A. Ivanov, and P. A. Lee, *A VMC Study of the Current Carried by a Quasiparticle*, Phys. Rev. B **73**, 104502 (2006).
- [101] B. Edegger, V. N. Muthukumar, C. Gros, and P. W. Anderson, *Electronic Structure of Strongly Correlated d-wave Superconductors*, Phys. Rev. Lett. **96**, 207002 (2006).
- [102] S. Bieri and D. Ivanov, *Quasiparticle spectral weights of Gutzwiller-projected high- $T_c$  superconductors*, Phys. Rev. B **75**, 035104 (2007).
- [103] F. Tan and Q.-H. Wang, *Two-mode VMC study of QP excitations in cuprate superconductors*, Phys. Rev. Lett. **100**, 117004 (2008).
- [104] F. Becca, L. Capriotti, and S. Sorella, in *Open Problems in Strongly Correlated Electron Systems*, ed. J. Bonca, P. Prelovsek, A. Ramsak, and S. Sarkar, NATO ARW, Sci. Ser. II, Vol. 15 (Kluwer, Dordrecht, 2001).
- [105] H. Yang, F. Yang, Y.-J. Jiang, and T. Li, *On the origin of the tunneling asymmetry in the cuprate superconductors: a variational perspective*, J. Phys.: Condens. Matter. **19**, 016217 (2007); cond-mat/0604488.
- [106] Ch. P. Chou, T. K. Lee, and Ch.-M. Ho, *Spectral weights, d-wave pairing amplitudes, and particle-hole tunneling asymmetry of a strongly correlated superconductor*, Phys. Rev. B **74**, 092503 (2006).
- [107] L. Spanu, M. Lugas, F. Becca, and S. Sorella, *Magnetism and superconductivity in the  $t$ - $t'$ - $J$  model*, Phys. Rev. B **77**, 024510 (2008).
- [108] D. Pines and P. Nozières, *The Theory of Quantum Liquids*, Addison-Wesley, Reading, MA (1966).
- [109] J. M. Luttinger, *Analytic Properties of Single-Particle Propagators for Many-Fermion Systems*, Phys. Rev. **121**, 942 (1961).
- [110] I. Dzyaloshinskii, *Some consequences of the Luttinger theorem: The Luttinger surface in non-Fermi liquids and Mott insulators*, Phys. Rev. B **68**, 085113 (2003).
- [111] C. Gros, B. Edegger, V. N. Muthukumar, and P. W. Anderson, *Determining the underlying Fermi surface of strongly correlated superconductors*, Proc. Natl. Acad. Sci. **103**, 14298 (2006).
- [112] R. Sensarma, M. Randeria, and N. Trivedi, *Can one determine the underlying Fermi surface in the superconducting state of strongly correlated superconductors?*, Phys. Rev. Lett. **98**, 027004 (2007).

- [113] Y. Hasegawa and D. Poilblanc, *Hole dynamics in the  $t$ - $J$  model: An exact diagonalization study*, Phys. Rev. B **40**, 9035 (1989).
- [114] D. Poilblanc, J. Riera, and E. Dagotto,  *$d$ -wave bound state of holes in an antiferromagnet*, Phys. Rev. B **49**, 12318 (1994).
- [115] K. Park, *Quantum antiferromagnetism and high  $T_c$  superconductivity: A close connection between the  $t$ - $J$  model and the projected BCS Hamiltonian*, Phys. Rev. B **72**, 245116 (2005).
- [116] Y. Ohta, T. Shimozato, R. Eder, and S. Maekawa, *Bogoljubov quasiparticle excitations in the two-dimensional  $t$ - $J$  model*, Phys. Rev. Lett. **73**, 324 (1994).
- [117] S. Yunoki, private communication (2006).
- [118] S. Yunoki, *Single-particle anomalous excitations of Gutzwiller-projected BCS Superconductors and Bogoljubov Quasiparticle characteristics*, Phys. Rev. B **74**, 180504(R) (2006).
- [119] H. Matsui, T. Sato, T. Takahashi, S.-C. Wang, H.-B. Yang, H. Ding, T. Fujii, T. Watanabe, and A. Matsuda, *BCS-Like Bogoljubov Quasiparticles in High- $T_c$  Superconductors Observed by Angle-Resolved Photoemission Spectroscopy*, Phys. Rev. Lett. **90**, 217002 (2003).
- [120] K. M. Shen, F. Ronning, D. H. Lu, F. Baumberger, N. J. C. Ingle, W. S. Lee, W. Meevasana, Y. Kohsaka, M. Azuma, M. Takano, and Z.-X. Shen, *Nodal Quasiparticles and Antinodal Charge Ordering in  $\text{Ca}_{2-x}\text{Na}_x\text{CuO}_2\text{Cl}_2$* , Science **307**, 901 (2005).
- [121] X. J. Zhou, T. Yoshida, A. Lanzara, P. V. Bogdanov, S. A. Kellar, K. M. Shen, W. L. Yang, F. Ronning, T. Sasagawa, T. Kakeshita, T. Noda, H. Eisaki, S. Uchida, C. T. Lin, F. Zhou, J. W. Xiong, W. X. Ti, Z. X. Zhao, A. Fujimori, Z. Hussain, and Z.-X. Shen, *Dichotomy between Nodal and Antinodal Quasiparticles in Underdoped  $\text{La}_{2-x}\text{Sr}_x\text{CuO}_4$  Superconductors*, Phys. Rev. Lett. **92**, 187001 (2004).
- [122] A. Ino, C. Kim, M. Nakamura, T. Yoshida, T. Mizokawa, A. Fujimori, Z.-X. Shen, T. Kakeshita, H. Eisaki, and S. Uchida, *Doping-dependent evolution of the electronic structure of  $\text{La}_{2-x}\text{Sr}_x\text{CuO}_4$  in the superconducting and metallic phases*, Phys. Rev. B **65**, 094504 (2002).
- [123] T. Yoshida, X. J. Zhou, T. Sasagawa, W. L. Yang, P. V. Bogdanov, A. Lanzara, Z. Hussain, T. Mizokawa, A. Fujimori, H. Eisaki, Z.-X. Shen, T. Kakeshita, and S. Uchida, *Metallic Behaviour of Lightly Doped  $\text{La}_{2-x}\text{Sr}_x\text{CuO}_4$  with a Fermi Surface Forming an Arc*, Phys. Rev. Lett. **91**, 027001 (2003).
- [124] A. Himeda and M. Ogata, *Spontaneous Deformation of the Fermi Surface due to Strong Correlation in the Two-Dimensional  $t$ - $J$  Model*, Phys. Rev. Lett. **85**, 4345 (2000).

- [125] W. O. Putikka, M. U. Luchini, and R. R. P. Singh, *Violation of Luttinger's Theorem in the Two-Dimensional  $t$ - $J$  Model*, Phys. Rev. Lett. **81**, 2966 (1998).
- [126] P. Lee and X.-G. Wen, *Vortex structure in underdoped cuprates*, Phys. Rev. B **63**, 224517 (2001).
- [127] S. Bieri and D. A. Ivanov, *An  $SU(2)$  approach to the pseudogap phase: electronic spectral functions*, arXiv:0809.5230; submitted to Phys. Rev. B.
- [128] T. Timusk and B. Statt, *The pseudogap in HTSC: an experimental survey*, Rep. Prog. Phys. **62**, 61 (1999).
- [129] M. Norman, D. Pines, and C. Kallin, *The pseudogap: friend or foe of high- $T_c$  ?*, Adv. Phys. **54**, 715 (2005).
- [130] D. S. Marshall, D. S. Dessau, A. G. Loeser, C-H. Park, A. Y. Matsuura, J. N. Eckstein, I. Bozovic, P. Fournier, A. Kapitulnik, W. E. Spicer, and Z.-X. Shen, *Unconventional electronic structure evolution with hole doping in  $Bi_2Sr_2CaCu_2O_{8+\delta}$ : angle-resolved photoemission results*, Phys. Rev. Lett. **76**, 4841 (1996).
- [131] A. G. Loeser, Z. X. Shen, D. S. Dessau, D. S. Marshall, C. H. Park, P. Fournier, and A. Kapitulnik, *Excitation gap in the normal state of underdoped  $Bi_2Sr_2CaCu_2O_{8+\delta}$* , Science **273**, 325 (1996).
- [132] H. Ding, T. Yokoya, J. C. Campuzano, T. Takahashi, M. Randeria, M. R. Norman, T. Mochiku, K. Kadowaki, and J. Giapintzakis, *Spectroscopic evidence for a pseudogap in the normal state of underdoped high- $T_c$  superconductors*, Nature (London) **382**, 51 (1996).
- [133] M. R. Norman, H. Ding, M. Randeria, J. C. Campuzano, T. Yokoya, T. Takeuchi, T. Takahashi, T. Mochiku, K. Kadowaki, P. Guptasarma, and D. G. Hinks, *Destruction of the Fermi surface in underdoped high- $T_c$  superconductors*, Nature (London) **392**, 157 (1998).
- [134] A. Kanigel, U. Chatterjee, M. Randeria, M. R. Norman, S. Souma, M. Shi, Z. Z. Li, H. Raffy, and J. C. Campuzano, *Protected Nodes and the Collapse of Fermi Arcs in High- $T_c$  Cuprate Superconductors*, Phys. Rev. Lett. **99**, 157001 (2007).
- [135] T. Giamarchi and C. Lhuillier, *Dispersion relation of a single hole in the  $t$ - $J$  model determined by a VMC method*, Phys. Rev. B **47**, 2775 (1993).
- [136] K.-Y. Yang, C. T. Shih, C. P. Chou, S. M. Huang, T. K. Lee, T. Xiang, and F. C. Zhang, *Low-energy physical properties of HTSC superconducting Cu oxides: A comparison between RVB and experiments*, Phys. Rev. B **73**, 224513 (2006).

- [137] I. Affleck and J. B. Marston, *Large- $n$  limit of the Heisenberg-Hubbard model: Implications for high- $T_c$  superconductors*, Phys. Rev. B **37**, 3774 (1988); I. Affleck, Z. Zou, T. Hsu, and P. W. Anderson,  *$SU(2)$  gauge symmetry of the large- $U$  limit of the Hubbard model*, *ibid.* **38**, 745 (1988).
- [138] E. Dagotto, E. Fradkin, and A. Moreo,  *$SU(2)$  gauge invariance and order parameter in strongly coupled electronic systems*, Phys. Rev. B **38**, 2926(R) (1988).
- [139] X.-G. Wen and P. A. Lee, *Theory of underdoped cuprates*, Phys. Rev. Lett. **76**, 503 (1996).
- [140] P. Lee, N. Nagaosa, T.-K. Ng, and X.-G. Wen,  *$SU(2)$  formulation of the  $t$ - $J$  model: Application to underdoped cuprates*, Phys. Rev. B **57**, 6003 (1998).
- [141] W. Rantner and X.-G. Wen, *Tunneling Density of States of High- $T_c$  Superconductors:  $d$ -Wave BCS Model versus  $SU(2)$  Slave-Boson Model*, Phys. Rev. Lett. **85**, 3692 (2000).
- [142] D. A. Ivanov, P. A. Lee, and X.-G. Wen, *Staggered-vorticity Correlations in a lightly doped  $t$ - $J$  model*, Phys. Rev. Lett. **84**, 3958 (2000).
- [143] P. A. Lee and N. Nagaosa, *Collective modes in the superconducting ground states in the gauge theory description of cuprates*, Phys. Rev. B **68**, 024516 (2003).
- [144] C. Honerkamp and P. A. Lee, *Staggered Flux Fluctuations and the Quasiparticle Scattering Rate in the  $SU(2)$  Gauge Theory of the  $t$ - $J$  Model*, Phys. Rev. Lett. **90**, 246402 (2003).
- [145] C. Honerkamp and P. A. Lee, *Staggered Flux Vortices and the Superconducting Transition in the Layered Cuprates*, Phys. Rev. Lett. **92**, 177002 (2004).
- [146] Z. A. Xu, N. P. Ong, Y. Wang, T. Kakeshita, and S. Uchida, *Vortex-like excitations and the onset of superconducting phase fluctuations in underdoped LSCO*, Nature (London) **406**, 486 (2000); Y. Wang, Z. A. Xu, T. Takeshita, S. Uchida, S. Ono, Y. Ando, and N. P. Ong, *Onset of the vortexlike Nernst signal above  $T_c$  in  $La_{2-x}Sr_xCuO_4$  and  $Bi_2Sr_{2-y}La_yCuO_6$* , Phys. Rev. B **64**, 224519 (2001); Y. Wang, N. P. Ong, Z. A. Xu, T. Kakeshita, S. Uchida, D. A. Bonn, R. Liang, and W. N. Hardy, *High Field Phase Diagram of Cuprates Derived from the Nernst Effect*, Phys. Rev. Lett. **88**, 257003 (2002).
- [147] J. Graf, G.-H. McElroy, S. Y. Zhou, C. Jozwiak, E. Rotenberg, A. Bill, T. Sasagawa, W. Eisaki, U. Uchida, H. Takagi, D.-H. Lee, and A. Lanzara, *Universal High Energy Anomaly in the Angle-Resolved Photoemission Spectra of High Temperature Superconductors: Possible Evidence of Spinon and Holon Branches*, Phys. Rev. Lett. **98**, 067004 (2007).

- [148] W. Zhang, G. Liu, J. Meng, L. Zhao, H. Liu, X. Dong, W. Lu, J. S. Wen, Z. J. Xu, G. D. Gu, T. Sasagawa, G. Wang, Y. Zhu, H. Zhang, Y. Zhou, X. Wang, Z. Zhao, Ch. Chen, Z. Xu, and X. H. Zhou, *High Energy Dispersion Relations for the High Temperature Bi<sub>2</sub>Sr<sub>2</sub>CaCu<sub>2</sub>O<sub>8</sub> Superconductor from Laser-Based Angle-Resolved Photoemission Spectroscopy*, Phys. Rev. Lett. **101**, 017002 (2008).
- [149] M. R. Norman, A. Kanigel, M. Randeria, U. Chatterjee, and J. C. Campuzano, *Modelling the Fermi arc in underdoped cuprates*, Phys. Rev. B **76**, 174501 (2007).

# Acknowledgements

First of all, I want to thank Dmitri for accepting me as his first doctoral student at the EPFL and for proposing this interesting topic of research to me. It was a pleasure learning from him, not only at the Institute of Theoretical Physics, but on many skiing and hiking trips to the close Swiss Alps. From the other members of our research group, I specially want to thank George Jackeli for the countless discussions about physics and many other things that we shared. George made my entrance to the field of solid state physics very pleasant. I also want to thank Benoît Crouzy and Sylvain Tollis for the great time we spent together, discussions and coffee, the climbing and skiing trips, their proof reading of my work, and much more.

I also want to thank the other members of the ITP, for their teaching, support, and advice I enjoyed from them over the years I spent at the EPFL: Profs. A. Baldereschi, Ch. Gruber, H. Kunz, Ph.-A. Martin, F. Mila, V. Savona, C. Scrucca, and M. Shaposhnikov. I specially want to thank Prof. F. Mila for the interesting journal clubs that he initiated and which allowed me to learn about ongoing research. Not to forget about Ioannis Rousochatzakis for the ungrateful task of motivating speakers for the journal club. From the other graduate students, I specially want to thank Pascal Bünzli, Julien Dorier, Aric Gliesche, Valeria Lante, Gaetano Parascandolo, Claude Plocek, Rico Rueedi, Davide Sarchi, Thierry Schuepbach, and Guillaume Tarel for the pleasant coffee breaks, many interesting discussions, and outings. Not to forget about Noemi Porta and Leonor Camporeale for their excellent administrative support. The other valuable members of the institute which I cannot mention here are also greatly acknowledged. I also want to thank the numerous undergraduate students who asked the right questions throughout my teaching activities.

At this place, I would like to express my thanks to the members of the jury for their useful comments on the manuscript. I also thank the Swiss National Science Foundation for the financial support.

I greatly profited from the numerous visitors who stayed regularly at the ITP over the years: Sasha Abanov, Misha Skvortsov, Yasha Vominov, Mike Zhitomirsky. In particular, I want to thank Bruce Normand. Not only for the physics he brought to the EPFL, but also for the various long and impressive mountain trips which I would never have done without him.

Last but not least, I want to cordially thank my parents for their support, love, and confidence. I also thank my brother Tobias and my sister Sara. My girlfriend Simone gave me substantial support and help during the last months of my thesis, I want to thank her for this.

# Curriculum Vitae

## Samuel Bieri

Born on March 8, 1978 in Bern, Switzerland  
Swiss citizen, languages: German, French, English

Institute of Theoretical Physics (ITP)  
Ecole Polytechnique Fédérale de Lausanne, Station 3, CH-1015 Lausanne  
e-mail: samuel.bieri@a3.epfl.ch

## EDUCATION

**Swiss Federal Institute of Technology (EPFL), Lausanne, Switzerland**

Doctor of Philosophy (Docteur ès sciences) expected **12/2008**

- Title of the thesis:  
*Resonating-valence-bond approaches to high-temperature superconductivity*
- Advisor: Prof. Dmitri A. Ivanov
- Area of study: strongly correlated electrons, doped Mott insulators,  $t$ - $J$  model, Gutzwiller-projected wavefunctions, spin liquids, quantum dimer models, topological order, field-theoretic approaches, random matrices, and high-temperature superconductivity.

Master of Science (Physicien Diplômé EPF) **03/2004**

- Title of the thesis:  
*Stability of the soliton in the broken  $O(3)$  nonlinear  $\sigma$ -model in  $2+1$  dimensions*
- Advisor: Prof. Mikhail Shaposhnikov
- Area of study: quantum field theory, topological and nontopological solitons, integrable models, high-energy and particle physics.

**Université de Montréal, Montreal, Canada** **2001 - 2002**  
One year exchange programm, accredited and financially supported by the EPFL

**Collège Sainte-Croix, Fribourg, Switzerland** **09/1999**  
Matura of Kanton Fribourg

**Rudolf Steiner Schule, Berne, Switzerland** **1985 - 1997**



## PUBLICATIONS

- S. Bieri and D. A. Ivanov, *SU(2) approach to the pseudogap phase of high-temperature superconductors: electronic spectral functions*, Physical Review B **79**, 174518 (2009).
- H. Ribeiro, S. Bieri, and D. Ivanov, *Single hole and vortex excitations in the triangular-lattice quantum dimer model*, Physical Review B **76**, 172301 (2007).
- S. Bieri and D. Ivanov, *Quasiparticle spectral weights of Gutzwiller-projected high- $T_c$  superconductors*, Physical Review B **75**, 035104 (2007).

## CONFERENCE PROCEEDINGS

- S. Bieri and D. Ivanov, *Coherent spectral weights of Gutzwiller-projected superconductors*, presented at the “11th Training Course in the Physics of Strongly Correlated Systems and high- $T_c$  Superconductors”, Vietri sul Mare, Salerno, Italy, October 2006, AIP Conf. Proc. **918**, 277 (2007).

## TEACHING ACTIVITIES

<i>Teaching Assistant</i> , EPFL	<b>2004 - 2008</b>
Advanced quantum mechanics, Prof. D. Ivanov	2007, 2008
Proseminar on full counting statistics, Prof. D. Ivanov	2007
Physique générale, Prof. G. Meylan	2007
Proseminar on supersymmetry, Prof. D. Ivanov	2006
Electrodynamique classique, Prof. R. Durrer	2006
Proseminar on quantum dimer models, Profs. D. Ivanov and F. Mila	2005
Electrodynamique classique, Prof. M. Shaposhnikov	2005
<i>Student Teaching Assistant</i> , EPFL	<b>2001 - 2003</b>
Physique générale, Prof. M. Grioni	2002, 2003
Mécanique classique, Prof. R. Gotthardt	2001, 2002

## OTHER EXPERIENCE

<i>Consultant</i> , e-globe technologies AG, Bern	<b>03/2004 - 10/2004</b>
<i>Research student</i> , Centre Hospitalier de l'Université de Montréal, Center for Biomedical Research	<b>04/2002 - 10/2002</b>
<i>Management support</i> , Swisscom AG, Bern	<b>02/1999 - 04/1999</b>